Dissertation

submitted to the

Combined Faculty of Natural Sciences and Mathematics

of the Ruperto Carola University Heidelberg, Germany

for the degree of

Doctor of Natural Sciences

Presented by

Mgr. Klára Obrová

born in: Mělník, Czech Republic

Oral examination: 19th October 2018

In depth functional characterization of *Plasmodium berghei* ferlin-like protein

Referees: Prof. Dr. Michael Lanzer
Dr. Ann-Kristin Mueller

Declaration of own work

I hereby declare that this dissertation contains my own work, and it has not been submitted previously for any assessment or other purposes. I have acknowledged all sources and provided these in the reference section.

Klára Obrová

Acknowledgments

At the first place, I want to thank **Dr. Ann-Kristin Mueller** for being a leader rather than a boss. No matter how bad my results looked, after talking with her I got a fresh supply of motivation to go on.

I am also very grateful to **Dr. Roland Frank** for endless discussions about even the tiniest piece of data or a stupid idea that came to my mind. Nobody ever reviewed my work and suggestions as carefully as him.

Thanks to **Dr. Kirsten Heiss**, **Dr. Britta Nyboer**, **Dr. Priyanka Fernandes** and **Kamil Wolanin**, the lab was always a friendly and relaxed working environment. Also, help was always just one question away. This thesis was partially supported by work of my talented and very friendly students. I was very glad to meet them all – **Valerie Oberhardt**, who contributed to chapters 3.1.2 and 3.2.4.1; **Vered Fijan** who contributed to chapters 3.1.3.1 and 3.2.4.3; **Kamil Wolanin** who helped with data in figure 3.20 and **Constanze Kroeber** whose extraordinary motivation significantly helped with data for chapter 3.1.3.2.

The role of FLP in the gametocyte stage was thoroughly discussed with **Dr. Gunnar R. Mair**, whose honest, straightforward and clever comments sometimes ruined and sometimes supported my complex plans. He also contributed to chapters 3.1.3.2 and 3.3.5 by providing vectors. Many methods would have taken much longer to establish without the help of **Jessica Kehrer**, who provided protocols and troubleshooted with me.

Dr. Marcel Deponte kindly ran analysis on the FLP sequence (which was until then more of a black box for me) and helped design fragments for chapter 3.1.2. **Dr. Mirko Singer** helped me substantially with generating the vector and especially with microscopy in chapter 3.1.3.2. **Christina Schulte-Huxel** was a master student interested in FLP before I joined the lab. Although I never met her, her data were a useful starting point. She also generated the line used in chapter 3.1.4.1.

I am very grateful to **my parents**, who keep thinking that my work is fascinating, even at times when I don't. I want to thank **my sister**, who decided to become a biologist as well, for occasional chats about how tough life can be.

Especially, I want to thank **Dr. Martin Obr**, my husband, for sharing my (and his) happy moments, helping me overcome trouble and discussing literally everything. He probably knows more about gametogenesis in *Plasmodium* than most other virologists.

Summary

Proteins of the ferlin family mediate calcium-dependent vesicular fusion. Although present throughout eukaryotic evolution, their function in unicellular organisms including apicomplexan parasites is unknown.

This study defined for the first time a crucial role for a ferlin-like protein (FLP) in host-to-vector transmission of the rodent malaria parasite *Plasmodium berghei*. Analysis of *flp* expression profile revealed a peak in the gametocyte stage. Endogenous tagging of the protein confirmed high abundance of FLP in this stage. In agreement with the reported vesicular localization of ferlins, HA-tagged FLP labelled intracellular speckles in asexual and sexual blood stages. The FLP-labelled vesicles relocalized to the cell periphery during gamete maturation, suggesting that they might act in the process of the gamete egress from the red blood cell.

Infection of the mosquito vectors requires the formation of free gametes and their fertilization in the mosquito midgut. Mature gametes will only emerge upon secretion of factors that stimulate the disruption of the red blood cell membrane and the parasitophorous vacuole membrane. Lysis of the surrounding membranes is a critical step in host-to-vector transmission and its failure prevents infection of the mosquito.

Genetic depletion of FLP in sexual stages led to a complete life cycle arrest in the mosquito. Although mature gametes formed normally, mutants lacking FLP remained trapped in the red blood cell. FLP function was restricted to egress as the observed phenotype was rescued by detergent-mediated *in vitro* membrane lysis facilitating escape from the host cell and allowing normal life cycle progression of the FLP-depleted gametocytes. The data of this work define FLP as a novel critical factor for *Plasmodium* fertilization and transmission and suggest an evolutionarily conserved example of ferlin-mediated exocytosis.

Zusammenfassung

Proteine aus der Familie der Ferline vermitteln die Calcium-abhängige Fusion zellulärer Vesikel. Obwohl Ferline in der eukaryotischen Evolution konserviert sind, ist ihre Funktion in einzelligen Organismen, die Parasiten der Apicomplexa inbegriffen, bislang unbekannt.

In dieser Studie wird erstmals die entscheidende Rolle eines Ferlin-ähnlichen Proteins (FLP, Ferlin-like protein) für die Übertragung des Nagetiermalariaerregers *Plasmodium berghei* vom Wirt auf den Moskitovektor beschrieben. Die Analyse des FLP-Expressionsprofils zeigte ein Maximum im Gametozytenstadium. Die endogene Markierung (tagging) des Proteins bestätigte die starke Anreicherung in diesem Parasitenstadium. In Übereinstimmung mit der bekannten vesikulären Lokalisation von Ferlinen, konnte Hämagglutinin (HA)-markiertes FLP in punktförmigen Bereichen innerhalb asexueller und sexueller Blutstadien visualisiert werden. Während der Gametogenese kam es zu einer Relokalisierung der Vesikel an der Zellperipherie, was einen Hinweis darauf lieferte, dass diese am Prozess des Austritts der Gameten aus dem Erythrozyten beteiligt sein könnten.

Die Infektion des Moskitovektors ist abhängig von der Bildung freier Gameten und deren Fertilisation im Mitteldarm der Stechmücke. Nur durch die Sekretion von Faktoren, die zur Auflösung der parasitophoren Vakuolen- und Erythrozytenmembran führen, können reife Gameten entstehen. Die Lyse dieser umhüllenden Membranen stellt einen essentiellen Schritt bei der Übertragung vom Wirt auf den Vektor dar. Ein Ausbleiben dieser Membranlyse verhindert die erfolgreiche Infektion der Stechmücke.

Die genetische Depletion von FLP in Sexualstadien führte zu einer vollständigen Unterbrechung des Lebenszyklus in der Stechmücke. Obwohl sich reife Gametozyten normal ausbildeten, blieben mutierte Parasiten ohne FLP im Erythrozyten eingeschlossen. Die Funktion von FLP konnte auf den Austritt der Gameten eingegrenzt werden, da der beobachtete Phänotyp durch eine *in vitro* Membranlyse unter Verwendung eines Detergenz rückgängig gemacht werden konnte. Dies ermöglichte den Austritt aus der Wirtszelle und resultierte folglich in einer normalen Weiterentwicklung FLP-depletierter Gametozyten. Die Ergebnisse dieser Arbeit definieren FLP als einen neuen und entscheidenden Faktor bei der Fertilisation und Übertragung von *Plasmodium* und weisen auf ein evolutionär konserviertes Beispiel Ferlin-vermittelter Exozytose hin.

Contents

List of abbreviations

AID	auxin-inducible degron
AMA1	apical membrane antigen 1
AP2-G	Apetala 2 - gametocytes
BAPTA-AM	1,2-Bis(2-aminophenoxy)ethane-N,N,N′,N′-tetraacetic acid tetrakis(acetoxymethyl ester)
C. elegans	*Caenorhabditis elegans*
C	clonal line
CCP	Coagulation factor C domain-containing protein
CDPK	calcium-dependent protein kinase
CelTOS	cell traversal protein for ookinetes and sporozoites
CITH	Car-I/Trailer Hitch homologue
CSP	circumsporozoite protein
D+/-	drug pressure on/off
DD	destabilization domain
DHFR	dihydrofolate reductase
DMSO	dimethyl sulfoxide
DOC2	double C2 protein
DOZI	development of zygote inhibited
DysF	dysferlin domain
E. coli	*Escherichia coli*
ECM	experimental cerebral malaria
ECP1	egress cysteine protease 1
Fer-1	Fertility factor 1
FISH	fluorescent *in situ* hybridization

FLP	ferlin-like protein
FLP/FRT system	flippase/flippase recognition target system
FMN	flavin monophosphate
GAM	gametocyte-enriched sample
GC	guanylyl cyclase
GEST	gamete egress and sporozoite traversal protein
GFP	green fluorescent protein
glms	glucosamine-6-phosphate activated ribozyme
HCM	host cell membrane
HDA2	histone deacetylase 2
HOP	heat shock organizing protein
HP1	heterochromatin protein 1
hpi	hours post infection
HSP70	heat shock protein 70
i.v.	intravenously
IPTG	Isopropyl β-D-1-thiogalactopyranoside
IP3	inositol tri-phosphate
iRBCs	infected red blood cells
kb	kilo base pair
kDa	kilo dalton
KO	knock-out
MAOP	membrane attack ookinete protein
MAP2	mitogen-activated protein kinase 2
MBS	mixed blood stages
MDV1/PEG3	male development-1/protein of early gametocyte 3

MO	membranous organelles
MTOC	microtubule organizing centre
MTRAP	merozoite thrombospondin-related adhesive protein
ND	not determined
OBs	osmiophilic bodies
ORF	open reading frame
P.	*Plasmodium*
P	parental line
PAT	putative small solute transporter
PC	positive control
PDE	phosphodiesterase
PKG	cGMP-dependent protein kinase
PI-PLC	phosphoinositide phospholipase C
PPLP2	*Plasmodium* perforin-like protein 2
PPM	parasite plasma membrane
PV(M)	parasitophorous vacuole membrane
qPCR	quantitative PCR
R	recycled line
3'RACE	3' rapid amplification of cDNA ends
RBC(M)	red blood cell (membrane)
RESA	ring-infected erythrocyte surface antigen
RFP	red fluorescent protein
RIPA buffer	radioimmunoprecipitation assay buffer
RPMI medium	Roswell Park Memorial Institute medium
RT	reverse transcriptase

S. japonicum	*Schistosoma japonicum*
SAS6	spindle assembly abnormal 6 homologue
SCHI	schizont-enriched sample
SEM	standard error of mean
SEP1	small exported protein 1
SERA	serine repeat antigen
*Sj*DF	*Schistosoma japonicum* dysferlin
SNAP-25	synaptosome-associated protein of 25 kDa
(Mid./Sal.gl.) spz	(Midgut/Salivary gland) sporozoite
SUB1	subtilisin-like protease 1
T. gondii	*Toxoplasma gondii*
T	transfer parasite population
TAE buffer	Tris-acetate-EDTA buffer
TM domain	transmembrane domain
UIS4	upregulated in sporozoites 4
UTR	untranslated region
V	vector
WT	wildtype
XA	xanthurenic acid

List of figures

List of tables

1 Introduction

1.1 The life cycle of *Plasmodium*

Plasmodium, the pathogenic single-celled protist causing malaria, alternates between the mammalian host and the mosquito vector in a complex life cycle with a number of intra- and extracellular stages (Fig. 1.1). The *Plasmodium* parasite was first reported as a live organism linked to the malaria fever in 1881. Interestingly, it was the process of exflagellation, the clearly distinguishable and unique event of rapid motility in the blood, that led to the discovery [1]. This drew attention to the causative agent of malaria and the whole life cycle was described in 1897 [2]. Both these contributions were awarded a Noble Prize in Physiology or Medicine in 1907.

1.1.1 Vector development

The mosquito vector is infected by ookinetes, tetraploid and motile invasive stages that develop in the mosquito midgut from a zygote several hours after infectious blood meal (Fig. 1.1). Ookinetes are extracellular stages, which leaves them vulnerable in the hostile environment of the mosquito midgut [3]. This, together with the fact that ookinete formation (unlike other invasive stages) is not preceded by a replicative stage, leads to significant reduction of the parasite numbers in this stage [4]. Ookinetes penetrate the mosquito wall using the perforin MAOP (membrane attack ookinete protein). In the membrane epithelium, ookinetes transmigrate several cells with the help of CelTOS (cell traversal protein for ookinetes and sporozoites) [5]. Eventually, ookinetes leave the epithelium and form an oocyst on its outer side, a perfectly round stage that can be observed already several days after the infectious blood meal (Fig. 1.1). Oocyst formation seems to be mainly dependent on laminin as ookinete-to-oocyst transformation proceeds in a laminin-supplemented Matrigel [6]. Inside the oocyst, syncytium with intense DNA replication is established. Subsequently, haploid sporozoites bud from sporoblast (syncytial lobes marked by the protein CSP (circumsporozoite protein)) in a complex process called sporogony [7]. Sporogony (a type of schizogony, discussed in chapter 1.1.3) is dependent on the organization of MTOC (microtubule organizing center) and the assembly of attached microtubules [8]. Mature sporozoites are curved with uneven microtubule distribution underneath their plasma membrane [9]. Motility of sporozoites precedes their release from the oocyst around day 14 post infection [10], but also proteins play a role in the release – SERA protease ECP1 [11], CSP [12] and others. After the release, sporozoites are passively carried through the mosquito body by the hemolymph and only recognition of salivary gland-specific molecules leads to their attachment [13]. The migration through the hemolymph leads to severe loss in parasite numbers, representing a second

bottleneck in the mosquito development [14]. Sporozoites migrate through acinar cells into the salivary gland duct [15], where they reside until the next blood meal.

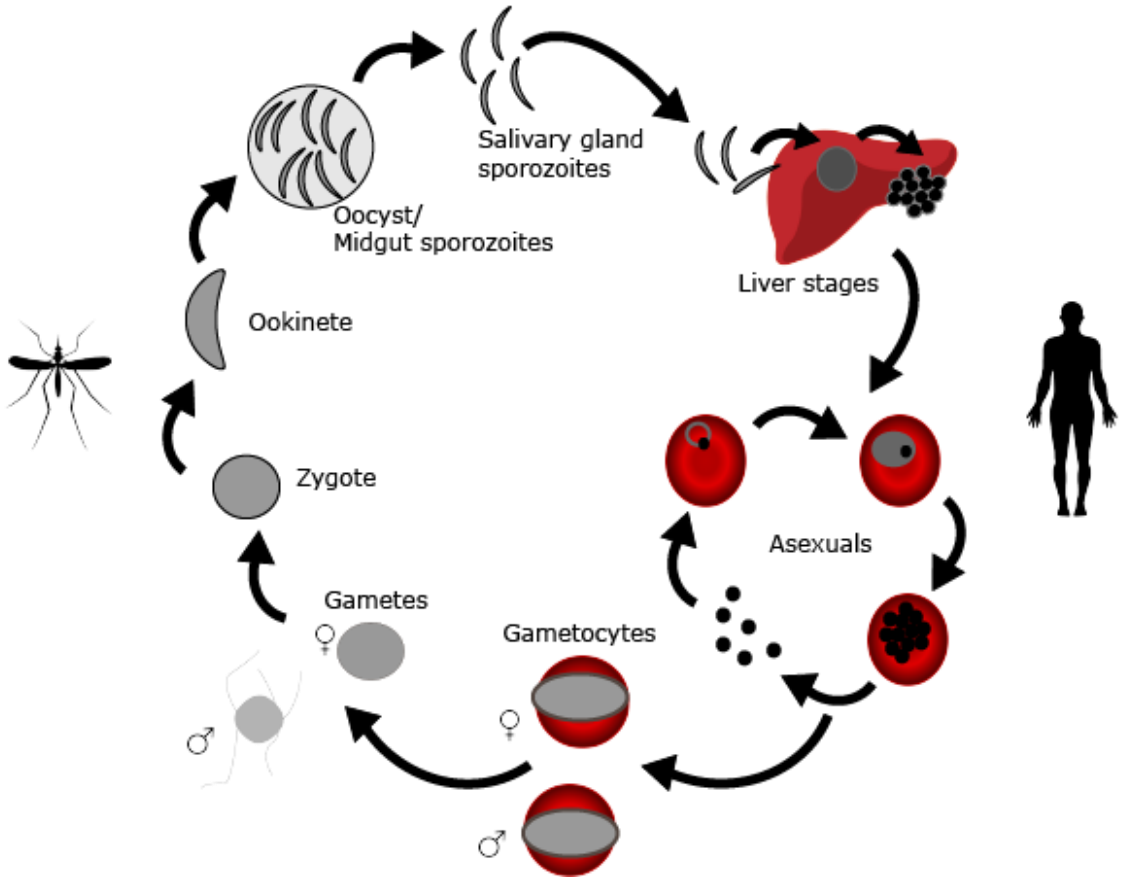

Figure 1.1 Life cycle of *Plasmodium*. The life cycle alternates between mammalian host (right side) and mosquito vector (left side) and includes a number of intracellular (liver stages, asexual blood stages – except merozoites, gametocytes) and extracellular (merozoites, gametes, zygotes, ookinetes, sporozoites) stages. Salivary gland sporozoites are injected into the human host during infectious blood meal. They use blood circulation to travel to the liver, where they establish the first replicative stage. After several days, thousands of merozoites are released into the blood stream, where they start the pathological asexual blood stage cycle (merozoites, rings, trophozoites and schizonts). Some parasites develop into gametocytes inside red blood cells and are transmitted to the mosquito vector during blood meal. Inside the mosquito midgut, gametocytes mature into fertilization-competent gametes and fuse to produce a zygote. Zygote differentiates into motile ookinete that penetrates the midgut wall and establishes an oocyst, in which replication followed by sporozoite budding takes place. Mature sporozoites travel through the mosquito haemocoel to the salivary glands, where they await the next blood meal.

1.1.2 Vector-to-host transmission

Sporozoites (Fig. 1.1) are passively transmitted to the host during blood meal. Experiments showed that despite general belief, sporozoites are not deposited directly into blood vessels, but instead into the host skin [16]. Interestingly, about half of the deposited sporozoites are left in the skin, about 20 % are taken up to local lymph nodes and only the rest glides in a corkscrew manner in search of a blood vessel [17].

1.1.3 Mammalian development

The first parasite destination is the liver, to which sporozoites are passively carried by the blood stream. Although the process is largely unclear, sporozoites recognize and cross the sinusoidal barrier, possibly via Kupfer cells, and enter hepatocytes [18]. After transmigrating through and killing several hepatocytes, the parasite finally establishes a protective parasitophorous vacuole (PV) [19] and settles in one cell [20]. Hidden from the immune system, the parasite develops for several days (around 2 days in a mouse, around a week in a human), eventually releasing large membranous assemblies of thousands of merozoites, called merosomes, into the blood stream [21–23]. Merosomes eventually rupture in small lung capillaries [22,23] and release the first generation of infectious merozoites. This stadium infects red blood cells (RBC) within minutes and extensively rearranges the cell to fit its needs. Blood asexual cycle is repeated every 48 hours with sequential development of ring stage, trophozoite stage, schizont stage and release of mature merozoites (Fig. 1.1). In some species, like the human *P. falciparum*, the blood cycle is synchronized, leading to massive synchronous releases of merozoites and causing periodical fevers to the host. *P. berghei* develops asynchronously in the blood stage. The asexual blood stage cycle is currently the only permissive stage for transgenesis [24], which excludes genes essential for this stage from the possibility of knock-out studies.

A typical feature of *Plasmodium* common to mosquito, liver and blood stages is the schizogony. Schizogony is a process of several DNA replications and mitoses without nuclear envelope breakage and cytokinesis [25]. This allows the parasite to produce tens (in the blood stage) or thousands (in the oocyst and liver stage) of new merozoites (merogony) or sporozoites (sporogony) with a single cytokinesis and to achieve extremely short doubling time.

The disease-causing blood stage is referred to as asexual stage to distinguish it from the subsequent sexual transmission stage, represented by gametocytes (Fig. 1.1). Male and female gametocytes form inside RBCs from sexually committed parasites. Although the process of sexual commitment is not completely clarified, recent findings shed light on the main switches. The decision to leave the asexual cycle and become sexually committed is triggered by external stimuli

[26] and mediated by epigenetic and transcriptional changes. In the first step, chromatin rearrangement leads to expression of Ap2-G [27–29], a gametocyte-specific plant-like transcription factor. This triggers a cascade that involves epigenetic rearrangements mediated by HDA2 (histone deacetylase 2) and HP1 (heterochromatin protein 1) [30,31]. Interestingly, the commitment to gametogenesis takes place in the schizont stage [32], leading to production of gametocytes from all the daughter merozoites. Already very early on, male- and female- specific markers can be detected, indicating that the sex determination takes place shortly after or at the time of commitment [33,34]. While male gametocytes are three times less abundant than females [35], their specialization is more pronounced as 36 % of their proteins are specific to the gametocyte stage (only 19 % in females) [36]. After formation, gametocytes remain developmentally silent in the mammalian host [37].

1.1.4 Host-to-vector transmission

Gametocytes are taken up by the mosquito during blood meal. In response to defined external stimuli in the mosquito midgut (drop in temperature of about five degrees [38], presence of xanthurenic acid (XA) [39]), calcium ions are released from the parasite's intracellular stores and trigger gametogenesis (calcium signalling in this process is further discussed in chapter 1.3.1). This developmental program yields fertile gametes, female (macro-) and motile male (micro-) gametes, which are capable of fertilization (Fig. 1.1).

Each female gametocyte develops into a single macrogamete. The macrogamete specifically represses translation of a large amount of proteins by mRNA-binding proteins DOZI and CITH [40,41]. Male gametocytes synthetize flagella and undergo mitosis in response to the calcium trigger [42], yielding eight flagellated microgametes. The flagella are supported by microtubules, assembly of which is regulated by PF16 and SAS6, followed by MAP2-mediated cytokinesis [43–46]. After mature microgametes are formed, they become motile and egress from the residual body with the help of actin II [47], MAP2 [44,46], PF16 [43] and many other factors discussed in chapter 1.1.4.1.

After fertile gametes are formed, microgametes actively move in search for their mating partners. Although no chemotaxis was reported in the process [48], in the restricted area of mosquito midgut microgametes and macrogametes encounter each other and fuse. Cellular fusion is followed by nuclear fusion and the formation of a zygote, the only diploid stage of the life cycle (Fig. 1.1). In the zygote stage, translational de-repression of mRNAs is mediated by CDPK1 [49]. Zygote undergoes DNA replication, differentiation and elongation, giving rise to the tetraploid, motile and invasive ookinete [50] (Fig. 1.1). Given the tetraploidy, it is not surprising that ookinetes

extensively regulate their transcription and, except for *de novo* transcribed genes, all genes are expressed from the maternal set [51].

1.1.4.1 Gametocyte egress

Gametogenesis of both sexes involves egress from the two membranes surrounding the gametocyte [26]; i.e. RBC membrane (RBCM) and PV membrane (PVM, delineating the intraerythrocytic niche of the parasite [19]) (Fig. 1.2). The sequence of RBCM and PVM disruption remained unclear for a long time with several models tested. It was first established for the egress of *P. falciparum* asexual blood stage that PVM rupture precedes RBCM rupture in so called inside-out model [52]. The same model was shown to hold true for *P. falciparum* gametocytes [53]. Only recently, a complete sequence of events confirming the inside-out model was reported for egress of *P. berghei* gametocytes [54]. While PVM rupture initiates in several sites, RBCM ruptures from one site only [53]. The egress of both *P. falciparum* and *P. berghei* gametocytes consists of similar sequence of events, namely swelling of the host cell followed by rupture and vacuolisation of the PVM and afterwards rupture of the RBCM and its vacuolisation take place (Fig. 1.2) [53,54]. Interestingly, similar events were identified in the egress of *P. falciparum* asexual blood stages [55]. The sequence of events in gametocyte egress seems to be more tightly regulated in *P. falciparum* [53] than in *P. berghei*, in which both male and female gametocytes show highly variable delays in between individual events [54].

Disruptions of both PVM and RBCM are dependent on proteases and exocytosis of secretory vesicles (Fig. 1.2), although different subsets are linked to each process [53]. The first reported vesicles that undergo exocytosis during egress were named osmiophilic bodies (OBs) due to their prominent staining in electron microscopy [56]. Although egress needs to be completed by male and female gametocytes alike, OBs defined by the marker protein G377 are only present in females [36,57,58]. Other gamete egress factors (MDV1/PEG3, GEST, PAT and MTRAP) were reported to localize to OBs but at the same time, both male and female gametocytes express these factors [59–61]. Additionally, perforin PPLP2 was reported to play a role in egress but to occupy egress vesicles distinct from OBs [62]. PPLP2 is the only molecule involved specifically in the lysis of RBCM reported to date [62,63]. Interestingly, in *P. berghei* its expression is restricted to male gametocytes, while in *P. falciparum* both sexes express the protein [62,63]. More proteins participating in egress were reported sex-specific in one *Plasmodium* species and sex-independent in another [57,58,62], suggesting that egress molecules have evolved to fulfil slightly different functions in different *Plasmodium* species.

Female OBs (Fig. 1.3. A and C) are defined by the protein G377, which plays a major role in their biogenesis in both *P. falciparum* [58] and *P. berghei* [57]. While in *P. falciparum* G377 also plays a role in egress and female gametocytes lacking the protein transmit less efficiently, this effect is much less prominent in *P. berghei*, where egress of macrogametes is only delayed in the absence of G377 with no impact on transmission [57]. While in both *P. falciparum* and *P. berghei*, G377 plays a role in biogenesis of female OBs, these roles differ. In *P. falciparum*, G377 absence leads to reduction of OB number, which explains the observed egress impairment [58]. In *P. berghei*, female OBs are formed in the absence of G377, however their shape and size is significantly reduced. MDV1/PEG3 (an egress molecule defining egress vesicles in both males and females) localizes to these reduced OBs, and they still react to induction of gametogenesis by relocalization to the cell periphery and exocytosis [57]. This differential role in OBs biogenesis between the two parasites explains why in the absence of G377, *P. falciparum* macrogametes egress less efficiently while *P. berghei* macrogametocytes egress is only delayed. Interestingly, no other molecule implicated in biogenesis of OBs was reported so far.

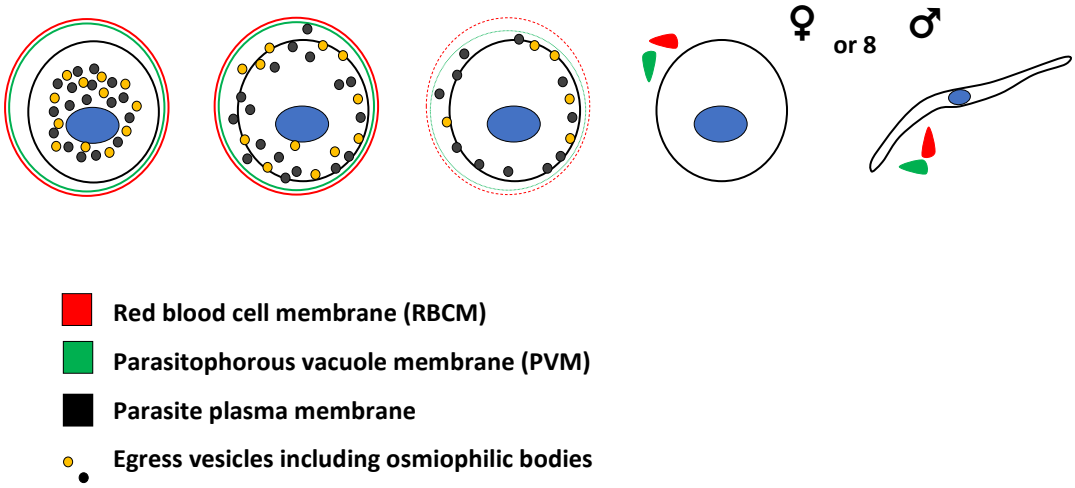

Figure 1.2 Gametocyte egress. Sequence of events (from left to right) leads from a mammal-resident gametocyte to a fully differentiated fertile gamete. In the mammalian host, gametocyte resides inside the RBC surrounded by PVM and RBCM and contains cytoplasmic egress vesicles. In reaction to the change of environment after transmission, the cell undergoes swelling, exocytosis of egress vesicles followed by permeabilization and rupture of PVM and RBCM. Remnants of membranes remain in the proximity of the egressed gametocyte. Female gametocyte only produces one gamete. Male gametocytes produce eight flagellated sperm-like gametes. Figure was kindly provided by Gunnar R. Mair and was adapted from Smith and Barillas-Mury, 2016 [197].

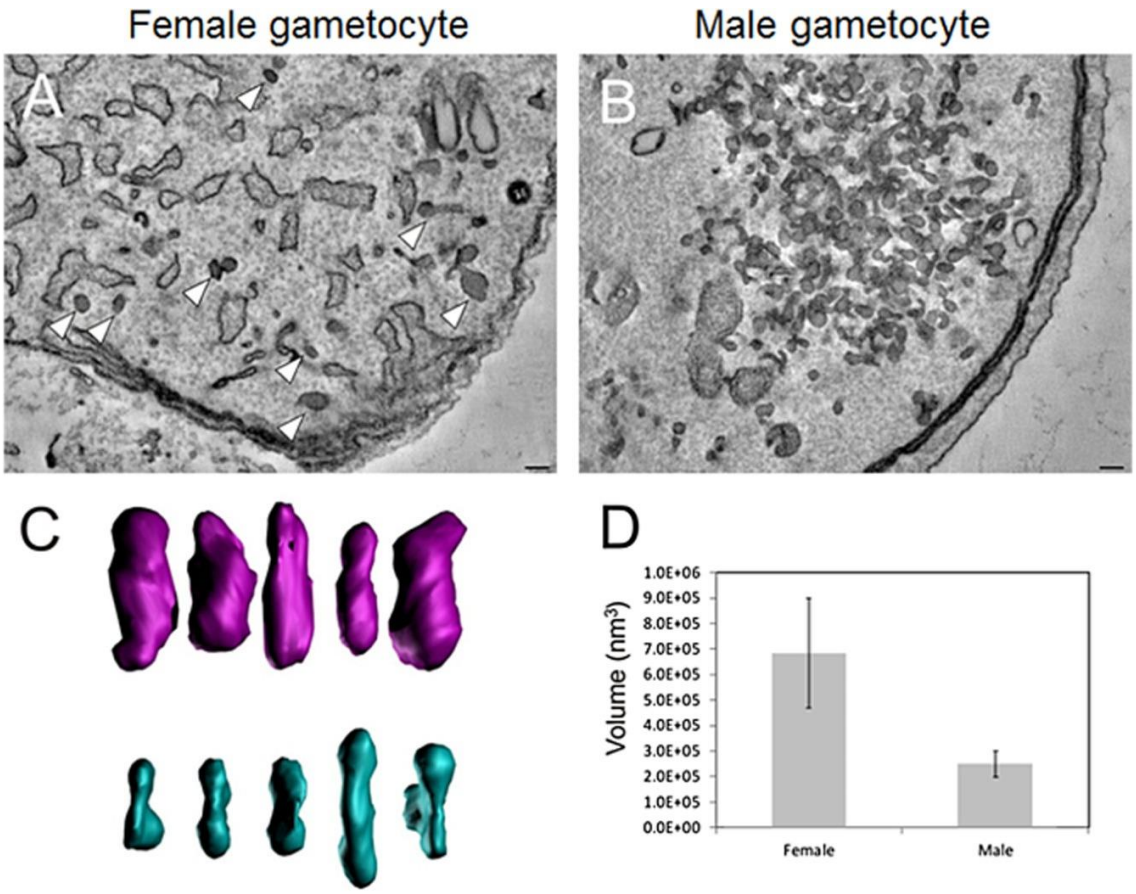

Figure 1.3 Male and female gametocytes harbour different OBs. Sections of female (**A**) and male (**B**) gametocytes from electron microscopy (5 nm thick, scale bar 100 nm) show difference in shape, size and localization pattern of male and female OBs. Electron tomograms visualizing OBs (**C**) show that female OBs (magenta, upper row) are bigger and different in shape compared to male OBs (cyan, lower row). Measurement of male and female OB volume from electron tomograms (**D**) confirms three-fold difference. Figure was published by Olivieri *et al.*, 2014 [57].

Male gametocytes do not express G377 in either *P. falciparum*, nor in *P. berghei* [57,58]. However, their egress is dependent on discharge of secretory vesicles as well. Several egress molecules (including MDV1/PEG3) define egress vesicles in both male and female gametocytes [57,59–61,64]. An electron microscopic study suggested that male gametocytes harbour so-called male OBs, vesicles different from female OBs in size, shape and exocytosis [57]. The comparison of MDV1/PEG3-positive vesicles showed that female OBs were oval, while male OBs were club shaped and three times smaller in volume compared to female OBs (Fig. 1.3). Gametocyte activation led to exocytosis of both male and female OBs, but their trafficking differed. While female OBs relocalized individually to the cell periphery and formed several foci underneath the

PVM, male OBs first formed clusters in the cytoplasm [57,65], but each vesicle remained intact. These clusters of individual vesicles were later transported to the cell periphery for exocytosis. While clustering of male OBs was induced by temperature drop, their exocytosis required additional stimuli [57]. Interestingly, all relocalization events were strongly dependent on calcium signalling as chelation of calcium prevented both the clustering of male OBs and relocalization of both male and female OBs to the cell periphery [57].

An additional difference between male and female OBs is the number of PVM lysis points. While female OBs fused with PVM in several foci [53,57], male OB clusters relocalized to the PVM and fused in one or very few spots [57] similarly to RBCM lysis [53]. This difference might be explained by the different nature of male and female gametes. While male gametes are defined by the formation of eight highly motile and vigorously beating flagella, which can easily emerge from the PVM through a single pore, female gametes do not exert any forces and lysis of PVM in several points might be necessary for the efficient disruption and removal of the membrane.

Male OBs were first defined by the presence of protein MDV1/PEG3, which colocalizes with G377 in females [57]. The absence of MDV1/PEG3 leads to severe impairment of egress of both sexes [61]. Similarly, a *P. berghei* specific protein GEST colocalizes with MDV1/PEG3 in both female and male OBs and its absence leads to impairment of egress from the PVM and RBCM [59]. MTRAP is another egress molecule that localizes to vesicles and is essential for gametocyte egress in both *P. berghei* and *P. falciparum* [64,66]. Interestingly, vesicles occupied by MTRAP, despite their clear secretory nature and role in egress, are not colocalizing with G377 nor with MDV1/PEG3 [64]. PPLP2 secretion is not impaired in parasites lacking MTRAP, indicating that the RBCM lysis is regulated independently of MTRAP [64]. PAT, a recently described essential egress factor, localizes to membranes of egress vesicles and partially colocalizes with both (male-specific) PPLP2 and (female-specific) G377, which indicates that PAT localizes to more than one subset of OBs.

Although MTRAP is indispensable for the egress to proceed, it occupies vesicles distinct from the originally defined OBs [64]. Similarly, PAT is necessary for egress but localizes to vesicles previously shown to localize to different cells (males and females) [60]. These studies together show that egress vesicles contain a range of different cargo combinations with yet unclear roles. Some proteins seem to occupy more subsets of these vesicles, e.g. MDV1/PEG3 or PAT [57,59–61]. This notion was supported by two high-throughput screenings analysing the proteome of gametocyte egress vesicles [66]. In this screening, proteins released to supernatant after gametocyte activation (when egress took place) were compared to a list of MDV1/PEG3 interaction partners (analysed using a BioID). The list of exocytosed proteins contained over eighty proteins, of which

about one fourth matched the list of MDV1/PEG3-interaction partners. This further confirms that MDV1/PEG3 likely localizes to several subsets of vesicles, as its interaction partners included proteins previously shown not to colocalize [62,64,66]. Previously reported gametocyte egress molecules as well as proteases SUB1 and the SERA family were found in the lists [66]. The drawback of the egressome approach is the absence of transmembrane proteins, which remain associated with the parasite membrane after discharge of egress vesicles and cannot be detected in the supernatant. This is the reason why PAT colocalization with PPLP2 and G377 could not be verified [66].

1.2 Egress of Apicomplexans

Apicomplexan parasites spend most of their life cycle hidden inside host cells, with the need to periodically egress. Apicomplexan egress is underlined by host cell lysis with severe effect on the host organism [67] as shown by periodical fevers caused by synchronized egress of *P. falciparum* merozoites. Egress is mediated by apical complex, a cytoskeletal structure bound to secretory vesicles typical for apicomplexans [67]. *Plasmodium, Toxoplasma* and other organisms from the phylum contain a number of secretory vesicles, discharge of which is typically calcium-dependent (Fig. 1.4). Calcium signalling either triggers vesicular trafficking or directly induces exocytosis [67]. While some vesicles play a role in both invasion and egress (micronemes), others are specific for one step only (rhoptries and dense granules for invasion and exonemes for egress) [68]. Exonemes are the critical secretory organelles for *Plasmodium* asexual blood stage egress since they carry the necessary protease SUB1. Calcium-dependent discharge of SUB1 into the PV and its activation by calcium ions leads to activation of SERA proteases, which cleave a number of substrates and trigger the egress cascade [69].

Egress from the host cell is taking place in three stages within the *Plasmodium* life cycle, namely the asexual blood stage, sexual blood stage and liver stage (Fig. 1.5). The three processes are generally considered different as involved players were often identified in just one life-cycle stage. On the other hand, several common features can be found, among others the involvement of secretory vesicles, proteases and calcium signalling. One feature common to all three egressing stages is the inside-out model discussed in chapter 1.1.4.1. In all stages, PVM rupture precedes the host cell membrane rupture (Fig. 1.5) [21,53,70]. Only the liver stage resides in a metabolically active cell, PVM rupture is followed by the death of the host hepatocyte and its detachment from the tissue (Fig. 1.5) [23,71]. This cell death is different from apoptosis or necrosis as the cell membrane remains intact and DNA is not processed [23]. All three stages that egress are furthermore characterized by a sharp increase of calcium levels [72–74] and some common

players such as proteases from the SERA family, SUB1, falcipain-1/berghepain-1, plasmepsins IX and X [52,53,66,69,74–81]).

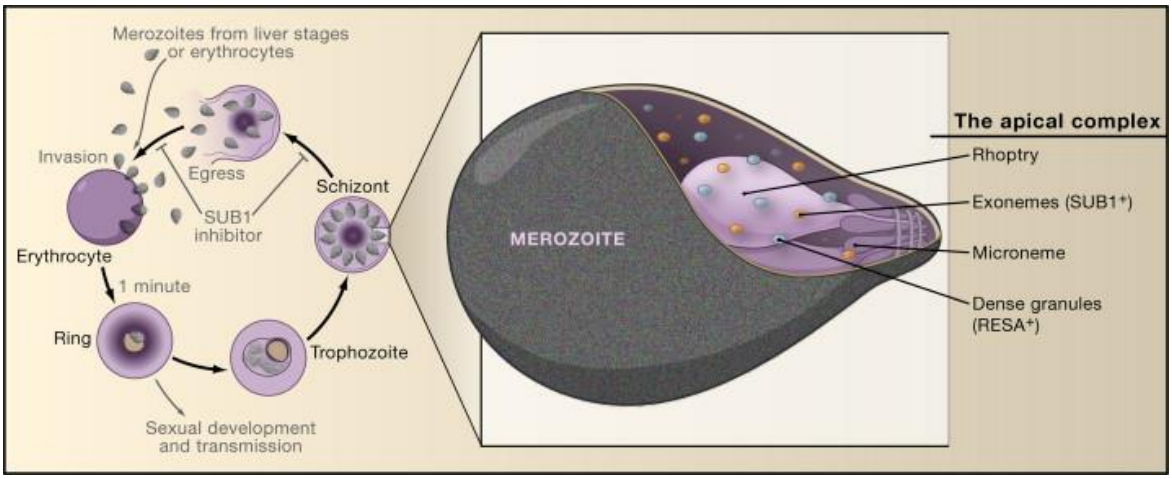

Figure 1.4 Secretory organelles of *Plasmodium*. The asexual blood stage cycle includes release of mature merozoites from the RBC (egress) and their invasion into new ones. These processes depend on parasite organelles that discharge their content calcium-dependently with a precise timing. Organelles necessary for merozoite egress are micronemes and exonemes (that contain SUB1). Organelles necessary for merozoite invasion include rhoptries, micronemes and dense granules (that contain the protein RESA). Figure was published by Janse and Waters, 2007 [198].

The evolutionary conservation of molecular processes in egress can be demonstrated on the comparison of *Plasmodium* and *Toxoplasma*, related apicomplexan parasites, with very distinct life cycles but some common molecular processes. Screening of egress-deficient mutants of *Toxoplasma* led to a discovery of DOC2, a C2 domain containing protein. The egress defect caused by DOC2 mutation was further characterized as micronemal secretion impairment, a process critically dependent on calcium signalling [82]. In *Plasmodium*, the link between calcium signalling and exocytosis of micronemes and exonemes and subsequent egress is not known. Based on the example of C2 domain-regulated egress in *Toxoplasma*, it was suggested that calcium trigger could be sensed by a C2 domain containing protein [67]. Although *Plasmodium* encodes the DOC2 protein, its depletion did not result in egress impairment, but instead inhibited invasion [82]. This phenotype can be explained by the differences in micronemal populations between *Plasmodium* and *Toxoplasma*. While *Toxoplasma* contains just one type of micronemes, necessary for both invasion and egress [83], *Plasmodium* uses for both events a separate type of micronemes [84]. This leaves the possibility that another C2-domain containing protein is involved in egress of *Plasmodium* asexual blood stages still open.

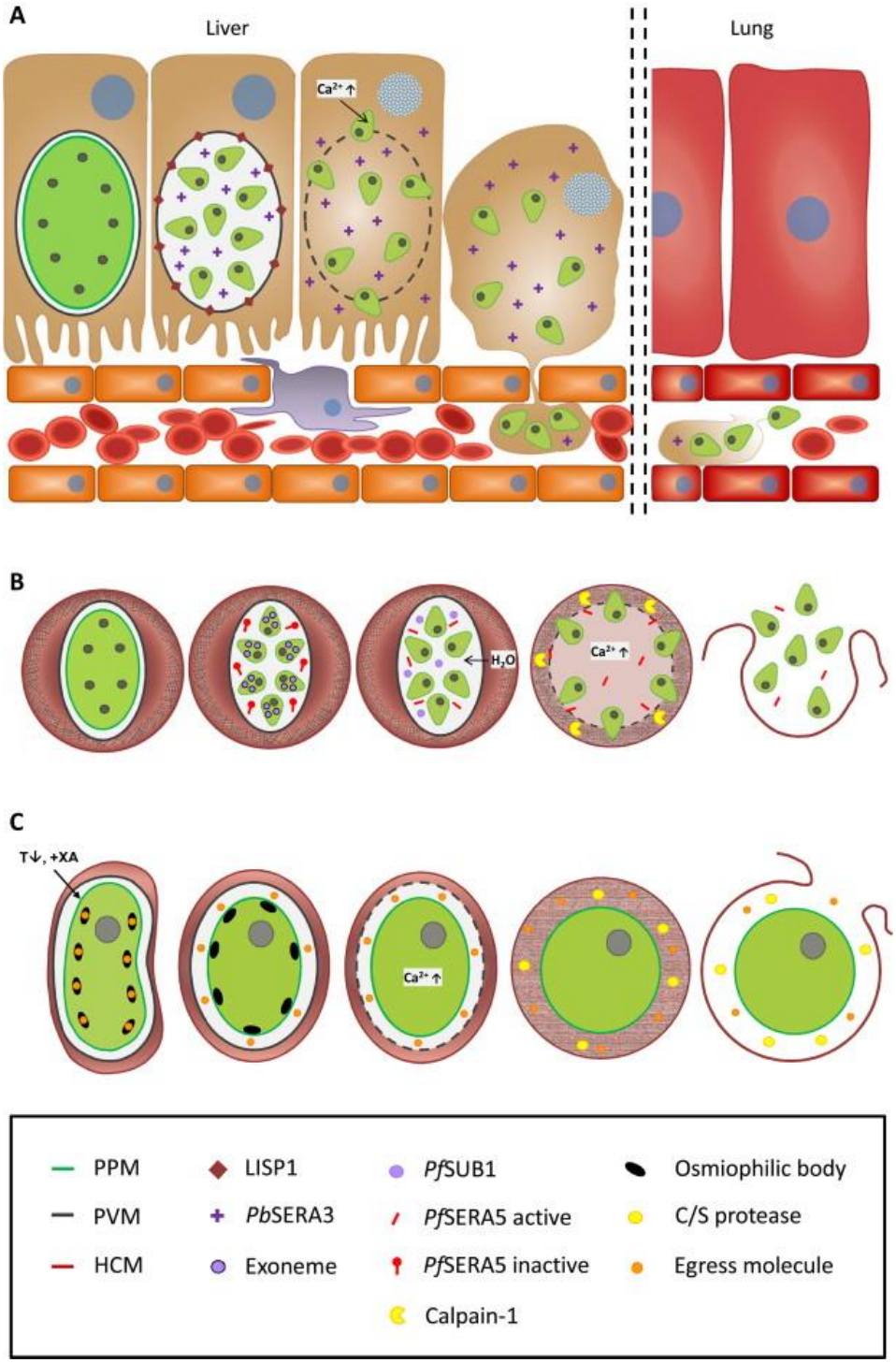

Figure 1.5 Egress of *Plasmodium* liver, asexual blood and sexual blood stages. Despite clear differences, egress of liver stages (A), asexual blood stages (B) and gametocytes (C) share common features. For example: parasitophorous vacuole membrane (PVM) always ruptures before the host cell membrane (HCM), egress vesicles are discharged, calcium ions and proteases are involved in the process, cells swell before the egress. PPM = parasite plasma membrane. Figure was published by Wirth and Pradel, 2010 [199].

1.3 Calcium signalling in *Plasmodium*

Signalling via the second messenger Ca^{2+} is in molecular terms a conserved pathway in eukaryotes [85]. *Plasmodium* heavily relies on calcium signalling, with some typical eukaryotic pathways missing and some additional unique pathways involved. A large number of pathways is regulated by calcium during the complex *Plasmodium* life cycle – e.g. invasion, egress, secretion, motility or cell cycle (Fig. 1.6) [42].

Calcium regulation is challenging for the *Plasmodium* parasite due to very different calcium levels in its host environments – invasive stages in the mammalian host (i.e. sporozoites and merozoites) are transiently present in blood, an environment very rich in calcium. On the other hand, cell-resident stages (liver trophozoites and schizonts and blood rings, trophozoites and schizonts) are exposed to a very low concentration of calcium. The parasite stores calcium ions in the endoplasmic reticulum [86], mitochondria [87,88], acidocalcisomes [89] and partially in the food vacuole [86]. Two types of calcium-binding domains can be found in Plasmodial proteins: EF hands that are present in calcium-dependent protein kinases (CDPKs) [90] and other proteins, and less abundant C2 domains [91], present for example in PI-PLC or in ferlin proteins. The complexity of calcium signalling and homeostasis in the parasite is far from being fully understood. One of the reasons for that is the small size of the parasite, hindering detailed analysis of calcium sources. Another challenge is the fact that analysis of calcium homeostasis and signalling typically relies on the use of inhibitors. *Plasmodium* with a large number of unknown proteins and evolutionary quite distinct targets represents a huge risk of off-targeting of inhibitors needed for the calcium study [42].

Upstream of the calcium release into the parasite cytosol is the cGMP-dependent protein kinase (PKG) pathway activated by cGMP and triggered by various and usually unknown stimuli (Fig. 1.6). PKG can trigger calcium release directly or by phosphoinositide-specific phospholipase C (PI-PLC)-induced production of inositol-triphosphate (IP_3) [92,93], which opens calcium channels on endoplasmic reticulum. A typical feature of calcium signalling in *Plasmodium* are the plant-specific CDPKs [94]. *Plasmodium* encodes seven CDPKs with functions in different stages of the life cycle. CDPKs represent promising potential drug targets due to their critical roles in several stages and a complete absence of similar genes from the mammalian genome.

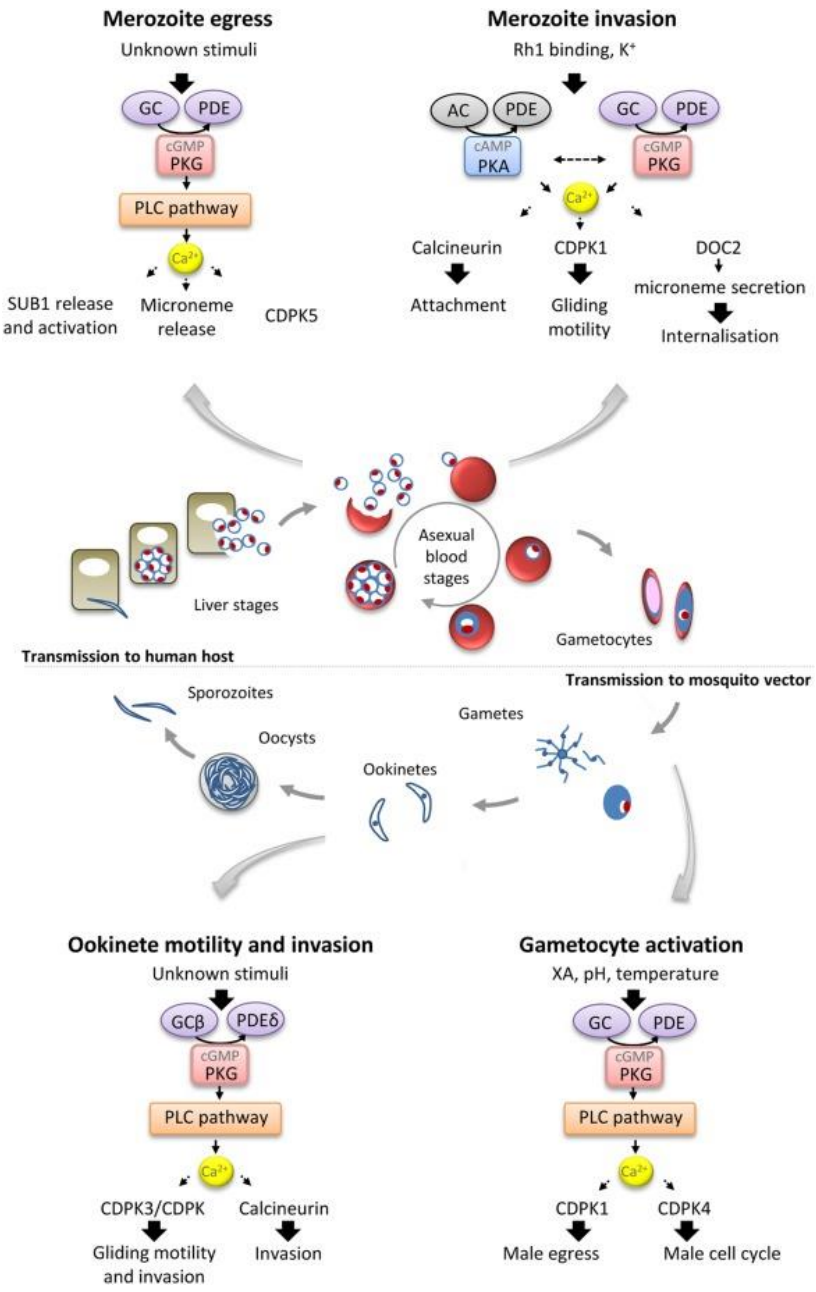

Figure 1.6 Selected calcium-regulated pathways in *Plasmodium* life cycle. In response to different stimuli, cGMP is produced and activates PKG. This pathway induces calcium release from internal stores. The Ca^{2+} second messenger acts in merozoite invasion (attachment and micronemal secretion), merozoite egress (micronemal and exonemal secretion, activation of SUB1), gametocyte activation (assembly of flagella, egress), ookinete motility and others. GC = guanylyl cyclase, PDE = phosphodiesterase. Figure was published by Brochet and Billker, 2016 [42].

Extracellular source of calcium is necessary only for the invasion of merozoites (Fig. 1.6) [95] and subsequent development of the asexual stages [96,97]. Other pathways depend on intracellular

stores of calcium as shown by chelation experiments with membrane-permeable and -impermeable chelators [42]. During invasion, calcium signalling induces the discharge of rhoptries [95], which induces calcium peak inside the erythrocyte to be invaded. Interestingly, melatonin induces a calcium peak in the parasite cytosol [98], which initiated speculations on involvement of this pathway in parasite synchronization during the asexual blood cycle observed in some *Plasmodium* species.

Another pathway critically dependent on calcium is the merozoite egress (Fig. 1.6) [97]. Unknown trigger leads to the universal pathway of PKG-mediated release of calcium ions [99] and subsequently to microneme release, exoneme release and CDPK5 activation [100,101]. Calcium is also necessary for SUB1 activation after its release from exonemes into the PV [102]. Interestingly, CDPK5 is also necessary for merozoite egress, but its function is independent on exonemal secretion [101].

Ookinete gliding requires high concentration of intracellular calcium (Fig. 1.6) [99], which triggers CDPK3 and calcineurin [99,103]. CDPK3 acts in attachment to the midgut epithelium and motility of the ookinete [104,105]. Sporozoite activation by serum leads to sharp peak of calcium, which transforms into oscillating peaks later on [106] and mediates motility. Hepatocyte invasion depends on calcium, which activates calcineurin [103]. During the liver development [107], similarly to blood stage development [97], calcium concentration in the parasite cytoplasm gradually rises, with the need for calcium-activated SUB1 for merozoite egress from the liver cells [80,108].

1.3.1 Calcium signalling in host-to-vector transmission

Gametogenesis, taking place after host-to-vector transmission, is critically dependent on calcium (Fig. 1.6). The trigger is represented by the environmental changes between mammalian host and the mosquito vector. The environment is sensed by the parasite by two particular features, drop in temperature by at least five degrees [38] and the presence of a mosquito specific molecule, XA [39]. XA induces GC that produces cGMP [109,110], which in turn activates PKG [109]. Afterwards PI-PLC produces IP3 [92,93], which mediates opening of calcium channels on endoplasmic reticulum and leads to a sharp increase of intracellular calcium after a lag phase of about 30 seconds after the initial trigger [73]. This triggers several pathways, including the male-specific CDPK4 pathway inducing the synthesis of flagella and cell cycle regulation [73], the CDPK1 pathway involved in changes in gene expression [49] and the discharge of egress vesicles [49] (Fig. 1.6).

Despite the clear calcium-dependent nature of gamete maturation [73,111], the known and putative gamete egress molecules lack calcium binding domains and the calcium-dependent factor linking these two events remains unclear. CDPK1 has been the only calcium-dependent egress factor suggested to date (Fig. 1.6) [42,49]. However, its depletion leads only to a delay of egress and after few minutes of active flagellar beating within the host RBC, free microgametes lacking CDPK1 eventually emerge [49]. This suggests that egress can be mediated in the absence of CDKP1 function.

1.4 The Ferlin protein family

Calcium ions regulate, among many others, the function of ferlins, proteins that contain the largest number of C2 domains. The ferlin protein family is conserved in most eukaryotes with the exception of plants or fungi [112]. Their important role in secretory pathways remained elusive for a long time, likely due to their absence in the yeast genome [113], which served as the main model organism for secretory pathways.

1.4.1 Topology and common features

The typical feature of ferlins is their domain composition (Fig 1.7 C). These proteins contain the largest number of C2 domain (four two seven) of all protein families, typically labelled with letters (C2A – C2F). C2 domain is a well described structural unit formed by beta sheets with negatively charged calcium binding pockets (Fig. 1.7 A and B) [91]. It remains unclear why proteins encode more than one C2 domain, but a tandem role of the domains is anticipated. Some C2 domains have lost their ability to bind calcium, indicating that their role is probably extended beyond this basic function. Although the main structural features are common between C2 domains, the sequence variability is significant and details like exact localization of the calcium binding pockets cannot be predicted from comparisons of individual sequences (Fig. 1.7 A and B) [114].

Ferlins additionally harbor a C-terminal transmembrane domain, which localizes them to membranes, often vesicles (Fig. 1.7C, 1.8). In many cases, ferlins contain a Fer domain – a ferlin specific motif of unknown function [115]. Several Fer domains (FerA, FerB and FerI) can be distinguished in ferlins and they are typically placed between the first and second C2 domains (C2A and C2B), forming a tandem structure (Fig 1.7 C and 1.10 A) [113]. Ferlin proteins can be divided into type I and II based on the presence or absence of dysferlin domain (DysF) of unknown function. In general, invertebrates encode two ferlins, one type I and one type II. In vertebrates the family expanded to three type I and three type II members, indicating the conservation of two functional clusters of ferlins [113]. Interestingly, the C2 domains in ferlins show more evolutionary

conservation between ferlin homologues than between the individual domains in one protein. In general, the C-terminal (C2E and C2F) domains are highly conserved, while N-terminal domains show more variability [113]. N-terminal C2A domain plays the major functional role in many ferlins, explaining its evolutionary variability underlined by adjusting to specific functions.

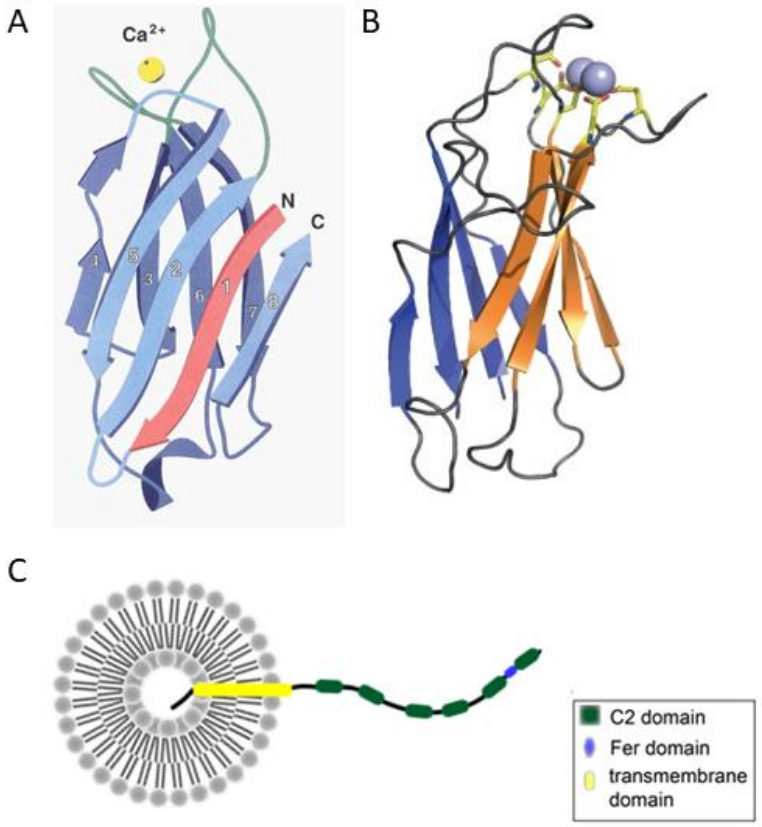

Figure 1.7 Schematic of C2 domains and ferlin insertion into membranes. C2 domain is an independent structural unit formed by beta sheets and connecting loops. Ribbon diagram of synaptotagmin I C2A domain (A) shows the typical structure of the C2 domain with calcium binding pocket located in one of the top loops. Ribbon diagram of myoferlin C2A domain (B) shows that main features are conserved and calcium is coordinated in the top loop, but overall the structure differs from (A). Ferlins are typically embedded in membranes (often vesicular) via their single C-terminal transmembrane domain. The short C-terminal part is facing the lumen of vesicle, while the major N-terminal portion (with C2 domains, DysF and Fer domains) faces the cytosol (C). Figures in (A) and (B) were published by Nalefski and Falke, 1996 [91] and Lek *et al.*, 2012 [151], respectively.

Calcium dependency of ferlin function has been shown for all proteins analysed [112,116–120]. Mutations hindering ferlin function localize mostly to their C2 domains and lead to insensitivity to

calcium [116,118]. Manipulation of calcium levels helped establish the dependency on calcium in many ferlins, although the exact mechanism by which calcium coordination into negatively charged pockets in the C2 domains (Fig. 1.7 A and B) mediates ferlin function is not clear. Two lines of evidence can be found in the literature, originating from *in vitro* biochemical studies with recombinant proteins. Some ferlin C2 domains were shown to bind phospholipids more efficiently in the presence of calcium [118]. This could explain why ferlin-mediated exocytosis only happens in the presence of calcium signaling. Another set of biochemical experiments with otoferlin C2 domains showed that these domains show high affinity for each other in the absence of calcium, while this affinity is lost in the presence of calcium [119]. This observation led the authors to propose a model, in which otoferlin (and perhaps other ferlins) resides in a closed conformation in the absence of calcium and only upon calcium signaling, its conformation opens (as C2 domains lose affinity for each other) and triggers vesicle exocytosis.

1.4.2 Mammalian ferlins

Mammalian ferlins are in the focus of active research as mutations in these genes lead to deafness (mutation of otoferlin, [121]) or muscular dystrophy (mutation of dysferlin [122]) in humans. Humans encode six ferlin genes distinguished by tissue-specific expression and by functions.

Inner ear hair cells, the whole vestibular system and cochlea and the brain express otoferlin [123]. Otoferlin binds syntaxin-1 and SNAP-25 in a calcium-dependent manner [124], this pathway is activated by synaptotagmins in other synapses and leads to neurotransmitter release. The inner hair cells lack expression of synaptotagmins and it seems that otoferlin has taken over the calcium-dependent regulation of neurotransmitter vesicle fusion [121]. Indeed, mice lacking otoferlin show profound deafness and impairment of synaptic vesicle exocytosis, despite their normal biogenesis and docking [125]. Although the deletion of otoferlin, unlike other genes involved in the neurostimulation in hearing, is not lethal, its absence leads to impaired neurotransmitter signaling and deafness. Instead of amplitudinal release copying the peaks of calcium concentration, in the absence of otoferlin, neurotransmitter is released slowly and regardless of stimulation [126]. In agreement with that, most otoferlin C2 domains bind lipids calcium-dependently and can induce membrane aggregation *in vitro*. Also, parts of the protein can accelerate SNARE-dependent membrane fusion *in vitro* but only in the presence of high calcium levels [127]. Interestingly, otoferlin seems to play an additional role in the recycling of synaptic vesicles [126]. A point mutation in the C2F domain, unlike the absence of otoferlin, leads to no impairment in synaptic exocytosis amplitudes. However, the mice bearing this mutation are still profoundly deaf. Closer examination revealed that synaptic vesicles are not efficiently

replenished, leaving the synapse unable to sustain signaling with high frequency amplitude [126]. This finding is further supported by otoferlin interaction with myosin VI [125,128] and Rab8a [129], which could mediate recycling of vesicles after exocytosis. The question remains, why the synaptotagmin regulation mediating neurotransmitter release in most synapses is replaced by otoferlin in the inner hair cells. One explanation might be the need for extremely high frequency of neurotransmitter release needed for the hearing. An estimate calculated that given the frequency of stimulation, in each synapse the synaptic vesicles need to be replenished up to 70 times per second. Such high frequency is beyond the rates reported for synapses without otoferlin [124].

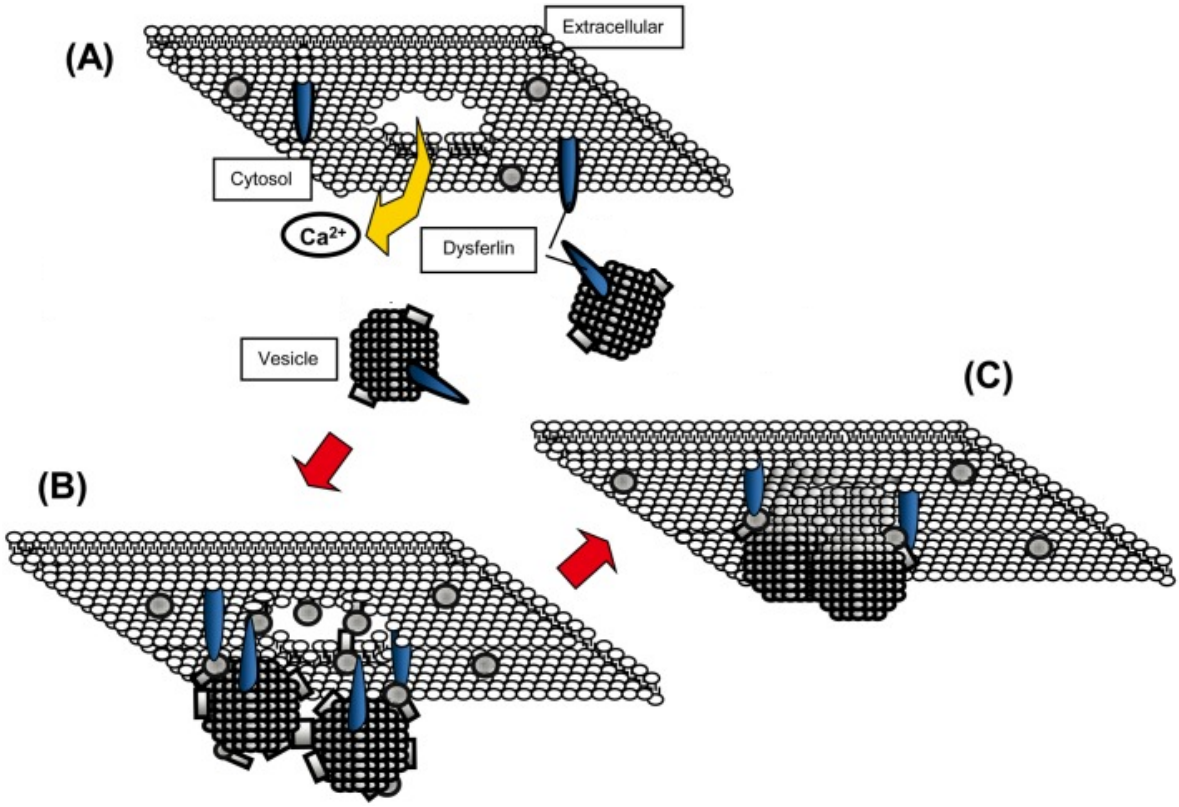

Figure 1.8 Mode of action of dysferlin. Membrane damage induces calcium ions transport from the extracellular environment into cytosol (A). This induces dysferlin-decorated vesicles to interact with annexins and SNARE proteins (B, not shown). Vesicles subsequently fuse with each other and the plasma membrane (C). The formed membrane patch reseals the membrane rupture. Figure was published by Kobayashi *et al.*, 2012 [187].

Two ferlin genes, dysferlin and myoferlin, are expressed ubiquitously [123]. However, their expression is highly enhanced in muscle tissue, heart tissue and placenta [122,130]. Although both proteins play a role in muscle membrane trafficking, their functions are strictly separated.

Myoferlin is important for myoblast fusion to myotubes with enriched abundance at the site of fusion [131] and hence is expressed mainly during muscle development [130,131] and partially after muscle injury and during regeneration [132]. Dysferlin is expressed after the development is finished, it localizes to plasma membrane and after membrane injuries, it relozalizes to cytoplasmic vesicles and reseals membrane ruptures (Fig. 1.8) [132,133]. Similarly overlapping but specialized roles are played by the two proteins in the placenta, with dysferlin expression peaking at fusion of placental syncytium [134]. Dysferlin was shown to interact with caveolin 3 [135] and calpain-3 [136]. Its absence leads to increased damage in skeletal muscles, similar to the one caused by absence of calcium, in mice. This further links dysferlin to calcium-mediated membrane repair in the muscle tissue (Fig. 1.8) [122,132,137–139]. Interestingly, in the dysferlin-deficient muscle, myoferlin is not upregulated, indicating no mutual redundancy between individual human ferlins [140]. Myoferlin, expressed mainly during the development of muscle tissue, is necessary for vesicular trafficking with highly reduced clathrin- and caveolin-dependent endocytosis, transferrin recycling [141] and impaired VEGF signaling in myoferlin-deficient cells. Trafficking of several growth factors (VEGF [142,143], IGFR [144] and others [145]) were linked to myoferlin and dysferlin, which along with their upregulation in several cancerous tissues [146–148] led to an increasing attention to their role in cancer.

However, very little was reported so far about the three remaining mammalian ferlins, Fer1L4, Fer1L5 and Fer1L6. Fer1L4 transcripts were detected predominantly in the stomach, but annotated as non-protein coding RNA (NCBI gene 80307) [123]. Fer1L5 is expressed in pancreas [123] and the developing muscle tissue with some indications for roles in myotube fusion, temporally preceding the role of myoferlin [113]. Fer1L6 expression was detected in the heart, kidney and stomach [123]. While Fer1L5 is quite similar to myoferlin, Fer1L4 and Fer1L6 are more similar to otoferlin [149]. Electronic databases of cDNA suggest alternative splicing for Fer1L4, Fer1L5 and Fer1L6 [149].

Some ferlins were reported to interact with SNARE proteins [119] and in general their function is considered similar to synaptotagmin function, replacing them in tissues where synaptotagmins are not expressed. However, in knock-out studies, otoferlin deficiency could not be rescued by synaptotagmin presence and vice versa [150]. Similarly to that, individual mammalian ferlins cannot compensate for each other's absence [151], which indicates high degree of specialization of individual proteins. Unlike synaptotagmins, ferlins serve as protein scaffold [120]. For example, dysferlin, additionally to vesicular fusion, mediates protein trafficking by recruitment of large protein complexes [152]. Interestingly, while this is not the case in *C. elegans* (discussed in chapter

1.4.3) [153], mammalian ferlins are implicated in vesicle docking and priming prior to fusion [124,154], a feature distinct from synaptotagmins.

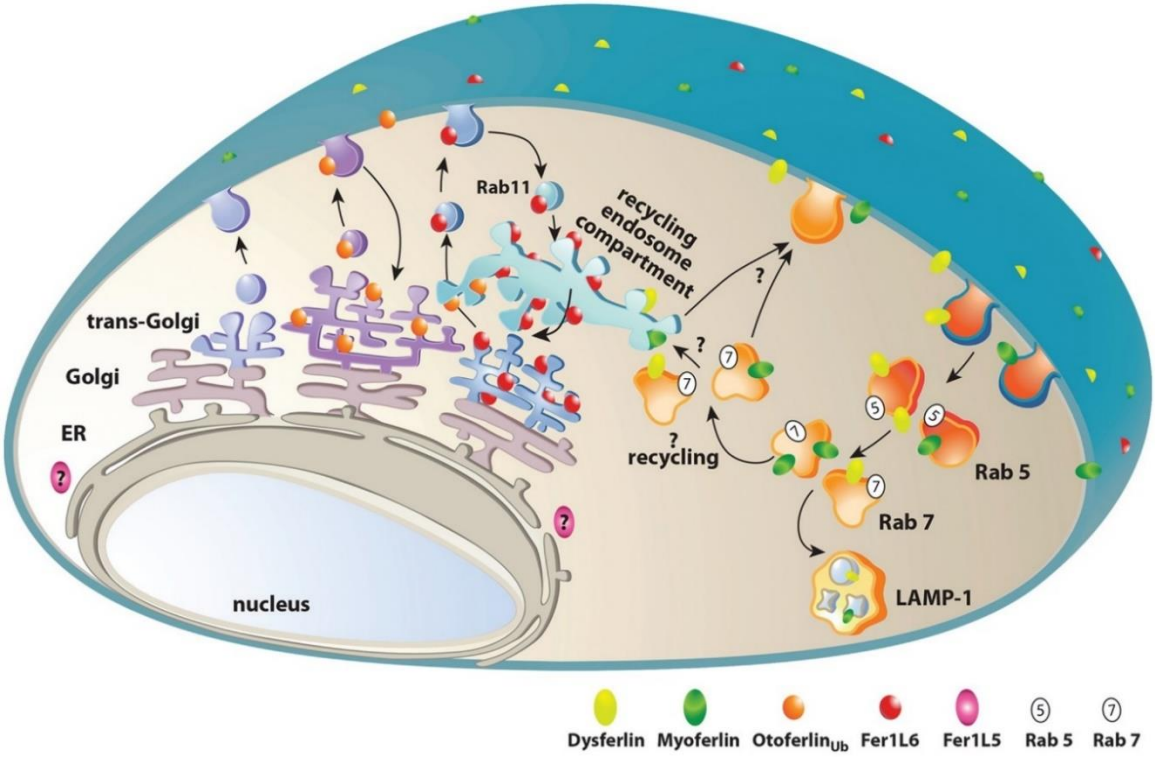

Figure 1.9 Model of human ferlins trafficking. Dysferlin (yellow) and myoferlin (green) are detected on the plasma membrane and in endosomal pathways, accumulating in Rab7-positive late endosomes. Otoferlin (orange) is detected in trans Golgi and very transiently on the plasma membrane. Fer1L6 is detected in trans Golgi, from where it recycles via Rab11-positive vesicles and it accumulates in the recycling endosome. Fer1L5 (magenta) is detected inside of the cell near the endoplasmic reticulum but the precise localization is not clear. Figure was published by Redpath *et al.*, 2016 [123].

The presence of DysF domain divides ferlins into type I and II. Type I (with dysferlin domain) in mammals is represented by dysferlin, myoferlin and Fer1L5, while otoferlin, Fer1L4 and Fer1L6 belong to the type II (without dysferlin domain). A complex study analysed several cell lines transfected with five human ferlins (leaving out the Fer1L4 pseudogene) tagged with small C-terminal tags [123]. Localization of individual tagged proteins along with their dynamics gave rise to a complex model of human ferlin pathways (Fig. 1.9). Interestingly, ferlins clustered into two groups distinguished by the presence of DysF domain – type I ferlins (myoferlin, dysferlin and Fer1L5) localized predominantly to plasma membrane and endosomes, while type II ferlins (otoferlin and Fer1L6) were found in trans-Golgi and recycling pathways. Myoferlin and dysferlin

colocalized with Rab7 in late endosomes, which together with evidence from other studies [145,155] indicates their role in transit of cargo through endosomes to lysosomes. Otoferlin and Fer1L6 localize to trans-Golgi and recycling networks, colocalizing with Rab11 and other markers of this compartment. Otoferlin additionally showed weak plasma membrane staining, which might suggest its transient residence in the membrane in between closely coupled exocytosis-endocytosis cycles. Fer1L5 appeared to localize to the endoplasmic reticulum but did not colocalize with ER markers calreticulin or calnexin [123].

1.4.3 Invertebrate ferlins

The first protein of the ferlin family was identified in the invertebrate *Caenorhabditis elegans* and named fertility factor 1 (Fer-1) as it acts in the process of spermatogenesis [153]. The protein was found in the testis tissue and is therefore male specific. When Fer-1 is mutated, sperm cells arrest in their development. In particular, membranous organelles (MO), vesicles filled with glycoproteins that need to fuse within the process of sperm development, do not fuse with the membrane and the worm is not fertile. As was shown later, MO are indeed decorated by Fer-1 with most of the protein facing the cytosol of the cell, a feature similar to SNARE proteins [112,153]. Also, Fer-1 function is calcium-dependent as shown by calcium chelation experiments [112]. Interestingly, most mutations interfering with Fer-1 function localize to C2 domains, further emphasizing their critical role in ferlin function [112]. Fer-1, apart from its role in fertility, is weakly expressed in the worm muscle. Mutation in Fer-1 additionally causes a mild impairment in total muscle power in the worm [156]. This is partially reminiscent of the roles of myoferlin and dysferlin in mammals (chapter 1.4.2).

Another invertebrate ferlin, the misfire protein from *Drosophila melanogaster*, also plays an essential role in fertility [157]. In the case of misfire, expression was detected both in testis and ovaries, with different splicing variants expressed in each tissue. However, only the longest transcript expressed in the testis was shown to be essential for *D. melanogaster* fertility, depletion in ovaries did not result in a phenotype. Misfire protein was linked to plasma membrane breakdown during the process of insemination [157]. This sterility is, similarly to the case of *C. elegans* [153], linked to a calcium-mediated fusion of membranous structures with the sperm membrane, as acrosome discharge necessary for plasma membrane breakdown is dependent on calcium signalling [158].

Not many non-mammalian ferlins were studied so far. One more example is a sea urchin ferlin, which is needed for exocytosis in wound repair. Interestingly, this ferlin is highly similar to dysferlin, as human dysferlin could compensate for the function in sea urchin [117,159]. This is an

unusual aspect, as human ferlins cannot complement each other [151]. *Schistosoma japonicum* expresses a ferlin gene similar to dysferlin, named *S. japonicum* dysferlin (*Sj*DF). The protein localizes to tegument, a partially liquid host-parasite interface layer. After knock-down of *Sj*DF by siRNA, worms showed reduced capacity to recover the tegument after injury. This suggests that the dysferlin role in membrane repair after injury is conserved in very ancient eukaryotes. The authors further considered *Sj*DF as an immune target for potential intervention strategies based on its high immunogenicity in mice [160].

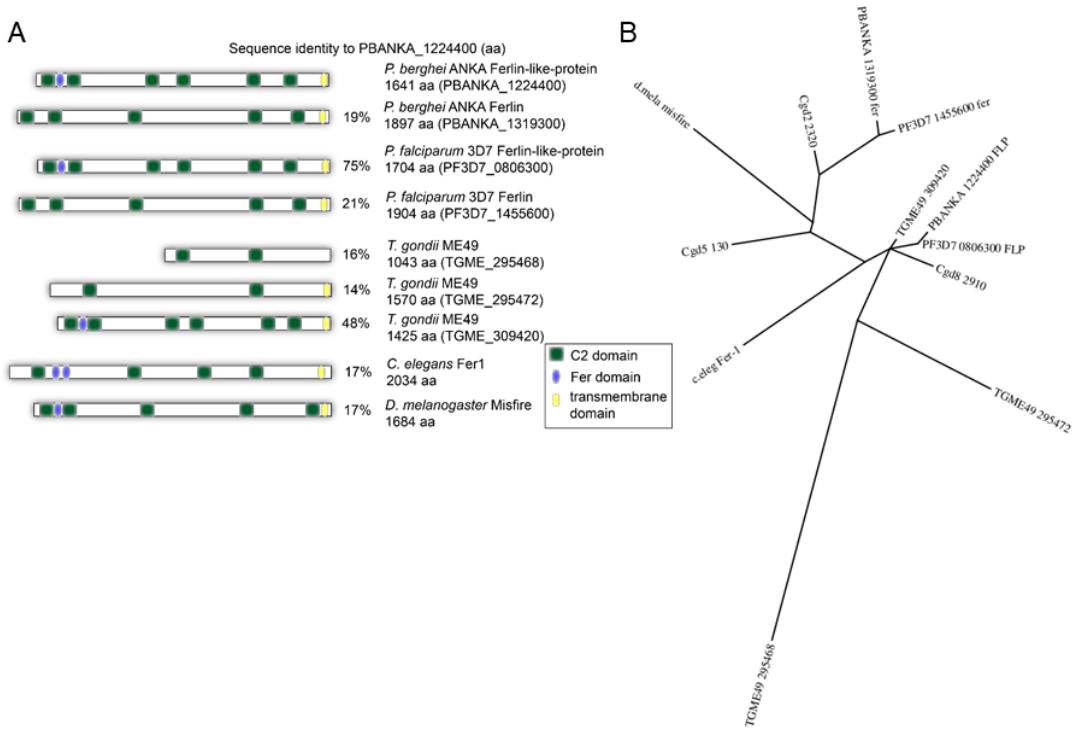

Figure 1.10 Apicomplexan ferlins. Protein domain analysis of selected ferlins (**A**) reveals highly conserved topology with multiple (2-6) C2 domains and a C-terminal transmembrane domain. Amino acid (aa) sequence identity in comparison to FLP (PBANKA_1224400) is shown in percent as calculated by Clustal. Phylogenetic tree of apicomplexan and selected invertebrate ferlins (**B**) FLP = ferlin-like protein, fer = ferlin, d.mela = *Drosophila melanogaster*, TGME49 = *Toxoplasma gondii* ME49, Cgd = *Cryptosporidium parvum* Iowa II, PF3D7 = *Plasmodium falciparum* 3D7, PBANKA = *Plasmodium berghei* ANKA, c.eleg = *Caenorhabditis elegans*. The tree was generated using amino acid sequence from eupathdb.org and uniprot.org and analysed in *Phylogeny.fr*.

Ferlins are present in most unicellular organisms, including apicomplexan parasites. *Plasmodium* harbors two ferlins - ferlin and ferlin-like protein (FLP) - with yet unknown functions (Fig. 1.10A).

T. gondii, the related apicomplexan parasite, encodes three ferlins. Two of them are very different and the third one is very similar to *Plasmodium* FLP (Fig. 1.10). Apicomplexan ferlins contain two to six C2 domains and a C-terminal transmembrane domain. Additionally, FLP and TGME_309420 harbor a Fer domain. Lower eukaryotes typically encode two ferlin genes, one of which usually harbors a DysF domain [113]. No typical DysF domain was assigned to apicomplexan ferlins. However, a typical feature of a DysF domain is the presence of repeats [113], FLP contains a repetitive region between C2D and C2E domains, which might be considered a pseudo-DysF domain.

1.5 The aim of the study

The ferlin protein family is conserved throughout the *Plasmodium* phylum and also in *Toxoplasma gondii* and other related apicomplexan parasites, suggesting an evolutionarily conserved function. *Plasmodium falciparum* ferlins were previously identified in our laboratory as potential immune targets [161]. *Plasmodium berghei*, a murine malaria parasite, represents a powerful tool to study the entire life cycle of this parasite in detail. The *P. berghei* life cycle alternating between laboratory mice and *Anopheles* mosquitoes is established in our laboratory. This model system allows for studying the life cycle as a whole, including the bottleneck transmission stages and other features, which are very difficult or impossible to tackle using the human parasite *P. falciparum*.

This study aimed at investigating the function of *P. berghei* ferlin-like protein (FLP). Deciphering FLP function should help its establishment as a novel immune target. Given the high degree of ferlin conservation throughout evolution, the role of FLP might additionally bring hints for roles of other ferlins in related organisms.

We set three aims in order to functionally characterize FLP. First aim was to analyse *flp* expression during the parasite life cycle. The protein abundance in each stage and especially the comparison between stages is critical for identifying the stages, in which it acts. The second aim was to analyse subcellular localization of FLP. Colocalization with known structures indicates in which processes might a given protein participate. To minimize risk of artefacts and maximize our chances for success, we set two independent aims for FLP visualization, namely preparation of polyclonal antibody and endogenous tagging. The third aim was to analyse FLP depletion phenotype. The comparison of wildtype and target-deficient parasites is the classical approach to study protein function. We attempted to generate a knock-out parasite. However, previous dat a from our laboratory indicated that *P. berghei* might be refractory to FLP deletion. We therefore investigated other ways to deplete FLP in parallel – namely inducible knock-down using small molecules, truncation of the protein and promoter swapping.

2 Materials and Methods

2.1 Material

2.1.1 Laboratory equipment

ABI 7500 Real-Time PCR System	Life Technologies, CA, USA
AMAXA Nucleofector II electroporator	Lonza, Cologne
Autoclave 5075 ELV	Systec, Wettenberg
Balances	
Analytical balance Pioneer	Ohaus, Nanikon, Switzerland
Precision balance	Mettler Toledo, Switzerland
BioPhotometer	Eppendorf, Hamburg
Camera (gel documentation)	INTAS Science Imaging Instruments, Goettingen
Centrifuges	
Megafuge 1.0R	Heraeus Instruments, Hanau
Megafuge 2.0R	Heraeus Instruments, Hanau
Microcentrifuge 5415 D	Eppendorf, Hamburg
Microcentrifuge 5415 R	Eppendorf, Hamburg
Centrifuge 5804	Eppendorf, Hamburg
Ultracentrifuge J2-MC	Beckman Coulter, Krefeld
Ultracentrifuge RCB5 Plus	Sorvall, Thermo Fisher Scientific, USA
Cold light source KL1500 LCD	Carl Zeiss, Oberkochen
Computer hardware	
Dell Inspiron 11	Dell Inc., TX, USA
Printer CX510de	Lexmark, KY, USA
Printer MS510dn	Lexmark, KY, USA
Scanner EPSON Perfection 2400 Photo	EPSON, Japan

Computer software

Adobe Photoshop elements 14	Adobe Systems Inc., CA, USA
AutoQuant X3	Media Cybernetics, Inc., MD, USA
Fiji (Image J) Version 1.51w	Wayne Rasband, NIH, USA
Image Studio Version 5.0.21	Li-Cor Biosciences, NE, USA
Prism 5	GraphPad Software Inc., CA, USA
Serial Cloner 2.6.1	Franck Perez, SerialBasics
Qiqqa Version v.79s	Quantisle Ltd.
Diaphragm vacuum pump laboport	KNG Neuberger, NJ, USA
Digital timer	NeoLab Migge, Heidelberg Carl Roth, Karlsruhe Oregon Scientific, CA, USA
EasyjecT Prima electroporator	EquiBio, TX USA
Electrophoresis Power Supply EPS 301	Amersham Pharmacia Biotech, Freiburg
Gel electrophoresis System Horizon 11.14	Biometra, Goettingen
Freezers -20^{o}C	Liebherr, Bulle, Switzerland
Freezer -80^{o}C	Thermo Fisher Scientific, MA, USA
Fridges	Liebherr, Bulle, Switzerland
Gas Burner Soudagaz X2000 PZ	Campingaz, Hungen-Inheiden
Haemocytometer chamber	Labotec Labor-Technik, Goettingen
Heating block thermomixer comfort	Eppendorf, Hamburg
Ice machine	Ziegra Eismachinen, Isernhagen

Incubators

Mosquito incubators	Mytron, Heilbad Heiligenstadt
Hera cell incubator	Heraeus Instruments, Hanau
Hera cell 150 incubator	Heraeus Instruments, Hanau
Heraeus function line incubator	Thermo Fisher Scientific, MA, USA
Shaking Incubator Innova 4300	New Brunswick Scientific, Nijmegen, Netherlands

Lab pH meter inoLab pH 7110	WTW, Weilheim
Li-Cor C-DiGit Blot Scanner	Li-Cor Biosciences, NE, USA
Liquid nitrogen tank Cryosystem 4000 series	Panasonic, Kadoma, Japan
Liquid nitrogen tank MVE XC 34/18	MTG, Bruckberg
Magnetic stirrer Heidolph MR3001	NeoLab Migge, Heidelberg
Micropistill for 1.5 ml tubes, conical	NeoLab Migge, Heidelberg

Microscopes

Confocal spinning disc microscope Nikon Eclipse TI-E	Nikon, Japan; Perkin Elmer, MA,USA
Fluorescence microscope	Carl Zeiss, Oberkochen
Stereomicroscope Stemi 2000-C	Carl Zeiss, Oberkochen
Widefield fluorescent microscope Axiovert 200M	Carl Zeiss, Oberkochen
Widefield light microscope Axioskop 40	Carl Zeiss, Oberkochen
Widefield light microscope Axiostar Plus	Carl Zeiss, Oberkochen
Widefield light microscope Axiovert 25	Carl Zeiss, Oberkochen

Microwave oven	Sharp electronics, Hamburg
Mosquito cages	BioQuip Products, CA, USA
PCR cycler GeneAmp System 9700	Life Technologies, CA, USA
PCR Mastercycler gradient	Eppendorf, Hamburg

Pipettes

Pipetman NEO	Gilson, WI, USA
Pipetman G	Gilson, WI, USA
Pipetman L	Gilson, WI, USA
Eppendorf Research	Eppendorf, Hamburg

Pipetus	Hirschman Laborgeraete, Eberstadt
PURIST Ultrapure Lab water systems	RephiLe Bioscience Ltd., China
Roller mixer CAT RM 5	NeoLab Migge, Heidelberg
Roller mixer SU 1400	NeoLab Migge, Heidelberg

Rotator SB3	Stuart, Staffordshire, UK
SDS PAGE XCell SureLock Mini-Cell	Thermo Fisher Scientific, MA, USA
Sterile workbench HeraSafe	Thermo Fisher Scientific, MA, USA
UV transilluminator	Vilber, Eberhardzell
Vortex Genie 2	Scientific Industries Roth, Karlsruhe
Water bath 1003	GFL, Burgwedel
Western blot XCell II Blot module	Thermo Fisher Scientific, MA, USA

2.1.2 Consumables

0.1 ml strip tubes and caps	Qiagen, Hilden
14 ml polystyrene round bottom tubes with lid	Greiner bio-one, Frickenhausen
24-well assay plate, clear bottom with lid, cell culture	Sigma-Aldrich, MO, USA
Aluminium foil	Carl Roth, Karlsruhe
BD Discardit II 20 ml syringes	Becton Dickinson, NJ, USA
BD Micro-Fine U-100, insulin syringes, 29G	Becton Dickinson, NJ, USA
BD Microlance 3 20G, 23G, 27G needles	Becton Dickinson, NJ, USA
BD Plastipak U-100, 1ml syringes	Becton Dickinson, NJ, USA
Biopur safelock tubes 1.5 ml	Eppendorf, Hamburg
Cell culture flasks Cell Star 25cm^2, 75 cm^2	Greiner bio-one, Frickenhausen
Cryotubes	Sigma-Aldrich, MO, USA
Disposable autoclave bags	Sarstedt, Nuembrecht
Disposable powder free gloves Semperguard	Sempermed, Austria
Electroporation cuvettes	Bio-Rad Laboratories, CA, USA
Falcon tubes 15 ml, 50 ml	Sarstedt, Nuembrecht
Filter tip Biosphere 20µl, 100µl, 200µl, 1000µl	Sarstedt, Nuembrecht
Filter tip FT 10 E 1 µl	Greiner bio-one, Frickenhausen

Folded filter paper	NeoLab Migge, Heidelberg
Glass pasteur pipettes	Brand GmbH, Heidelberg
Glass slides with marked circles	Medco, Munich
Immobilion-P transfer membrane, PVDF	Merck Millipore, MA, USA
Kimtech Science precision wipes	Kimberly-Clark, Ontario, Canada
Lab-Tek chamber slides, 8 well	Thermo Fisher Scientific, MA, USA
Membrane filters 0.1 µm	Merck Millipore, MA, USA
Micro tubes 1.5 ml, 2ml	Sarstedt, Nuembrecht
Micro-cuvettes 10 x 4 mm	Sarstedt, Nuembrecht
MicroAmp Optical 96-well reaction plate	Applied Biosystems, CA, USA
Microscopic cover glasses 18 x 18 mm, 24 x 50 mm	Marienfeld, Lauda-Koenigshofen
Microscopic slides, frosted ends, 76 x 25 x 1 mm	Marienfeld, Lauda-Koenigshofen
Parafilm M	Bemis, WI, USA
PCR tubes, RNase free, flat cap, 0.2 ml	Kisker Biotech, Steinfurt
Petri dishes 94/16 mm, 145/20 mm	Greiner bio-one, Frickenhausen
Pipette tips 0.1 – 10 µl	Kisker Biotech, Steinfurt
Pipette tips 200 µl, 1000 µl	Sarstedt, Nuembrecht
Polystyren cuvettes 10 x 4 x 45 mm	Sarstedt, Nuembrecht
qPCR seals, optical clear	Peqlab technology, Erlangen
Quali PCR-tube stripes with lid 0.2 ml	Kisker Biotech, Steinfurt
Self-adhesive labels 33 x 13 mm	NeoLab Migge, Heidelberg
Serological pipettes 1 ml, 5 ml, 10 ml, 25 ml	Sarstedt, Nuembrecht
Stericup express PLUS 0.22 µm filtration system	Merck Millipore, MA, USA
Syringe filter unit 0.22 µm	GE Healthcare, Little Chalfont, UK
TouchNTuff nitril gloves	Ansell, Brussels, Belgium

Tubee's self-adhesive dots	NeoLab Migge, Heidelberg
WesternSure Pen	Li-Cor Biosciences, NE, USA
Whatman paper	GE Healthcare, Little Chalfont, UK

2.1.3 Chemicals and Reagents

Acetic acid	Carl Roth, Karlsruhe
Agarose	Sigma-Aldrich, MO, USA
Albumin fraction V	Carl Roth, Karlsruhe
Alsever's solution	Sigma-Aldrich, MO, USA
Ampicillin	Carl Roth, Karlsruhe
100x Antibiotic-Antimycotic	Life Technologies, CA, USA
BactoTM-Agar	Becton Dickinson, NJ, USA
BactoTM-Tryptone	Becton Dickinson, NJ, USA
BAPTA-AM	Sigma-Aldrich, MO, USA
Bepanthen eye cream	Bayer AG, Leverkusen
Bis Tris	Carl Roth, Karlsruhe
Bromphenol blue	Serva Electrophoresis, Heidelberg
β-Mercaptoethanol	Carl Roth, Karlsruhe
Calcium chloride	AppliChem, Darmstadt
Cat food Cachet classic	Saturn petfood, Bremen
CF-11 Cellulose powder	Thermo Fisher Scientific, MA, USA
4-chloro-DL-phenylalanine	Sigma-Aldrich, MO, USA
Diethylether	Sigma-Aldrich, MO, USA
Dipotassium hydrogen phosphate	AppliChem, Darmstadt
Digitonin	Sigma-Aldrich, MO, USA
DMEM medium	Life technologies, CA, USA

DMSO	Gruessing, Filsum
Dry ice	Zentrallager UniKlinikum Heidelberg
DTT	AppliChem, Darmstadt
EDTA	AppliChem, Darmstadt
Ethanol	Sigma-Aldrich, MO, USA
Ethidium bromide	Carl Roth, Karlsruhe
FCS (South American or US origin)	Life technologies, CA, USA
5-Fluorocytosine	Sigma-Aldrich, MO, USA
Gentamicin	Life technologies, CA, USA
Giemsa staining solution	Carl Roth, Karlsruhe
Glass beads unwashed	Sigma-Aldrich, MO, USA
Glucose	Carl Roth, Karlsruhe
Glutaraldehyde	Merck Millipore, MA, USA
Glycerol	Carl Roth, Karlsruhe
Glycine	AppliChem, Darmstadt
Guanidine hydrochloride	Sigma-Aldrich, MO, USA
HBSS medium	Life technologies, CA, USA
Heparin	Ratiopharm, Ulm
Hoechst 33342	Life technologies, CA, USA
Hydrochloric acid	VWR International, PA, USA
Hypoxanthine	Sigma-Aldrich, MO, USA
Immersion oil	Waldeck, Muenster
IPTG	Adipogen life science, Switzerland
Kanamycin	Carl Roth, Karlsruhe
Ketamine	Bremen Pharma GmbH, Warburg

Lithium acetate	Sigma-Aldrich, MO, USA
Manganese chloride	Gruessing, Filsum
Magnesium sulphate	Merck Millipore, MA, USA
Methanol	AppliChem, Darmstadt
N-lauroylsarcosinate	Sigma-Aldrich, MO, USA
Nycodenz	Axis-Shield, Dundee, Scotland
Para-aminobenzoic acid	Sigma-Aldrich, MO, USA
Paraformaldehyde 4% in PBS	Carl Roth, Karlsruhe
PBS tablets	Sigma-Aldrich, MO, USA
Penicillin/Streptomycin	Life technologies, CA, USA
Potassium acetate	Sigma-Aldrich, MO, USA
Potassium dihydrogen phosphate	AppliChem, Darmstadt
Power SYBR Green PCR Master mix	Applied Biosystems, CA, USA
Propanol	Sigma-Aldrich, MO, USA
Protease inhibitor	Roche, Basel, Switzerland
Pyrimethamine	Sigma-Aldrich, MO, USA
Riboflavin	Sigma-Aldrich, MO, USA
RPMI	Life technologies, CA, USA
Rubidium chloride	Carl Roth, Karlsruhe
Saponin	Sigma-Aldrich, MO, USA
SDS	Carl Roth, Karlsruhe
Sea salt	Alnatura, Bickenbach
Sodium acetate	Gruessing, Filsum
Sodium deoxycholate	Sigma-Aldrich, MO, USA
Sodium dihydrogen phosphate	Sigma-Aldrich, MO, USA

Sodium fluoride	Sigma-Aldrich, MO, USA
Sodium hydrogen carbonate	AppliChem, Darmstadt
Sodium hydroxide	J. T. Baker, NJ, USA
Sulfadiazine	Sigma-Aldrich, MO, USA
Sucrose	AppliChem, Darmstadt
Tetracyclin	Carl Roth, Karlsruhe
TRIS	Carl Roth, Karlsruhe
Triton X-100	Sigma-Aldrich, MO, USA
Trypan Blue	Sigma-Aldrich, MO, USA
0.25% Trypsin/EDTA	Life technologies, CA, USA
Tween 20	Carl Roth, Karlsruhe
X-gal	NeoLab Migge, Heidelberg
Xanthurenic acid	Sigma-Aldrich, MO, USA
Xylazine	Ecuphar GmbH, Greifswald
Yeast extract	Carl Roth, Kalrsruhe
Western Lightning Plus-ECL	Perkin Elmer, MA, USA

2.1.4 Commercial kits

AMAXA Human T Cell Nucleofector Kit	Lonza, Cologne
First strand cDNA synthesis kit	Thermo Fisher Scientific, MA, USA
Gibson assembly cloning kit	New England Biolabs, MA, USA
NuPAGE MOPS Kit	Thermo Fisher Scientific, MA, USA
pGEM-T Easy Vector Systems	Promega, Mannheim
QIAamp DNA Blood Kit	Qiagen, Hilden
QIAprep Spin Plasmid Miniprep Kit	Qiagen, Hilden
QIAquick PCR Purification Kit	Qiagen, Hilden

QIAquick Gel Extraction Kit	Qiagen, Hilden
Qubit Protein Assay Kit	Thermo Fisher Scientific, MA, USA
3‘RACE System for Rapid Amplification of cDNA Ends	Thermo Fisher Scientific, MA, USA
RNeasy Mini Kit	Qiagen, Hilden
Turbo DNA free kit	Life technologies, CA, USA

2.1.5 Strains

2.1.5.1 Bacteria strains

BigEasy-TSA Electrocompetent bacteria	Lucigen, WI, USA
Chemocompetent *E. Coli* XL1 Blue	Agilent Technologies, CA, USA
Electrocompetent *E. Coli* PMC103	provided by Prof. Jude M. Przyborski, Heidellberg Universit Hospital
Competent *E. Coli* BL21(DE3)	provided by Dr. Julia Sattler, Heidelberg University Hospital
Competent *E. Coli* JM109	Promega, Mannheim

2.1.5.2 Cell lines

Human hepatoma cell line HuH7	provided by Prof. Bartenschlager, Heidelberg University Hospital

2.1.5.3 Parasite strains

Plasmodium berghei ANKA cl15cy1	[162]
Plasmodium berghei ANKA GFPcon	[163]
Plasmodium berghei ANKA 820cl1m1cl1	[61]

2.1.5.5 Mosquito strain

Anopheles stephensi	Max Planck Institute for Infection Biology, Berlin

2.1.5.6 Mice strains

Naval Medical Research Institute (NMRI), outbred	Charles River, MA, USA
C57BL/6	Janvier, France

2.1.6 Oligonucleotides

Primers were purchased form Life Technologies at concentration 0.1 nmol/µl.

2.1.6.1 Primers used for plasmid construction

Number	Purpose	Restriction site	Sequence (restriction site)
#1	Cloning of pET28a_Ab1 and pET28a_Ab4	BamHI	GGGGATCCAGTATAGGAAAAAAACAC
#2	Cloning of pET28a_Ab1 (**triple stop codon**)	XhoI	GTCTCGAG**TTAATTAATTA**CTGGGAATAAATAC
#3	Cloning of pET28a_Ab2	BamHI	GGGGATCCAATTTATATAAAAAAGACCAAAAAGG
#4	Cloning of pET28a_Ab2 (**triple stop codon**)	XhoI	CTCTCGAG**TTAATTAATTA**CTCTTCCAATAGATG
#5	Cloning of pET28a_Ab4 (**triple stop codon**)	XhoI	GACTCGAG**TTAATTAATTA**ATATACCCCAACA
#6	Cloning of flp_gfp	SpeI	CCCGACTAGTATTATGCCAATAGAAT
#7	Cloning of flp_gfp (**ORF shift**)	PshAI	CGGACTCCTGTC**C**TTTTAACAAAAAC
#8	Cloning of flp_gfp and dflp_TM		ACGTGGTCGACGAAGTACTTCGTTTAAACGCTGATTTAATAATGGCAAAT
#9	Cloning of flp_gfp and dflp_TM		ACGCGTGGGCCCCCTAGGTACGTATCTCGAGCCCGGGAAGACAGAAGTAATGAATTGTATCT
#10	Cloning of dflp_C2A		TATAGGGGACGATCGGTCGTGCACTGCCCCTAGAGCTTTTGATATAG
#11	Cloning of dflp_C2A		GTTGTACTTTTGAATATACATAATTTAAACTCATTTTATGGACGCATAAAT
#12	Cloning of dflp_C2A		TAAGAAATAAACTGATTTATGCGTCCATAAAATGAGTTTAAATTATGTATA

#13	Cloning of dflp_C2A		GCATGGCGCGCCCGTCTCGTACATCATATGGATATTTGATTTATTGAAC
#14	Cloning of dflp_TM	SacII	CTACCGCGGCAAATGAACCCATTGGTGA
#15	Cloning of dflp_TM (**triple stop codon**)	XbaI	GTCGCTCTAGA**TTAATTAATTA**TTTCAATCCTTGCATTATAGATG
#16	Cloning of flp_AID	PstI	GGGGCTGCAGAGACAGAAGTAATGAATTGTATC
#17	Cloning of flp_AID (**extra bp**)	SapI	TAGCTCTTC**CAGC**ACTGTATTCCTAACAACCGA
#18	Cloning of flp_AID	AscI	CTAGGCGCGCCCAAATGAACCCATTGGTGA
#19	Cloning of flp_AID	XhoI	GTCTCGAGTTTTAACAAAAACATTATAAAT
#20	Cloning of dflp_ook	NotI	GGAACTGCGGCCGCAAAATGAGTATAGGAAAAA
#21	Cloning of dflp_ook	SpeI	ATAATCACTAGTAGGCCCAGGGGCATGAGTTTT
#22	Cloning of dflp_spz and dflp_gam	KpnI	AAGGTACCCTAGAGCTTTGATATAG
#23	Cloning of dflp_spz and dflp_gam	HindIII	GGAAGCTTTTATGGACGCATAAATCAG
#24	Cloning of dflp_spz	BsmI	GGGGGAATGCTATGAGTATAGGAAAAAAAACAC
#25	Cloning of dflp_spz	SacII	AACCGCGGGCCAATACCGGCAACAGAC
#26	Cloning of dflp_liver		GGTCGACGAAGTACTTCGTTTAAACGGTACCCTAGAGCTTTTGATATAG
#27	Cloning of dflp_liver		CCTAGGTACGTATCTCGAGCCCGGGAAGCTTTTATGGACGCATAAATCA

#28	Cloning of dflp_liver		TGTTTTTTCCTTCAATTTCGAGC TCCGGATCGATTATTAATTTTA GAGG
#29	Cloning of dflp_liver		ATTATATTGTGTTTTTTTTCCTA TACTCATTTTATCACATCCCCTT TTC
#30	Cloning of dflp_liver		AAGTGAAAATAGGAAAAGGG GATGTGATAAAATGAGTATAG GAAAAAAA
#31	Cloning of dflp_liver		CGACGAAGTACTTCTCGCGAG CGCGCCCGCGGGCCAATACCG GCAACAG
#32	Cloning of dflp_gam	EcoRV	GAGATATCATGAGTATAGGAA AAAAAACAC
#33	Cloning of dflp_gam	AatII	GAGACGTCACCTCTAAATATAT TTATAC

2.1.6.2 Primers used for genotyping and other assays

Number	Purpose	Chapters	Sequence
#1	genotyping of *flp::gfp,* Δflp_{TM} and *flp::AID* parasites	3.1.3.1, 3.2.2.2, 3.2.3.1	GGAATTCCATATGGATGAATTGCAAAGAGAA GAAATG
#2	genotyping of *flp::gfp* and Δflp_{TM} parasites	3.1.3.1, 3.2.2.2	TGAATGCAACCATAACCCATACTC
#3	genotyping of *flp::gfp* and Δflp_{TM} parasites	3.1.3.1, 3.2.2.2	TAATACGACTCACTATAGGGCGA
#4	genotyping of *flp::gfp* and Δflp_{TM} parasites	3.1.3.1, 3.2.2.2	AATCCTTAAACGGGCTTGC
#5	genotyping of *flp::gfp* and Δflp_{TM} parasites	3.1.3.1, 3.2.2.2	GTTTACCTTCTACTGAAGAGGTTGTGG
#6	genotyping of *flp::gfp, flp::iLOV* and *flp::AID* parasites	3.1.3.1, 3.1.3.3, 3.2.3.1	GCCTCTTTTGTGTGTCATTTCATC
#7	genotyping of *gfp::flp,* $\Delta flp_{ook,}$ $\Delta flp_{spz,}$ Δflp_{liver} and Δflp_{gam} parasites	3.1.3.2, 3.2.4.1, 3.2.4.2, 3.2.4.3, 3.2.4.4	TCCCCGCGGGTCTGTTTGAATGTCAAACTGCT ATG

#8	genotyping of *gfp::flp,* $\Delta flp_{ook,}$ $\Delta flp_{spz,}$ Δflp_{liver} and Δflp_{gam} parasites	3.1.3.2, 3.2.4.1, 3.2.4.2, 3.2.4.3, 3.2.4.4	TGTTGGGTGGGTCATGTTCT
#9	genotyping of *gfp::flp*parasites	3.1.3.2	ATGAGTAAAGGAGAAGAACTTTTCA
#10	genotyping of *gfp::flp*parasites	3.1.3.2	TTATTTGTATAGTTCATCCATGCC
#11	*gfp::flp* transcript detectionm genotyping of *Δflp* parasites	3.1.3.2, 3.2.1.1	CGACGCCATTTGTTTCTCCA
#12	genotyping of *flp::iLOV* parasites	3.1.3.3	GCAGAATTCGTGAATCATCTCTTGATTTATCTGCTC
#13	genotyping of *flp::iLOV* parasites	3.1.3.3	TTGCGGCCGCGGACATGTTTTAAATGAGTTATGTGAGC
#14	genotyping of *flp::iLOV*, *Δflp* and Δflp_{C2A} parasites	3.1.3.3, 3.2.1.1, 3.2.2.1	CCGATTTAAGATTCGTGATTGTATG
#15	genotyping of *flp::iLOV* and *flp::HA* parasites	3.1.3.3, 3.1.3.4	TTAGAATTAGCGGCTGTACTCGGTCAGCTCCAGGAA
#16	genotyping of *flp::iLOV, flp::HA* and *Δflp* parasites	3.1.3.3, 3.1.3.4, 3.2.1.1	GACTTTGGTGACAGATACTACTGTG
#17	*flp::iLOV* transcript detection, 3'RACE	3.1.3.3, 3.1.5	AACTGGGAGATGCAACTGCAT
#18	genotyping of *flp::HA* parasites, 3'RACE, qPCR of *flp*	3.1.3.4, 3.1.5, 3.1, 3.2.4.1, 3.2.4.4, 3.3.4	CATCAAATGAACCCATTGGTGAATC
#19	genotyping of *flp::HA* parasites	3.1.3.4	CAATTCATTACTTCTGTCT
#20	genotyping of *flp::HA* and *Δflp* parasites	3.1.3.4, 3.2.1.1	GGCTATTCATACTAGCCATTTTATGTG
#21	genotyping of *Δflp*parasites	3.2.1.1	TCGGATCCCCTTATTTAAGAGCAACGATATTTAG
#22	genotyping of *Δflp*parasites	3.2.1.1	CGGGTACCGCTGACATTTCATATTTTAT
#23	genotyping of *Δflp*parasites	3.2.1.1	GGGGATGTACAAAGACATTG
#24	genotyping of *Δflp*parasites	3.2.1.1	GAAAAGATGATAATATAATTAAC
#25	genotyping of Δflp_{C2A} parasites	3.2.2.1	CGGGATCCATCTGGTTCTTCTACATCTTC
#26	genotyping of Δflp_{C2A} and *flp::AID* parasites	3.2.2.1, 3.2.3.1	CACATAAAATGGCTAGTATGAATAGCC
#27	genotyping of Δflp_{C2A} and *flp::HA* parasites	3.2.2.1, 3.2.3.1	TAATACGACTCACTATAGGG

#28	gentoyping of *flp::AID* parasites	3.2.3.1	CCCTATGTTTTATAAAATTTTTTATTTATTTATAAGC
#29	gentoyping of *Δflp$_{ook}$* parasites	3.2.4.1	TCCCCGCGGCATACCCACATACATGGATATACATATGG
#30	gentoyping of *Δflp$_{ook}$* parasites	3.2.4.1	CCCGCACGGACGAATCCAGATGG
#31	gentoyping of *Δflp$_{spz}$* parasites	3.2.4.2	CCGTGTGAATATGCTCATTTTGTATAC
#32	gentoyping of *Δflp$_{spz}$* parasites	3.2.4.2	CCCGCACGGACGAATCCAGATGG
#33	gentoyping of *Δflp$_{liver}$* parasites	3.2.4.3	CCGCATGTTTATTAACATT
#34	gentoyping of *Δflp$_{gam}$* parasites	3.2.4.4	CCCCGCGGCATTTAGGGCATAAAAATAG
#35	gentoyping of *Δflp$_{gam}$* parasites	3.2.4.4	CAAATTTTGAAGTATATGAGAAGAATGAT
#36	gentoyping of *Δflp$_{gam}$* parasites	3.2.4.4	GGAACTGCGGCCGCAAAATGAGTATAGGAAAAA
#37	gentoyping of *Δflp$_{gam}$* parasites	3.2.4.4	CTCCGGTTCCCAACGATCAAG
#38	genotyping of *flp::HA;g377::mCherry* parasites	3.3.5	TATGATAATTTTGATGAG
#39	genotyping of *flp::HA;g377::mCherry* parasites	3.3.5	TTATTTTTAGATCAAAGC
#40	genotyping of *flp::HA;g377::mCherry* and *flp::HA;pplp2::mCherry* parasites	3.3.5	GCATGAACTCCTTGATGATGGC
#41	genotyping of *flp::HA;g377::mCherry* and *flp::HA;pplp2::mCherry* parasites	3.3.5	GGTGTTCTCTCTGATGTCCAGGAGGAGAAA
#42	genotyping of *flp::HA;pplp2::mCherry* parasites	3.3.5	GCTTCTGCGGGATATAAAAATGC
#43	genotyping of *flp::HA;pplp2::mCherry* parasites	3.3.5	ACGCATATCCATTCG
#44	qPCR of *flp*	3.1, 3.2.4.1, 3.2.4.4, 3.3.4	TGCTGGGTGTTTACAAGAAATGG
#45	qPCR of *ferlin*	3.1	GGTAATAGTTTTTCATCATGCGG
#46	qPCR of *ferlin*	3.1	ATAGGGATTTTTGCTGCCTCT
#47	qPCR of *hop*	3.1, 3.2.4.1, 3.2.4.3,	GGTGCCTATTCAAGTTTAGGA

		3.2.4.4, 3.3.4	
#48	qPCR of *hop*	3.1, 3.2.4.1, 3.2.4.3, 3.2.4.4, 3.3.4	CTAGTTGTCTTAAACCATGCTC
#49	RT-PCR of *aldolase*	3.2.4.3	TGTATTTAAAGCTTTACATGATAATGG
#50	RT-PCR of *aldolase*	3.2.4.3	TTTTCCATATGTTGCCAATGAATTTGC
#51	qPCR of *clag*	3.2.4.4, 3.3.4	ACAGGCGTAATGACTCGACG
#52	qPCR of *clag*	3.2.4.4, 3.3.4	CGGAGTATAGCGTCTTCGCC
#53	qPCR of *ama1*	3.2.4.1	ATTTGGGTTGATGGTTATTG
#54	qPCR of *ama1*	3.2.4.1	TCCTTGTCGAAATTTGGTAG
#55	RT-PCR and qPCR of PBANKA_111780	3.2.4.3	GCAAACTGCAATGAAGCCCA
#56	RT-PCR and qPCR of PBANKA_111780	3.2.4.3	TCCATTATGTGGGAACATGGCT
#57	RT-PCR and qPCR of PBANKA_062260	3.2.4.3	GTATCTTATTTATCTGAG
#58	RT-PCR and qPCR of PBANKA_062260	3.2.4.3	GATATTCTCAATAATCCC
#59	RT-PCR and qPCR of PBANKA_121680	3.2.4.3	TGGAGTTACACAAATTACTGGAAAA
#60	RT-PCR and qPCR of PBANKA_121680	3.2.4.3	TTTCCACAAGAGGAGTTAGGTAAA
#61	RT-PCR and qPCR of PBANKA_121100	3.2.4.3	CCATTCCCTGGACCTGGTTT
#62	RT-PCR and qPCR of PBANKA_121100	3.2.4.3	ACGGCAAATGCTTGCCCTA

2.1.7 Antibodies

2.1.7.1 Primary antibodies

2.1.7.1.1 Immunofluorescence assay

mouse anti-CSP, hybridoma supernatant (1:300) [164]

mouse anti-GFP, monoclonal (1:100) Roche Diagnostics, IN, USA

mouse anti-HSP70, hybridoma supernatant (1:100) [165]

mouse anti-βtubulin, monoclonal (1:400) Sigma-Aldrich, MO, USA

rat anti-HA tag, monoclonal, clone 3F10 (1:100) Roche Diagnostics, IN, USA

rat anti-TER-119, monoclonal (1:200) Santa Cruz Biotechnology, TX, USA

rabbit anti-SEP-1, polyclonal serum (1:200)	provided by Prof. Ponzi, Instituto Superiore di Sanita, Italy [166]

2.1.7.1.2 Western blot

mouse anti-GFP, monoclonal (1:500)	Roche Diagnostics, IN, USA
mouse anti-His tag, monoclonal (1:1000)	Novagen, Merck Millipore, MA, USA
mouse anti-Hsp70, hybridoma supernatant (1:100)	[165]
rabbit anti-iLOV, polyclonal serum (1:2000)	provided by Prof. Christie, University of Glasgow, UK [167]
rat anti-HA tag, monoclonal, clone 3F10 (1:1000)	Roche Diagnostics, IN, USA

2.1.7.2 Secondary antibodies

2.1.7.2.1 Immunofluorescence assay

goat anti-mouse Alexa 488 (1:300)	Life technologies, CA, USA
goat anti-mouse Alexa 546 (1:300)	Life technologies, CA, USA
goat anti-rat Alexa 488 (1:300)	Life technologies, CA, USA
goat anti-rat Alexa 546 (1:300)	Life technologies, CA, USA
goat anti-rabbit Alexa 488 (1:300)	Life technologies, CA, USA

2.1.7.2.2 Western blot

goat anti-mouse IgG-Peroxidase (1:10000)	Sigma-Aldrich, MO, USA
goat anti-rabbit IgG-Peroxidase (1:5000)	Jackson ImmunoResearch, PA, USA
goat anti-rat IgG-Peroxidase (1:5000)	Jackson ImmunoResearch, PA, USA

2.1.8 Enzymes

Alkaline Phosphatase	New England Biolabs, MA, USA
DNase I	Sigma-Aldrich, MO, USA
Fast Digest enzymes	Life technologies, MA, USA

Gateway LR Clonase	Thermo Fisher Scientific, MA, USA
Lysozyme	Sigma-Aldrich, MO, USA
Phusion DNA Polymerase	New England Biolabs, MA, USA
Proteinase K	Life technologies, MA, USA
Restriction endonucleases	New England Biolabs, MA, USA
T4 DNA ligase	New England Biolabs, MA, USA
Taq DNA Polymerase	Thermo Fisher Scientific, MA, USA

2.1.9 Buffers, media and solutions

2.1.9.1 Antibiotic stock solutions

Ampicilin	100 mg/ml in 50% EtOH
Kanamycin	50 mg/ml in H_2O
Tetracycline	5 mg/ml in 100% EtOH

2.1.9.2 Buffers for molecular biology

Fixing buffer IFA	PBS 4% paraformaldehyde 0.0075% glutaraldehyde
2x Laemmli buffer	250mM Tris pH 6.8 10mM EDTA 6.6% SDS 24% glycerol 6% mercaptoethanol bromphenol blue
Permeabilization buffer IFA	PBS 125mM glycine 0.1% Triton X-100

RIPA buffer	50mM Tris pH 7.5 150mM sodium chloride 5mM EDTA 50mM sodium fluoride 0.5% sodium deoxycholate 0.1% SDS 1% Triton X-100
TAE buffer	400M Tris 1mM EDTA 200mM acetic acid
TBS(T) buffer	2mM Tris 137mM sodium chloride (0.1% Tween 20)
Transfer buffer	25mM Tris 250mM glycine 20% Methanol

2.1.9.3 Buffers and media for microbiology

Chemocompetent cells Tfb I buffer	30mM potassium acetate 100mM rubidium chloride 10mM calcium chloride 50mM manganese chloride 15% glycerol -> pH 5.8, autoclave + store at 4^{o}C
Chemocompetent cells Tfb II buffer	10mM MOPS 10mM rubidium chloride 75mM calcium chloride 15% glycerol -> pH 6.5, autoclave + store at 4^{o}C

LB medium (agar)	10 g/l BactoTryptone 5 g/l Yeast Extract 10 g/l sodium chloride (15 g/l BactoAgar) -> autoclave + add antibiotic (1:1000) -> for pGEM blunt cloning IPTG and X-gal added
Lysis buffer	PBS 20 U/ml DNase I 10 µg/ml lysozyme 100mM β-mercaptoethanol inhibitors of proteases
Lysis buffer basic pH (with detergent)	50 mM Tris 2 mM EDTA 1 M sodium chloride 100 µM β-mercaptoethanol inhibitors of proteases (0.1 % N-lauroylsarcosinate) -> pH adjusted to 8.3
Lysis buffer acidic pH (with detergent)	50 mM Bis-Tris 2 mM EDTA 1 M sodium chloride 100 µM β-mercaptoethanol inhibitors of proteases (0.1 % N-lauroylsarcosinate) -> pH adjusted to 6
Solubilization buffer	6 M guanidine hydrochloride 2 mM EDTA 50 mM sodium dihydrogen phosphate 50 mM DTT

SB medium	35 g/l BactoTryptone 20 g/l Yeast Extract 5 g/l sodium chloride 7 mM sodium hydroxide -> autoclave
TB medium	10.8 g/l BactoTryptone 9.6 g/l Yeast Extract 9.4 g/l dipotassium hydrogen phosphate 2.29 g/l potassium dihydrogen phosphate -> autoclave + add 4 ml glycerol and antibiotic (1:1000)
SOC medium	20 g/l BactoTryptone 5 g/l Yeast Extract 0.5 g/l sodium chloride 5 g/l magnesium sulphate -> autoclave + add 20 ml of sterile 1M glucose
YEG-Cl agar	5 g/l Yeast Extract 5 g/l sodium chloride 2 g/l 4-Chloro-DL-phenylalanine 15 g/l BactoAgar -> autoclave + add 0.4% glucose and kanamycin (1:1000)

2.1.9.4 Buffers and media for HuH7 cell culture

Culture medium	DMEM 10% FCS antibiotic-antimycotic -> kept sterile, stored at 4^{o}C

2.1.9.5 Buffers and media for parasitology

5-FLuorocytosine drinking water	1 g/l in tap water

Nycodenz stock	5mM Tris pH 7.5 3mM potassium chloride 0.3mM EDTA 276 g/l Nycodenz -> autoclave + store in dark at 4°C
Ookinete medium	RPMI 20% FCS 50 mg/l hypoxanthine Pen/Strep 2 g/l sodium hydrogen carbonate 100µm xanthurenic acid
Overnight blood culture medium	RPMI 20% FCS 2 mg/l gentamicin -> sterile filtered, heparin added
Pyrimethamine drinking water	70 mg/l in tap water with sucrose, pH 3.5-5
Riboflavin drinking water	5 mg/l in tap water
Sulfadiazine in drinking water	10 mg/l in tap water with sucrose

2.1.9.6 Anaesthetics for mice

Ketamine-Xylazine (K/X)	PBS 25% Ketamine 4% Xylazine

2.1.9.7 Anopheles breeding

Salt solution	1 g/l sea salt in dH_2O
Sugar solution	100 g/l sucrose in dH_2O supplemented with para-aminobenzoic acid

2.1.9.8 Protein/DNA ladder and loading dye

Gene ruler 1 kb	Thermo Fisher Scientific, MA, USA
6x Loading dye	Thermo Fisher Scientific, MA, USA
Low MW ladder	New England Biolabs, MA, USA

PageRuler prestained	Thermo Fisher Scientific, MA, USA

2.1.10 Plasmids

2.1.10.1 Circular vectors

The pET28a vector (Fig. 2.1A) was used as a backbone for recombinant production of parts of the FLP protein. The vector carries kanamycin resistance and a machinery for recombinant protein expression inducible with IPTG in BL21DE5 *E. coli* bacteria. The pET28a vector offers the possibility of both N-terminal (cleavable by thrombin) and C-terminal fusion of the recombinant protein to a His-tag. Parts for recombinant expression were selected based on structural analysis of FLP. We cloned parts of *flp* gene (PCR amplified from genomic DNA) into the vector using the *XhoI* and *BamHI* restriction sites, fusing the sequence to the N-terminal His-tag and omitting the C-terminal one (Fig. 2.1B-D). Fragments corresponding to the 5'end of *flp* (Ab1 and Ab4) were amplified without the start codon, all fragments were terminated by a triple stop codon. Sizes of the fragments were as follows, Ab1 – 903 bp (primers #1 and #2), Ab2 – 936 bp (primers #3 and #4) and Ab4 – 429 bp (primers #1 and #5). All primer sequences are listed in chapter 2.1.6.1.

The pBAT-SIL6 vector (Fig. 2.2A, [168]) was used to generate the flp_gfp vector (for generation of *flp::gfp* parasite line). The vector carries an ampicillin resistance cassette and a recyclable hDHFR/yFcu resistance cassette, which can be used to select for parasites that carry the cassette by Pyrimethamine selection and afterwards for parasites that recycled the cassette (via 3'UTR homology regions) by 5' fluorocytosine selection [169]. Fragment corresponding to the 3'end of *flp* sequence without the stop codon (1035 bp, primers #6 and #7) was PCR amplified from genomic DNA and cloned into the backbone using the *SpeI* and *PshAI* restriction sites. Fragment corresponding to the 3'UTR of *flp* (693 bp, primers #8 and #9) was PCR amplified from genomic DNA and cloned into the *KpnI/HindIII*-opened backbone using Gibson assembly. The final vector (Fig. 2.2B) was linearized using the *SpeI* and *KpnI* restriction sites and used for transfection. All primer sequences are listed in chapter 2.1.6.1.

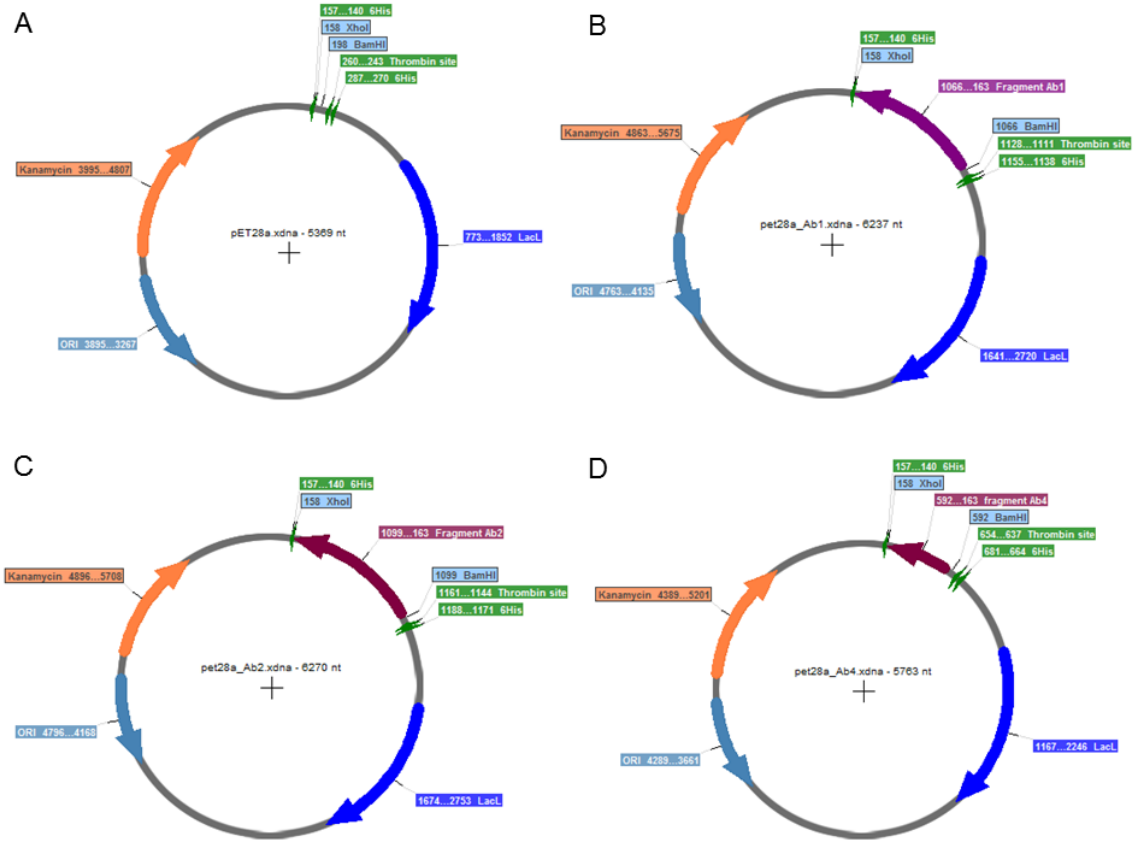

Figure 2.1 Plasmids used for recombinant expression of FLP fragments in *E. coli*. A) The backbone plasmid pET28a carries the kanamycin resistance cassette (orange), the *E. coli* origin of replication (ORI, light blue), LacL (dark blue), a cleavable (thrombin site, green) His-tag for N-terminal fusion (green) and a non-cleavable His-tag for C-terminal fusion. **B)**-**D)** Fragments corresponding to different parts of *flp* (purple) were cloned into the backbone using *BamHI* and *XhoI* restriction sites.

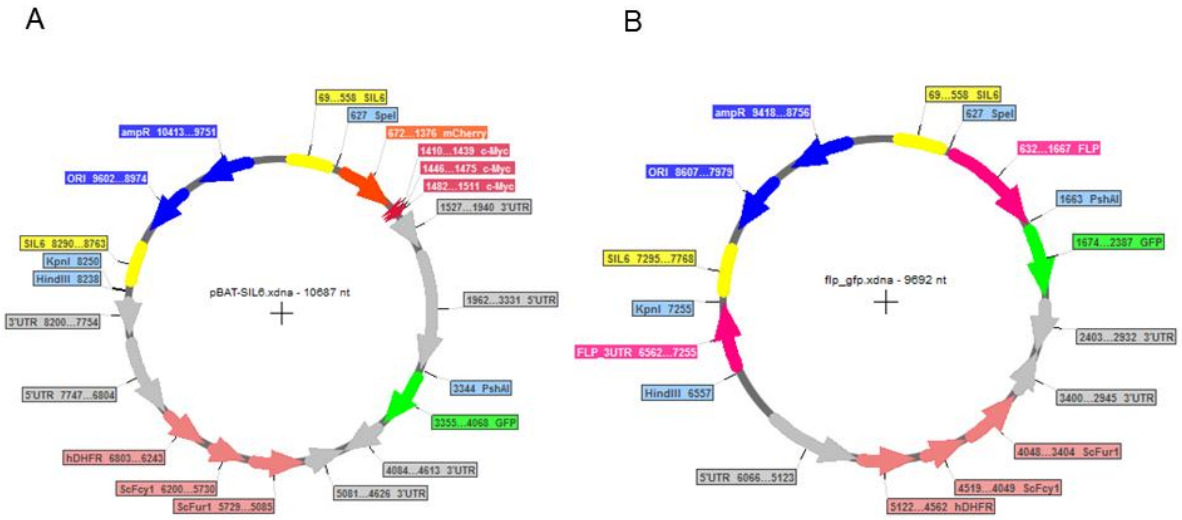

Figure 2.2 Backbone and final plasmids used for generation of *flp::gfp* parasite line. A) The backbone plasmid pBAT-SIL6 carries the ampicillin resistance cassette (ampR, dark blue), the *E. coli* origin of replication (ORI, dark blue), homology arms for integration into a silent locus on chromosome 6 (SIL6, yellow), a recyclable selection cassette (hDHFR, ScFcy, salmon), *mCherry* (orange), triple c-myc tag (red) and *gfp* (green). **B)** Fragments corresponding to 3'end and 3'UTR of *flp* (pink) were cloned into the backbone using *SpeI, PshAI*, *KpnI* and *HindIII* restriction sites.

The gfp_flp vector (used for generation of *gfp::flp* parasite line) was generated and transfected by Gunnar R. Mair. In brief, fragments corresponding to 5'UTR of *flp* (1498 bp) and 5'end of *flp* without the start codon (1197 bp) were cloned upstream and downstream of *gfp* and triple HA tags, respectively (Fig. 2.3). Vector was linearized using the *EcoRV* restriction site and used for transfection. All primer sequences are listed in chapter 2.1.6.1.

The pBAT-SIL6-MCS vector (Fig. 2.4A), generated by Franziska Hentzschel from the pBAT-SIL6 backbone (Fig. 2.2A, [168]), was used to generate the dflp_C2A vector (for generation of *Δflp*$_{C2A}$ parasite line). Similarly to pBAT-SIL6, the vector carries an ampicillin resistance cassette and a recyclable hDHFR/yFcu resistance cassette, which can be used to select for parasites that carry the cassette by Pyrimethamine selection and afterwards for parasites that recycled the cassette (via 3'UTR homology regions) by 5' fluorocytosine selection [169]. Fragment corresponding to the 5'UTR of *flp* (1019 bp, primers #10 and #11) and the *flp* sequence starting after C2A domain and with a newly introduced start codon (1402 bp, primers #12 and #13) were PCR amplified from genomic DNA and cloned into the *NaeI*/*NdeI*-open backbone using Gibson assembly. The final

vector (Fig. 2.4B) was linearized using the *BstBI* restriction site and used for transfection. All primer sequences are listed in chapter 2.1.6.1.

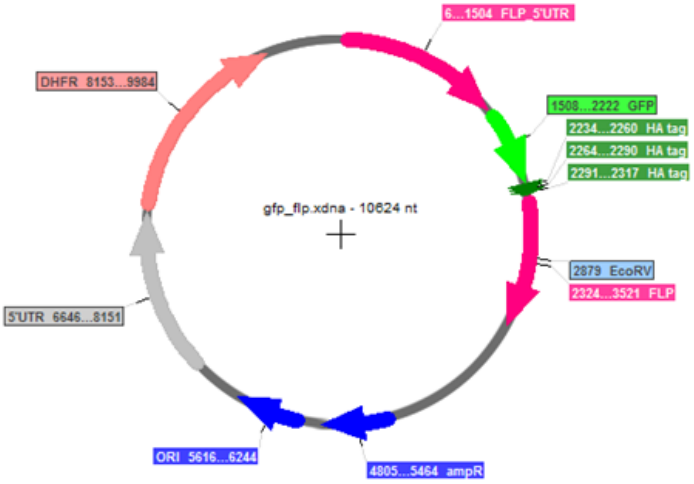

Figure 2.3 Final plasmid used for generation of *gfp::flp* parasite line. The plasmid carries the ampicillin resistance cassette (ampR, dark blue), the *E. coli* origin of replication (ORI, dark blue), the selection cassette (hDHFR, salmon), *gfp* (green) and triple HA tag. Fragments corresponding to parts of 5'end and 5'UTR of *flp* (pink) were cloned into the backbone.

The pBAT-SIL6-MCS vector (Fig. 2.5A, introduced above) was used to generate the dflp_TM vector (for generation of Δflp_{TM} parasite line). Fragment corresponding to the 3'UTR of *flp* (1003 bp, primers #8 and #9) and the 3'end of *flp* ending before the transmembrane domain and with a newly introduced stop codon (1035 bp, primers #14 and #15) were PCR amplified from genomic DNA and cloned into the backbone using *KpnI* and *HindIII* and *SacII* and *BamHI* restriction sites, respectively. The final vector (Fig. 2.4B) was linearized using the *SacII* and *KpnI* restriction sites and used for transfection. All primer sequences are listed in chapter 2.1.6.1.

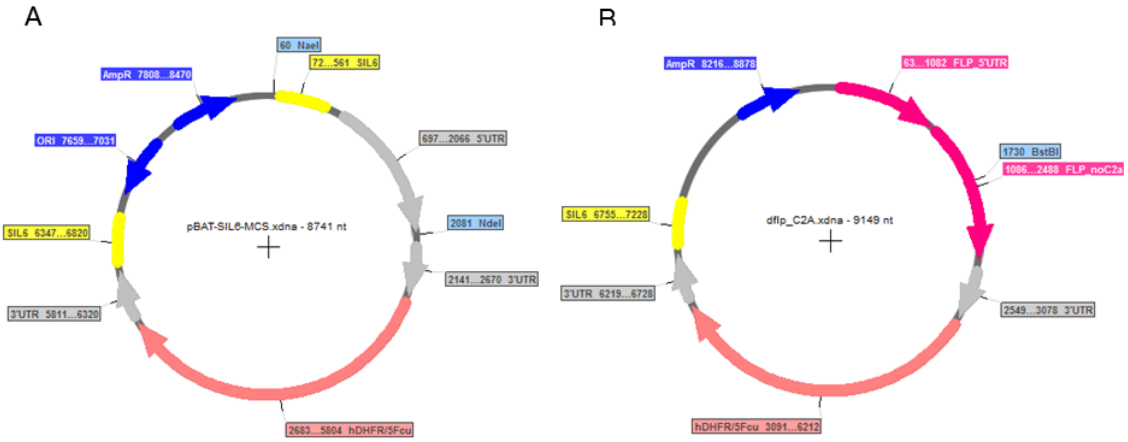

Figure 2.4 Backbone and final plasmids used for generation of *Δflp*$_{C2A}$ parasite line. A) The backbone plasmid pBAT-SIL6-MCS carries the ampicillin resistance cassette (ampR, dark blue), the *E. coli* origin of replication (ORI, dark blue), homology arms for integration into a silent locus on chromosome 6 (SIL6, yellow) and a recyclable selection cassette (hDHFR, ScFcy, salmon). **B)** Fragments corresponding to parts of 5'UTR of *flp* and its open reading frame starting after the C2A domain (pink) were cloned into the backbone using *NaeI* and *NdeI* restriction sites.

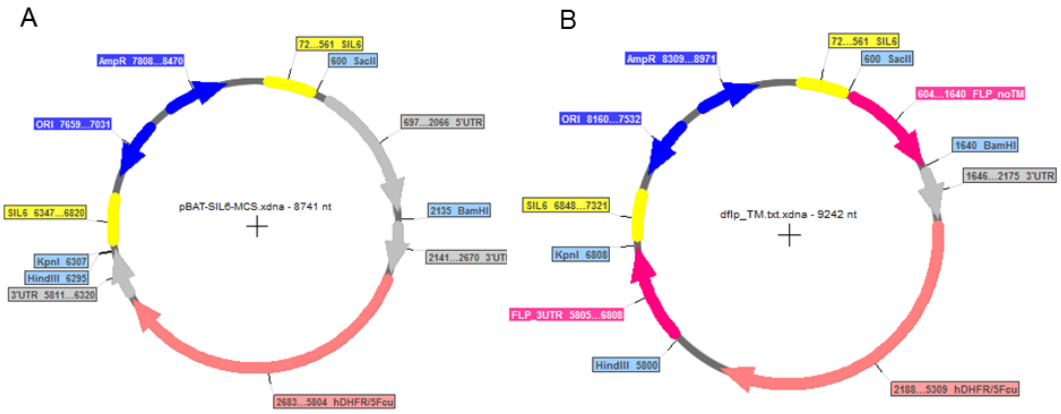

Figure 2.5 Backbone and final plasmids used for generation of *Δflp*$_{TM}$ parasite line. A) The backbone plasmid pBAT-SIL6-MCS carries the ampicillin resistance cassette (ampR, dark blue), the *E. coli* origin of replication (ORI, dark blue), homology arms for integration into a silent locus on chromosome 6 (SIL6, yellow) and a recyclable selection cassette (hDHFR, ScFcy, salmon). **B)** Fragments corresponding to parts of 3'UTR of *flp* and its open reading frame ending before the TM domain (pink) were cloned into the backbone through *KpnI*, *HindIII, SacII* and *BamHI* restriction sites.

The AID-GFP vector (Fig. 2.6A, kind gift from Nisha Philip [103]) was used to generate the flp_AID vector (for generation of *flp::AID* parasite line). The vector carries an ampicillin resistance cassette, *gfp* and a hDHFR resistance cassette, which can be used to select for parasites that carry the cassette by Pyrimethamine selection. Fragment corresponding to the 3'UTR of *flp* (624 bp, primers #18 and #19) and the 3'end of *flp* without the stop codon (643 bp, primers #16 and #17) were PCR amplified from genomic DNA and cloned into the backbone using the *PstI* and *SapI* and *SacII* and *XhoI* restriction sites, respectively. The final vector (Fig. 2.6B) was linearized using the *SacII* and *AhdI* restriction sites and used for transfection.

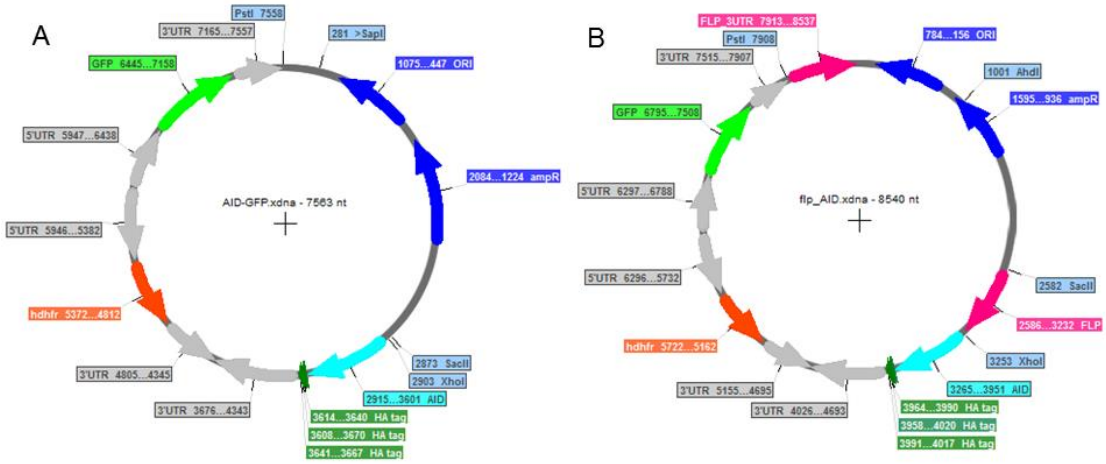

Figure 2.6 Backbone and final plasmids used for generation of *flp::AID* parasite line. A) The backbone plasmid AID-GFP carries the ampicillin resistance cassette (ampR, dark blue), the *E. coli* origin of replication (ORI, dark blue), *gfp* (green) and a selection cassette (hDHFR, salmon). **B)** Fragments corresponding to parts of 3'UTR of *flp* and its 3'end (pink) were cloned into the backbone through *PstI*, *SapI*, *SacII* and *XhoI* restriction sites.

The b3D-ama1 vector (Fig. 2.7A), generated by Kirsten Heiss from the b3D.DT^H.^D backbone [24], was used to generate the dflp_ook vector (for generation of Δflp_{ook} parasite line). Similarly to b3D.DT^H.^D, the vector carries an ampicillin resistance cassette, a TgDHFR resistance cassette, which can be used to select for parasites that carry the cassette by Pyrimethamine selection and *ama1* promoter. Fragment corresponding to the 5'end of *flp* (1205 bp, primers #20 and #21) was PCR amplified from genomic DNA and cloned into the open backbone using *NotI* and *SpeI* restriction sites. The final vector (Fig. 2.7B) was linearized using the *BstBI* restriction site and used for transfection. All primer sequences are listed in chapter 2.1.6.1.

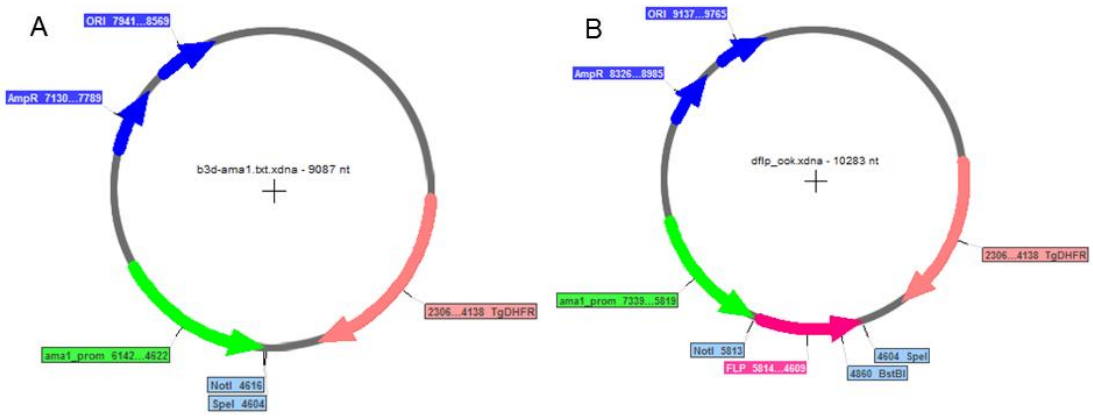

Figure 2.7 Backbone and final plasmids used for generation of *Δflp$_{ook}$* parasite line. A) The backbone plasmid b3D-ama1 carries the ampicillin resistance cassette (ampR, dark blue), the *E. coli* origin of replication (ORI, dark blue), *ama1* promoter (green) and a selection cassette (TgDHFR, salmon). **B)** Fragment corresponding to the 5'end of *flp* (pink) was cloned into the backbone using *NotI* and *SpeI* restriction sites.

The pLIS0185 vector (Fig. 2.8A), generated by Gunnar R. Mair, was used to construct the dflp_spz vector (for generation of *Δflp$_{spz}$* parasite line). The vector carries an ampicillin resistance cassette, a TgDHFR resistance cassette, which can be used to select for parasites that carry the cassette by Pyrimethamine selection and *ccp* promoter. Fragments corresponding to the 5'UTR (1021 bp, primers #22 and #23) and 5'end of *flp* (979 bp, primers #24 and #25) were PCR amplified from genomic DNA and cloned into the backbone using *KpnI* and *HindIII* and *BsmI* and *SacII* restriction sites, respectively. The final vector (Fig. 2.8B) was linearized using the *KpnI* and *SacII* restriction sites and used for transfection. All primer sequences are listed in chapter 2.1.6.1.

The pBAT-SIL6-MCS vector (Fig. 2.9A, introduced above) was used to generate the dflp_liver vector (for generation of *Δflp$_{liver}$* parasite line). Fragment corresponding to the 5'UTR of *flp* (1079 bp, primers #26 and #27), 5'UTR of PBANKA_062260 (1498 bp, primers #28 and #29) and the 5'end of *flp* (1040 bp, primers #30 and #31) were PCR amplified from genomic DNA and cloned into the *KpnI*/*HindIII*- and *SacII*/*EcoRV*-opened backbone, respectively, using Gibson assembly. The final vector (Fig. 2.9B) was linearized using the *ScaI* restriction site and used for transfection. All primer sequences are listed in chapter 2.1.6.1.

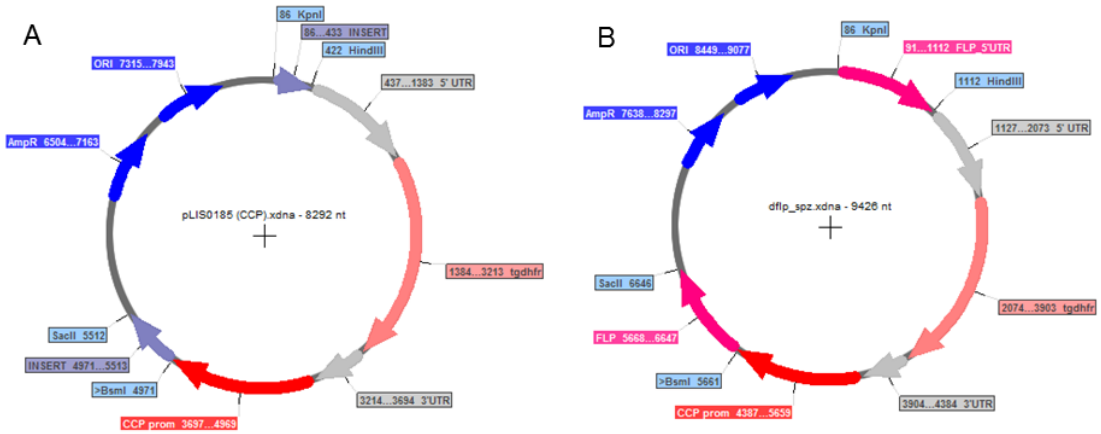

Figure 2.8 Backbone and final plasmids used for generation of *Δflp*$_{spz}$ parasite line. A) The backbone plasmid pLIS0185 carries the ampicillin resistance cassette (ampR, dark blue), the *E. coli* origin of replication (ORI, dark blue), *ccp* promoter (red) and a selection cassette (TgDHFR, salmon). **B)** Fragments corresponding to 5'UTR and 5'end of *flp* (pink) were cloned into the backbone through *KpnI, HindIII*, *BsmI* and *SacII* restriction sites.

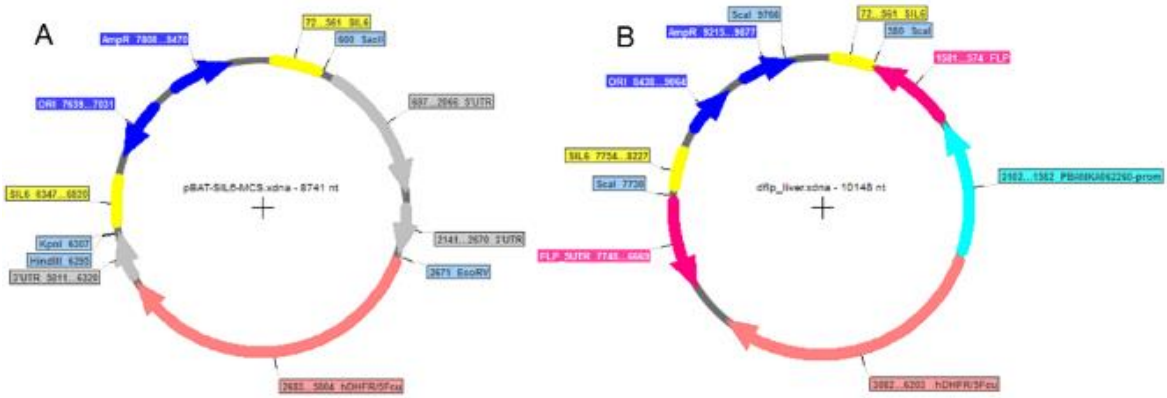

Figure 2.9 Backbone and final plasmids used for generation of *Δflp*$_{liver}$ parasite line. A) The backbone plasmid pBAT-SIL6-MCS carries the ampicillin resistance cassette (ampR, dark blue), the *E. coli* origin of replication (ORI, dark blue), homology arms for integration into a silent locus on chromosome 6 (SIL6, yellow) and a recyclable selection cassette (hDHFR, ScFcy, salmon). **B)** Fragments corresponding to parts of 5'UTR of *flp* (pink), 5'UTR of PBANKA_062260 (cyan) and 5'end of *flp* (pink) were cloned into the backbone using *KpnI*, *HindIII*, *SacII* and *EcoRV* restriction sites.

The pLIS0209 vector (Fig. 2.10A), generated by Gunnar R. Mair, was used to construct the dflp_gam vector (for generation of *Δflp*$_{gam}$ parasite line). The vector carries an ampicillin resistance

cassette, a hHDFR resistance cassette, which can be used to select for parasites that carry the cassette by Pyrimethamine selection and *clag* promoter. Fragments corresponding to the 5'UTR (1021 bp, primers #22 and #23) and 5'end of *flp* (558 bp, primers #32 and #33) were PCR amplified from genomic DNA and cloned into the open backbone using *KpnI* and *HindIII* and *EcoRV* and *AatII* restriction sites, respectively. The final vector (Fig. 2.10B) was linearized using the *KpnI* and *AatII* restriction sites and used for transfection. All primer sequences are listed in chapter 2.1.6.1.

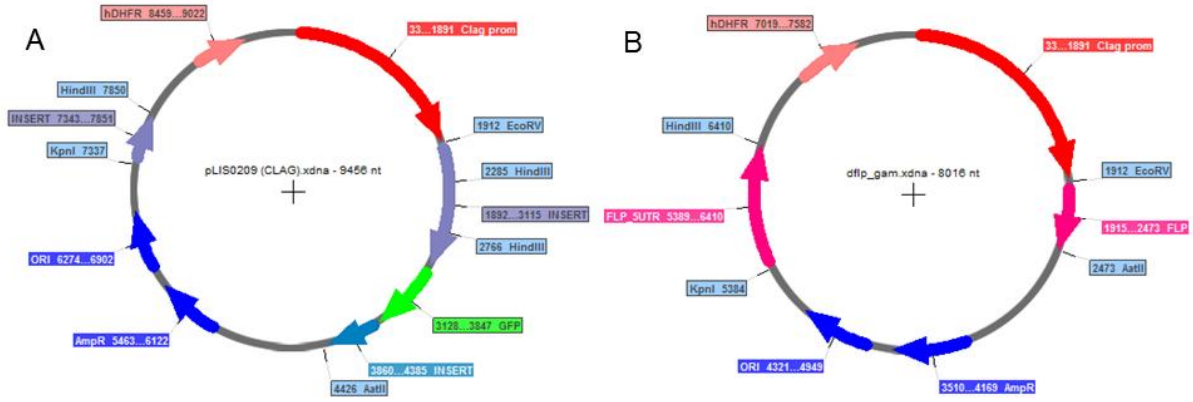

Figure 2.10 Backbone and final plasmids used for generation of *Δflp$_{gam}$* parasite line. A) The backbone plasmid pLIS0185 carries the ampicillin resistance cassette (ampR, dark blue), the *E. coli* origin of replication (ORI, dark blue), *clag* promoter (red) and a selection cassette (hDHFR, salmon). **B)** Fragments corresponding to 5'UTR and 5'end of *flp* (pink) were cloned into the backbone using *KpnI, HindIII*, *BsmI* and *SacII* restriction sites.

The g377_mCherry vector (used for generation of *flp::HA; g377::mCherry* parasite line) was generated by Gunnar R. Mair. In brief, fragment corresponding to 3'end of *g377* without the stop codon (1479 bp) was cloned upstream of an *mCherry* tag (Fig. 2.11A). Vector was linearized using the *BstZ17I* restriction site and used for transfection.

The pplp2_mCherry vector (used for generation of *flp::HA; pplp2::mCherry* parasite line) was generated by Gunnar R. Mair. In brief, fragment corresponding to 3'end of *pplp2* without the stop codon (1440 bp) was cloned upstream of an *mCherry* tag (Fig. 2.11B). Vector was linearized using the *PmeI* restriction site and used for transfection. All primer sequences are listed in chapter 2.1.6.1.

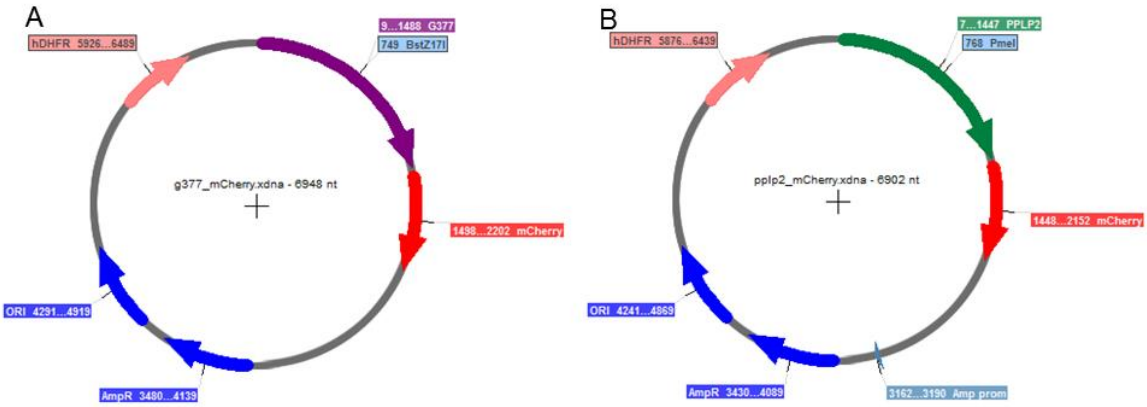

Figure 2.11 Final plasmids used for generation of *flp::HA;g377::mCherry* and *flp::HA;pplp2::mCherry* parasite lines. A) The plasmid carries the ampicillin resistance cassette (ampR, dark blue), the *E.coli* origin of replication (ORI, dark blue), a selection cassette (hDHFR, salmon) and *mCherry* (red). Fragment corresponding to 3'end of *g377* (purple) was cloned into the backbone. **B)** The plasmid carries the ampicillin resistance cassette (ampR, dark blue), the *E.coli* origin of replication (ORI, dark blue), a selection cassette (hDHFR, salmon) and *mCherry* (red). Fragment corresponding to 3'end of *pplp2* (green) was cloned into the backbone.

2.1.10.2 Linear PlasmoGEM vectors

The PlasmoGEM project has brought a substantial improvement in the field of *Plasmodium berghei* genetic manipulation. Sanger Institute in London, offers a large library of linear vectors (based on pJAZZ vector [170]) that can be used for manipulation of *Plasmodium berghei* and show high transfection efficiencies thanks to very long homology arms [171,172].

The intermediate tagging vector for *flp* (PGEM-049911, Fig. 2.12A) was used to generate the flp_iLOV vector (for generation of *flp::iLOV* parasite line). The vector carries ampicillin resistance cassette (not shown), long homology arms for the *flp* locus and an intermediate cassette with zeocin resistance cassette surrounded by Gateway attR sites. We generated the final vector using a Gateway reaction between the intermediate vector and a circular plasmid carrying the final cassette (which carries hDHFR/yFCU recyclable cassette that can be used to select for parasites that carry the cassette by Pyrimethamine selection and afterwards for parasites that recycled the cassette (via 3'UTR homology regions) by 5' fluorocytosine selection [169].) surrounded by Gateway attL sites (Fig. 2.12B). The final vector (Fig. 2.12C) was linearized using the *NotI* restriction sites and used for transfection.

The final tagging vector for *flp* (PGEM-049911, Fig. 2.13A) was used for generation of *flp::HA* parasite line. The vector carries ampicillin resistance (not shown), long homology arms for the *flp* locus and a final cassette (which carries triple HA tag and hDHFR/yFCU recyclable cassette that can be used to select for parasites that carry the cassette by Pyrimethamine selection and afterwards for parasites that recycled the cassette (via 3'UTR homology regions) by 5' fluorocytosine selection [169]). The vector was linearized using the *NotI* restriction site and used for transfection.

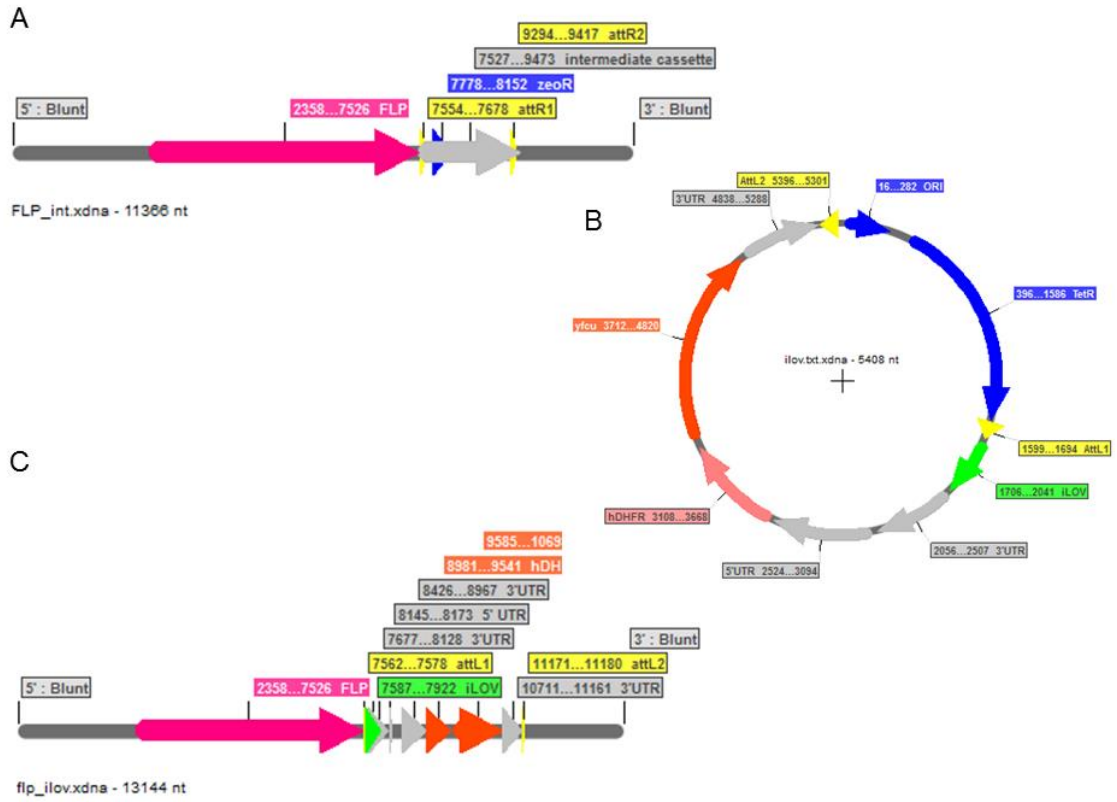

Figure 2.12 Backbone, cassette and final plasmids used for generation of *flp::iLOV* parasite line. A) The intermediate plasmid for *flp* tagging carries the zeocin resistance cassette (zeoR, dark blue), homology arms for integration into the *flp* locus (pink and dark grey) and Gateway attR sites (yellow). **B)** The iLOV final cassette plasmid carries tetracycline resistance cassette (TetR, dark blue), *E. coli* origin of replication (ORI, dark blue), a recyclable selection cassette (hDHFR, ScFcy, salmon), *iLOV* (green) and Gateway attL sites (yellow). **C)** Final plasmid for *flp* iLOV-tagging carries *iLOV* sequence fused to *flp* sequence followed by the resistance cassette.

The final knock-out vector for *flp* (PGEM-120990, Fig. 2.13B) was used for generation of *Δflp* parasite line. The vector carries ampicillin resistance (not shown), long homology arms for the *flp*

locus and a final cassette (which carries triple HA tag and hDHFR/yFCU recyclable cassette that can be used to select for parasites that carry the cassette by Pyrimethamine selection and afterwards for parasites that recycled the cassette (via 3'UTR homology regions) by 5' fluorocytosine selection [169]). The vector was linearized using the *NotI* restriction site and used for transfection.

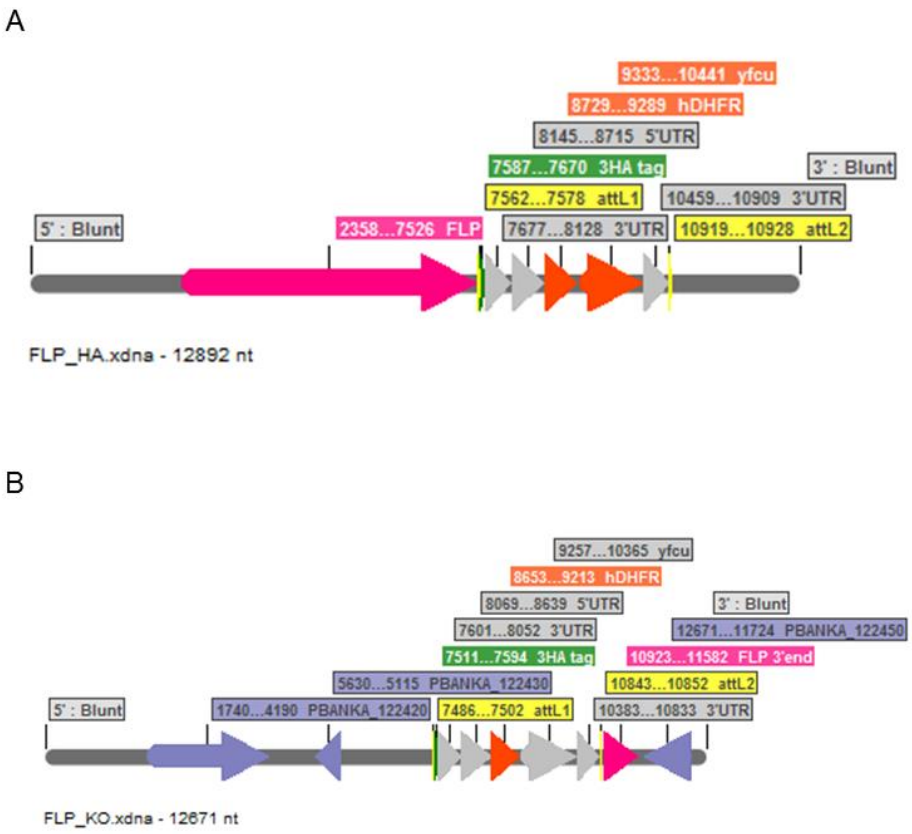

Figure 2.13 Final plasmids used for generation of *flp::HA* and *Δflp* parasite lines. A) The final plasmid for *flp* tagging carries long homology arms for integration into the *flp* locus (pink and dark grey) and the final cassette (with triple HA tag (green) and a recyclable selection cassette (hDHFR, ScFcy, salmon)) and Gateway attL sites (yellow). **C)** The final plasmid for *flp* knock-out carries long homology arms for integration into the *flp* locus (pink and dark grey) and the final cassette (with triple HA tag (green) and a recyclable selection cassette (hDHFR, ScFcy, salmon)) and Gateway attL sites (yellow).

2.2 Methods

2.2.1 Molecular biology

2.2.1.1 Isolation of RNA and cDNA preparation

Parasite material was isolated as described in chapter 2.2.3. RNA was isolated using the RNeasy Mini kit and DNA was digested in samples using Turbo DNA free kit. Concentration was measured by absorbance at 260 nm (A260) measurement using the Biophotometer. Up to 500 µg of RNA in 10 µl was used to reverse transcribe cDNA using the First strand cDNA synthesis kit. Each cDNA production was performed in duplicates – sample and a control lacking reverse transcriptase (-RT). Both cDNA samples were tested by Taq PCR (chapter 2.2.1.4) with aldolase primers (a housekeeping gene expressed by all parasite stages). Only samples positive for aldolase and with negative -RT control were used further.

2.2.1.2 Quantitative PCR

Parasite cDNA was added as a template into Power SYBR Green PCR Master mix along with primers (final concentration 400nM). Samples were analysed in MicroAmp Optical 96-well reaction plate in triplicates, -RT control of the sample with the highest cDNA concentration and H_2O were used as controls. qPCR was performed using the ABI 7500 Real-Time PCR System and calculated with comparative C_T method accounting for primer efficiency (chapter 2.2.1.2.1). All primer sequences are listed in chapter 2.1.6.2.

2.2.1.2.1 Primer efficiency

Serial dilution of parasite gDNA was added as template into Power SYBR Green PCR Master mix along with primers (final concentration 400nM). Samples were analysed in MicroAmp Optical 96-well reaction plate in triplicates, H_2O was used as control. qPCR was performed using the ABI 7500 Real-Time PCR System. C_T values were plotted as function of gDNA concentration and five values best fitting the linear regression function were used to calculate the slope. Primer efficiency was calculated as 10^(-1/slope) and used for comparative C_T calculations. All primer sequences are listed in chapter 2.1.6.2.

2.2.1.3 3’ RACE

RNA was isolated from parasite samples as described in chapter 2.2.1.1. Afterwards, *flp* specific forward primers and polyT and adapter reverse primers (500nM) were used to produce cDNA (2mM dNTPS, 20mM Tris, 50mM KCl, 25mM $MgCl_2$, 10 units of SuperScript reverse transcriptase, 3’RACE System for Rapid Amplification of cDNA ends). The produced cDNA was used as a template in a standard Taq PCR reaction (chapter 2.2.1.4) with adapter and nested *flp* primers. All primer

sequences are listed in chapter 2.1.6.2. Both products (cDNA and PCR fragment) were analysed by agarose electrophoresis (chapter 2.2.1.9) and cloned into pGEM vectors using a kit from Promega. Briefly, purified PCR fragments (50 ng) were added as inserts into ligation mix, incubated for 1 hour at room temperature and used to transform bacteria. Transformed bacteria were plated onto X-gal LB plates and white colonies (in which the lac operon was interrupted by insert) were tested for insert presence and used for sequencing.

2.2.1.4 PCR and RT-PCR

PCR was performed in 10–50 µl reactions using the Taq polymerase (genotyping, colony PCR, RT-PCR and plasmid testing) or Phusion polymerase (fragments for cloning and problematic genotyping reactions). Taq reaction contained: 750mM Tris, 200mM $(NH_4)_2SO_4$, 1.5mM $MgCl_2$, 0.1% Tween 20, 1.5–5 units of Taq polymerase, 2mM dNTPs and 1mM primers. PCR was performed in a PCR cycler with initial denaturation (94°C, 3 minutes), 30 cycles of denaturation (94°C, 30 seconds), annealing (usually 55°C, 40 seconds) and synthesis (60°C, 0.5-7 minutes) and final synthesis phase (60°C, 7-20 minutes). Phusion reaction contained: 1x GC buffer, 0.4–4 units of Phusion, 2mM dNTPs and 1mM primers. PCR was performed in a PCR cycler with initial denaturation (98°C, 30 seconds), 30 cycles of denaturation (98°C, 10 seconds), annealing (usually 58°C, 30 seconds) and synthesis (68°C, 0.5-7 minutes) and final synthesis phase (68°C, 7-20 minutes). Plasmids, gDNA or cDNA were used as templates. All primer sequences are listed in chapters 2.1.6.1 and 2.1.6.2. PCR products were analysed by agarose electrophoresis (chapter 2.2.1.9). For further use, fragments were purified using the QIAquick PCR Purification Kit or cut from a gel and purified by the QIAquick Gel Extraction Kit. DNA concentration was measured by absorbance at 260 nm (A260) measurement using the Biophotometer.

2.2.1.4.1 Colony PCR

Colony PCR was performed in 20 µl reactions using the Taq polymerase. Bacterial colonies were reinoculated on fresh LB plates and residual bacteria were transferred directly into PCR reaction using a tip. Reaction contained: 750mM Tris, 200mM $(NH_4)_2SO_4$, 1.5mM $MgCl_2$, 0.1% Tween 20, 1.5–5 units of Taq polymerase, 2mM dNTPs and 1mM primers. PCR was performed in a PCR cycler with initial denaturation (94°C, 10 minutes), 30 cycles of denaturation (94°C, 30 seconds), annealing (usually 55°C, 40 seconds) and synthesis (60°C, 0.5-3 minutes) and final synthesis phase (60°C, 7-12 minutes). PCR products were analysed by agarose electrophoresis (chapter 2.2.1.9).

2.2.1.5 Plasmid isolation

Bacteria grown overnight in a liquid medium (37° C, shaking at 200 rpm) were spun (2879 G, 10 min) and pellets were frozen down at -20° C or directly used to isolate plasmid DNA with the

QIAprep Spin Plasmid Miniprep Kit. Plasmid DNA concentration was measured by absorbance at 260 nm (A260) measurement using the Biophotometer.

2.2.1.6 DNA digest

For cloning steps, 1–3 µg of plasmid DNA or 0.5–2 µg of purified PCR product were mixed with 10–40 units of restriction enzyme(s) and corresponding buffer and kept overnight at 37° C in an incubator or at the recommended temperature in a heating block. To prevent re-ligation of the digested plasmid, 10 units of alkaline phosphatase were added for the last hour of digest. Digested plasmid DNA was checked by agarose electrophoresis (chapter 2.2.1.9) and purified using the QIAquick Gel Extraction Kit. Digested PCR product was purified using the QIAquick PCR Purification Kit. DNA concentration was measured by absorbance at 260 nm (A260) measurement using the Biophotometer. For digest prior to transfection, >10 µg of plasmid DNA was mixed with 30 units of restriction enzyme(s) and kept overnight at 37°C in an incubator or at the recommended temperature in a heating block. For plasmid verification, 100 ng of plasmid DNA was mixed 5 - 10 units of restriction enzyme(s) and corresponding buffer and incubated for 2 – 3 hours at 37°C in an incubator or at the recommended temperature in a heating block. Digested plasmid DNA was checked by agarose electrophoresis (chapter 2.2.1.9).

2.2.1.7 Ligation

Purified DNA fragments (plasmid and PCR product(s)) were mixed in a molar ratio of 1:3 (1:2 for long inserts and 1:5 for short inserts), 400 units of T4 DNA ligase and T4 DNA ligase buffer were added. Reaction with no insert was used as control. Reactions were incubated overnight in a box of slowly melting ice/water mix and used to transform bacteria.

2.2.1.8 Gibson assembly

Purified DNA fragments (plasmid and PCR product(s)) were mixed in a molar ratio of 1:3 (1:2 for long inserts and 1:5 for short inserts) in a 5 µl sample. DNA was mixed with 5 µl of Gibson assembly enzyme mix and incubated in a PCR cycler (2 hours, 40° C). Afterwards, DNA was diluted 1:3 and used to transform bacteria.

2.2.1.9 Agarose electrophoresis

Solution of 1%-2% agarose in TAE buffer was dissolved while boiling. After cooling down, ethidium bromide was added (75 ng/ml) and gel solidified in electrophoresis chamber with combs. DNA samples supplemented with loading dye were loaded into pockets and voltage of 100 V was applied for 30–60 minutes. Gels were analysed with UV transilluminator and imaged with a camera. For further use, DNA was extracted from the gel using the QIAquick Gel Extraction Kit.

2.2.1.10 Ethanol DNA precipitation

Plasmid DNA digested for transfection (chapter 2.2.1.6) was precipitated by adding 2.5 volume of 100% EtOH and 0.1 volume of 3M NaAc (pH 5.2). The sample was incubated at -80° C for at least 30 minutes, spun (maximum speed, 4° C, 30 minutes), 500 µl of 70% EtOH was added, sample was spun again (maximum speed, 4° C, 5 minutes). Ethanol was removed by pipetting and evaporation, DNA was resuspended in 15 µl of ddH_2O, DNA concentration was measured by absorbance at 260 nm (A260) measurement using the Biophotometer. Digested plasmid was analysed by agarose gel (chapter 2.2.1.9).

2.2.1.11 Isolation of genomic DNA

Mixed asexual blood stages were purified as described in chapter 2.2.3.7.1. Genomic DNA was isolated using the QIAamp DNA Blood Kit and concentration was measured by absorbance at 260 nm (A260) measurement using the Biophotometer.

2.2.1.12 Gateway reaction

Intermediate plasmid (90 ng) and a plasmid carrying final cassette (25 ng) were mixed with the LR clonase enzyme (1.5 µl) and 1x clonase buffer. Mixture was incubated overnight in a PCR machine (25°C), treated with proteinase K (0.5 µl added, 37°C, 10 minutes), dialyzed against ddH_2O (RT, 1 hour) and electroporated into BigEasy-TSA Electrocompetent bacteria. Bacteria were inoculated onto YEG-Cl agar plates, incubated overnight (37°C) and colonies were tested by colony PCR (chapter 2.2.1.4.1).

2.2.1.13 Sequencing

Purified plasmid (2 µg) or PCR fragments (1 µg) in 20µl sample were sent for sequencing by GATC along with a 20µl sample of 10 µM primer.

2.2.1.14 Western blotting

Proteins were lyzed in RIPA buffer - 20 minutes incubation on ice with vortexing, spinning (maximum speed, 4°C, 5 min) and protein lysates were stored at -80°C. In protein expression experiments, bacterial lysates were generated as described in chapter 2.2.2.4. Protein lysates were mixed with Laemmli buffer and boiled for 5 minutes (10–15 minutes for bacterial pellets). Samples were loaded on a BisTris gradient gel (4-12%) and voltage of 150 V was applied until the gel front reached the bottom of the gel. Gel was incubated in transfer buffer along with methanol-activated PVDF membrane. Blotting sandwich was assembled from sponges, Whatman papers, PVDF membrane and the gel. Wet transfer was performed in the apparatus filled with transfer buffer at 30 V for 3 hours. Membrane was blocked in 5% milk in TBST for (1 hour, room temperature, rotator). Afterwards, primary antibody diluted in 5% milk in TBST was added and

membrane was incubated overnight at 4° C on a rotator. After three washing steps in TBST (10 minutes, room temperature, rotator), secondary antibody diluted in 5% milk in TBST was added (1 hour, room temperature, rotator). After three washing steps in TBST (10 minutes, room temperature, rotator), protein ladder was visualized with WesternSure pen and ECL was added to induce peroxidase reaction (5 minutes, room temperature, rotator). Membrane was scanned using the LiCor C-DiGit Blot Scanner and figures were processed using Image Studio. All antibodies and used concentrations are listed in chapter 2.1.7.

2.2.1.15 Immunofluorescence assay (IFA)

2.2.1.15.1 IFA of blood stages

Blood with mixed blood stages (chapter 2.2.3.7.1) or enriched schizonts (chapter 2.2.3.7.2) were fixed in fixing buffer. For activated gametocytes, blood was first incubated in an ookinete medium (15 – 20 min, room temperature, rotator) and fixed in fixing buffer. Samples were kept at 4° C or directly permeabilized with permeabilization buffer (20 min, room temperature, rotator). Samples were blocked in 10% FCS/PBS (1 hour, room temperature, rotator) and stained with primary antibody diluted in 10% FCS/PBS (1 hour, room temperature, rotator). Afterwards, samples were washed three times in 1% FCS/PBS (15 minutes, room temperature, rotator), stained with secondary antibody (1 hour, room temperature, rotator), washed twice in 1% FCS/PBS and once in 1% FCS/PBS supplemented with Hoechst (15 minutes, room temperature, rotator). Finally, samples were resuspended in PBS and stored at 4° C until imaging. All antibodies and used concentrations are listed in chapter 2.1.7. Samples were imaged using Confocal spinning disc microscope Nikon Eclipse TI-E or Widefield light miscroscope Axiovert 25, images were processed in FIJI and in some cases deconvolved in AutoQuant X3.

2.2.1.15.2 IFA of liver stages

Liver stages were cultured as described in chapter 2.2.3.6. At designated time points, cultures were fixed with ice cold methanol (20 minutes, room temperature, sterile hood), washed twice with 1% FCS/PBS and blocked with 10% FCS/PBS (30 minutes at 37° C or overnight at 4° C). Samples were stained with primary antibody diluted in 10% FCS/PBS (1 hour at 37° C), washed three times with 1% FCS/PBS, stained with secondary antibody (1 hour at 37° C, for the last 5 minutes Hoechst was added) and washed three times with 1% FCS/PBS. Samples were mounted using 30% glycerol, sealed with nail polish and kept at 4° C until imaging. All antibodies and used concentrations are listed in chapter 2.1.7. For size measurement, fifty images per well were taken using Widefield light microscope Axiovert 25 and liver stage size was measured in FIJI. Liver stage numbers were counted by hand using Fluorescence microscope.

2.2.1.15.3 Gliding assay

Sporozoites were purified as described in chapter 2.2.3.5. To precoat the surface with BSA (bovine serum albumin), 8 well slide was incubated with 3% BSA/RPMI (20 minutes, 37° C). Ten thousand isolated sporozoites in 20 µl of 3% BSA/RPMI was pipetted onto the coated wells and incubated (20–30 minutes, 37° C). Afterwards, medium was carefully removed, and samples were fixed with 4% PFA/PBS (15 minutes, room temperature). Samples were washed twice with 1% FCS/PBS and blocked with 10% FCS/PBS (30 minutes, 37 ° C). Sporozoites and their trails were stained with anti-CSP antibody diluted in 10 % FCS/PBS (1 hours, 37° C), washed three times with 1% FCS/PBS, stained with secondary antibody diluted in 10% FCS/PBS (1 hours, 37° C) and washed three times with 1% FCS/PBS. Afterwards, samples were mounted with 30% glycerol and sealed with nail polish and stored at 4° C until analysis. All antibodies and used concentration are listed in chapter 2.1.7. Samples were analysed by hand using Fluorescence microscope. Gliding capability of sixty sporozoites per well was assessed as gliders (one or more circles) or non-gliders (no or less than one circle).

2.2.1.15.4 Invasion assay

HuH7 cells were infected with sporozoites as described in chapter 2.2.3.6. Sporozoites were allowed to invade for two hours and cultures were fixed with 4% PFA/PBS (20 minutes, room temperature, sterile hood). Samples were blocked in 10% FCS/PBS (1 hour at 37° C) and stained with anti-CSP antibody diluted in 10% FCS/PBS (1 hour at 37° C). Afterwards, samples were washed three times with 1% FCS/PBS and stained with secondary antibody (anti-mouse conjugated to Alexa 488) diluted in 10% FCS/PBS (1 hour at 37° C) and washed three times with 1% FCS/PBS. Next, samples were permeabilized (to allow staining of intracellular sporozoites) with ice cold methanol (20 minutes, room temperature). Samples were blocked again in 10% FCS/PBS (1 hour at 37° C) and stained with anti-CSP antibody diluted in 10% FCS/PBS (1 hour at 37° C). Afterwards, samples were washed three times with 1% FCS/PBS and stained with secondary antibody (anti-mouse conjugated to Alexa 546) diluted in 10% FCS/PBS (1 hour at 37° C, for 5 last minutes Hoechst was added) and washed three times with 1% FCS/PBS. Finally, samples were mounted using 30% glycerol, sealed with nail polish and stored at 4° C until imaging. Samples were imaged using the Widefield light microscope Axiovert 25. At least fifty sporozoites per well were imaged and their invasion status was assessed. Invaded (red staining only) and non-invaded (red and green staining) sporozoites were counted.

2.2.2 Microbiology

2.2.2.1 Production and transformation of chemocompetent *E. coli*

Chemocompetent XL1 blue bacteria were inoculated from a master stock into 5 ml of LB medium supplemented with tetracycline and grew overnight (37° C, shaking at 200 rpm). Bacterial culture was diluted into 200 ml of LB medium supplemented with tetracycline to OD_{600} = 0.1. Culture was incubated (37° C, shaking at 200 rpm) until OD_{600} = 0.48. Bacteria were incubated on ice (15 mins), spun (2879 G, 4° C, 7 min) and resuspended in 80 ml of Tbf I buffer. Bacteria were incubated on ice (15 mins), spun (2879 G, 4° C, 7 min), resuspended in 8 ml of Tbf II buffer and incubated on ice (15 mins). Bacteria were aliquoted into Eppendorf tubes (50 µl) and were either used directly or frozen in liquid nitrogen and stored at -80° C. For transformation, bacteria were thawed on ice, mixed with DNA (ligation mix, Gibson assembly mix or plasmid) and incubated on ice for 30 mins. Bacteria were transformed by heat shock (30 seconds at 42°C followed incubation on ice for 2 minutes) and diluted in 1 ml LB medium and incubated for 1 hour (37° C, shaking at 200 rpm). Bacteria were inoculated onto LB agar plates with corresponding antibiotic and incubated overnight at 37° C. Successful transformation was tested by colony PCR (chapter 2.2.1.4.1) or by plasmid isolation and control digest (chapter 2.2.1.6).

2.2.2.2 Production and transformation of electrocompetent *E. coli*

Electrocompetent PMC 103 bacteria were inoculated into 10 ml of antibiotic-free SB medium and cultivated overnight (37° C, shaking at 200 rpm). Bacteria were diluted 100 times in 600 ml of antibiotic free SB medium and grew for 3.5 hours (37° C, shaking at 200 rpm). Bacteria were spun (2879 G, 4° C, 10 min), resuspended in 600 ml cold sterile ddH_2O, spun again (2879 G, 4° C, 10 min), resuspended in 600 ml cold sterile ddH_2O, spun again (2879 G, 4° C, 10 min) resuspended in 600 ml cold sterile 10% glycerol, spun again (2879 G, 4° C, 15 min) and resuspended in 1.2ml of 10% glycerol. Bacteria were aliquoted into cold Eppendorf tubes (50 µl, kept on dry ice/EtOH mix) and transferred to -80° C. All manipulations were sterile and on ice. For transformation, bacteria were thawed on ice, mixed with DNA (ligation mix, Gibson assembly mix or plasmid) and 100 µl of 10% glycerol and transferred into an electroporation cuvette. Bacteria were electroporated and immediately transferred into 1ml of warm SOC medium and incubated for 1 hour (37° C, shaking at 200 rpm). Bacteria were inoculated onto LB agar plates with corresponding antibiotic and incubated overnight at 37° C. Successful transformation was tested by colony PCR (chapter 2.2.1.4.1) or by plasmid isolation and control digest (chapter 2.2.1.6).

2.2.2.3 Preparation of bacterial glycerol stocks

Bacteria were inoculated into a liquid medium with antibiotics and grew overnight (37° C, shaking at 200 rpm). 500 µl of the culture was mixed with 500 µl of 30% glycerol in a cryotube and stored at -80° C. For inoculation, a small amount of frozen glycerol stock was scraped with a yellow tip and inoculated into liquid medium.

2.2.2.4 Protein expression

BL21DE3 bacteria transformed with pET28a vectors were inoculated into 5ml of LB medium with kanamycin and incubated overnight (37° C, shaking at 200 rpm). Bacterial culture was diluted in LB medium supplemented with kanamycin to OD_{600} = 0.1. Culture was incubated (37° C, shaking at 200 rpm) until OD_{600} = 0.6. At this point, 1 ml of culture was harvested (not induced sample) and recombinant expression was induced by addition of IPTG to final concentration of 1µM (or 0.1µM - 1µM in optimization experiments). Bacteria were cultivated for additional 4 hours (37° C or 15° C and 20° C in optimization experiments, shaking at 200 rpm). Bacteria were pelleted by centrifugation (2879 G, 4° C, 10 min) and stored at -20° C. For lysis, pellet was thawed on ice and resuspended in a lysis buffer. Suspension was sonicated, incubated (magnetic stirrer or rotator, 20 min, 4° C) and spun (2879 G, 4° C, 10 min). Supernatant was mixed with Laemmli buffer (95° C, 5 min), pellets were resuspended in Laemmli buffer (95° C, 5 min) and analysed on SDS-PAGE and Western blot (chapter 2.2.1.14).

2.2.3 Parasitology

2.2.3.1 Parasitaemia and gametocytonemia

A drop of tail blood from mice infected with parasites was smeared on a glass slide. After the blood film dried, the sample was fixed in methanol (30 seconds, room temperature) and stained in 10% Giemsa dye (25 minutes, room temperature). Parasitaemia (gametocytonemia) was determined using Widefield light microscope Axioskop 40 and counted by hand as number of parasites (gametocytes) per field of view (n = 15) divided by total erythrocytes per field of view (n = 3). Parasitaemia and gametocytonemia were plotted in percent.

2.2.3.2 Exflagellation assay

Drop of tail blood from infected mice was incubated on a glass slide at room temperature for 12 minutes. For digitonin rescue experiments, 5 µl of ookinete medium with or without 0.002% digitonin was added to the sample. Exflagellation was observed using Widefield light microscope Axioskop 40 or imaged using Widefield light microscope Axiovert 25.

2.2.3.3 Ookinete assay

Blood with parasites was collected by heart puncture and 20 million infected red blood cells were injected intraperitoneally into naïve mouse. Three days later, parasitaemia (chapter 2.2.3.1) and exflagellation (2.2.3.2) were analysed. For cross-fertilization assay, mice pairs with similar levels of parasites and gametocytes were matched. Blood was collected by heart puncture and transferred into 12 ml of ookinete medium (for digitonin rescue, medium was supplemented with 0.002% digitonin). Cultures were incubated for 20 hours (19° C, shaking at 25 rpm) and afterwards ookinetes were analysed by blood smear or directly imaged using Widefield light microscope Axiovert 25 or Confocal spinning disc microscope Nikon Eclipse TI-E. Alternatively, ookinetes were enriched over 63% Nycodenz/PBS - culture was layered over Nycodenz cushion and spun (1513 G, 15 min, room temperature). A ring containing ookinetes that established at the Nycodenz/medium interface was collected using a Pasteur pipette. Enriched ookinetes were resuspended in PBS supplemented with Hoechst and were analysed by blood smear or directly imaged using Widefield light microscope Axiovert 25 or Confocal spinning disc microscope Nikon Eclipse TI-E. For cross-fertilization assays, fifty random ookinetes were imaged using Widefield light microscope Axiovert 25 and red or green fluorescence was assessed using FIJI. For ookinete feedings (chapter 2.2.3.4), cultures were spun (404 G, 8 minutes, room temperature) and washed with RPMI medium (to remove digitonin). Cultures were resuspended in 800 µl of prewarmed blood (collected by heart puncture from naïve mice) and offered to mosquitoes in membrane feeder (warmed up to 37° C).

2.2.3.4 Mosquito feeding

Anopheles mosquitoes were fed on anaesthetized mice or using a membrane feeder. For feeding on mice, drop of tail blood from infected mice was analysed in exflagellation assay (chapter 2.2.3.2) for gametocyte presence. Mice were anaesthetized (chapter 2.2.4.1.1). After a few minutes, lack of reflexes was checked, and fully asleep mice were put on mosquito cages with an eye protecting cream. For membrane feeding, ookinete cultures (chapter 2.2.3.3) were resuspended in warm blood from naïve mice. This mixture was applied into parafilm-covered membrane feeders, which were connected to a constant flow of warm water. Membrane feeders were fixed above mosquito cages, so that mosquitoes could feed on the cultures. Mosquitoes were starved by removing the sugar and salt solutions 4 hours prior to feeding. The feeding proceeded for 20 minutes, with two position changes of the mice/feeders to allow all mosquitoes to feed. In case of membrane feeding, unfed mosquitoes were removed one day after feed. Mosquitoes were kept in the insectary incubators (21° C, 80% humidity) for up to 21 days.

2.2.3.5 Isolation of mosquito stages

Mosquitoes were dissected using sterile needles and Stereomicroscope Stemi 2000-C. For ookinetes, mosquito midguts were isolated 18 – 20 hours post feeding, mashed on one side of a glass slide and smeared. For oocyst examination, mosquito midguts were isolated, placed on a glass slide, covered with a cover slip and examined for oocyst presence using Widefield light microscope Axioskop 40. Midgut sporozoites were isolated from mosquito midguts at day 14 post feeding. Midguts were collected in an Eppendorf tube and squished with a micropistill. Mosquito tissues were spun (0.1 G, 3 min, 4° C), leaving the purified sporozoites in supernatant. Salivary gland sporozoites were isolated from mosquito salivary glands at day 17 - 21 post feeding. Salivary glands were collected in an Eppendorf tube and squished with a micropistill. Mosquito tissues were spun (0.1 G, 3 min, 4° C), leaving the purified sporozoites in supernatant.

2.2.3.6 Infection of HuH7 cells

Isolated salivary gland sporozoites were used to infect human hepatoma cell line (HuH7) in 8-well labteks or 24-well plates. HuH7 cells were seeded one day prior to infection (25 000 cells per labtek well, 50 000 cells per 24-well plate well). At the time of infection, cells were washed once with culture medium to remove dead cells. Sporozoites (10 000 in 100 µl for labtek well or 50 000 in 200 µl for 24-well plate well) were diluted in culture medium and put onto cells. Invasion proceeded for two hours in the cell culture incubator. Afterwards, suspension with uninvaded sporozoites was removed and cells were washed twice with culture medium. Cells were cultured with daily supplement of fresh medium for the designated times.

2.2.3.7 Isolation of blood stages

All blood stage parasite material was isolated from infected mice (chapter 2.2.4.1.2).

2.2.3.7.1 Mixed asexual stages

Infected mice were anesthetized and blood with parasites was collected by heart puncture. Blood was diluted in PBS (for RNA isolation, blood was filtered over a CF11 column to remove white blood cells), spun (404 G, 8 min, RT) and erythrocytes were lyzed in 0.2% saponin in PBS. Parasites were spun again (1410 G, 8 min, RT) and used further for gDNA (chapter 2.2.1.11), RNA (chapter 2.2.1.1) or protein (chapter 2.2.1.14) isolation.

2.2.3.7.2 Schizonts

Infected mice were anaesthetized, blood with parasites was collected by heart puncture and immediately transferred into 10 ml of warm medium for overnight culture. Blood was spun (404 G, 8 min, RT), resuspended in 35 ml of warm medium for overnight culture, transferred to a 75 cm^2 culture flask and incubated for 18 hours in a cell culture incubator supplemented with 5% O_2.

Cultures were underlayered with 55% Nycodenz in a Falcon tube and spun (120 G, 25 min, RT) and brown ring at the Nycodenz/medium interface was collected in a fresh tube. Schizonts were spun (404 G, 8 min, RT) and further used for IFA staining (chapter 2.2.1.15.1), RNA (chapter 2.2.1.1) or protein (chapter 2.2.1.14) isolation, transfection (chapter 2.2.3.8) or purification of rings and trophozoites (chapter 2.2.3.7.3).

2.2.3.7.3 Rings and trophozoites

Purified schizonts (chapter 2.2.3.7.2) were intravenously injected in naïve mice. Mice were anaesthetized, blood with parasites was collected by heart puncture at designated time points (5 hours post injection for rings and 17 hours post injection for trophozoites). Blood was filtered over a CF11 column to remove white blood cells, spun (404 G, 8 min, RT) and erythrocytes were lyzed in 0.2% saponin in PBS. Parasites were spun again (1410 G, 8 min, RT) and used for RNA isolation (chapter 2.2.1.1).

2.2.3.7.4 Gametocytes

Infected mice were treated with sulfadiazine in drinking water for 48 – 72 hours (until asexual blood stages were killed as assessed by blood smearing). Mice were anaesthetized, blood with gametocytes was collected by heart puncture, diluted in RPMI medium and spun (404 G, 8 min, RT). Gametocytes were resuspended in RPMI medium, underlayered by 48% Nycodenz in a Falcon tube and spun (1410 G, 15 min, RT) and brown ring at the Nycodenz/medium interface was collected in an Eppendorf tube. Gametocytes were spun (404 G, 8 min, RT) and washed in RPMI several times and further used for RNA (chapter 2.2.1.1) or protein (chapter 2.2.1.14) isolation.

2.2.3.8 Transfection of *Plasmodium berghei*

Parasites were transfected in the schizonts stage, enriched and purified as described in chapter 2.2.3.7.2. Parasite transfection was performed using the AMAXA Human T Cell Nucleofector Kit according to manufacturer's instruction and as described [24]. Transfected parasites were immediately injected intravenously into naïve mice and after one day of recovery, mice were treated with Pyrimethamine in drinking water to select for parasites carrying the *dhfr* cassette. Mice were followed by daily blood smears and after parasitaemia grew over 1 %, mice were anaesthetized and blood with parasites was collected by heart puncture (chapter 2.2.3.7.1). Parasite material was used to isolate gDNA (chapter 2.2.1.11) and PCR genotyping was performed (chapter 2.2.1.4). To obtain a clonal line, transfected parasites were used to infect a mouse and kept under Pyrimethamine selection pressure. When mouse reached parasitaemia of 0.1–1 %, it was anaesthetized and blood with parasites was collected by heart puncture. Blood was serially diluted and aliquots with 1 parasite in 100 µl of RPMI medium were injected into 4 - 10 naïve mice.

Mice (with no drug pressure) were followed by daily blood smears and after parasitaemia reached 1 %, mice were anaesthetized and blood with parasites was collected by heart puncture (chapter 2.2.3.7.1). Parasite material was used to isolate gDNA (chapter 2.2.1.11) and PCR genotyping was performed (chapter 2.2.1.4).

2.2.3.9 Recycling of selection cassette

In order to return the transgenic parasite into a Pyrimethamine-sensitive state, in selected cases (when *dhfr* cassette contained *yfcu* gene for negative selection), the *dhfr* cassette was recycled. For this, mouse was infected with clonal parasite line and after reaching 1% parasitaemia, mice were treated with 5'fluorocytosine in drinking water. After parasitaemia recovered and reached 0.5 %, the mouse was anaesthetized and blood with parasites was collected by heart puncture (chapter 2.2.3.7.1). Blood was serially diluted and aliquots with 1 parasite in 100 µl of RPMI medium were injected into 4 naïve mice. Mice (with no drug pressure) were followed by daily blood smears and after parasitaemia reached 1 %, mice were anaesthetized and blood with parasites was collected by heart puncture (chapter 2.2.3.7.1). Parasite material was used to isolate gDNA (chapter 2.2.1.11) and PCR genotyping was performed (chapter 2.2.1.4).

2.2.3.10 Cryopreservation of parasites

Blood was collected by heart puncture (chapter 2.2.3.7.1) from infected mice with parasitaemia of 1–3 %, aliquoted with two volumes of Alsever's solution with glycerol and immediately transferred into and stored in liquid nitrogen tanks.

2.2.4 Animal experiments

2.2.4.1 Maintenance of mice

Eight weeks old mice were kept in Makrolon cages type II in the central animal facility of the University of Heidelberg (Interfakultaere Biomedizinische Forschungseinrichtung). Mice were kept at constant room temperature of 22°C and 50-60% humidity with a 12/12 hours light/dark cycle. Animals were fed with standard dry pellet food.

2.2.4.1.1 Anaesthesia

Prior to mosquito feeding, mice were anaesthetized by intraperitoneal injection of ketamine/xylazine (100 µl/25 g). Eyes were covered with eye cream to prevent drying and mice were covered with paper tissues to reduce heat loss. Anaesthetized mice were offered to pre-starved mosquitoes (chapter 2.2.3.4).

2.2.4.1.2 Parasite infection

Mice were infected with asexual blood stages or sporozoites. Asexual blood stages were from cryopreserved samples (chapter 2.2.3.10) or collected from another mouse by heart puncture (2.2.3.7.1). Blood was injected intraperitoneally or intravenously into a naïve mouse. Isolated salivary gland sporozoites (chapter 2.2.3.5) were injected intravenously into a naïve mouse. For infection by bite, ten infected mosquitoes were transferred one day prior to the experiment into a separate cage. Mice were anesthetized (chapter 2.2.4.1.1) and offered to pre-starved mosquitoes for 15 minutes.

2.2.4.2 Mosquito breeding

All mosquito developmental stages (eggs, larvae, pupae and newly hatched adults) were bred in trays filled with salt solution, supplemented with cat pelleted food and covered with nets. Eggs were collected into glass dishes with filter paper and salt solution overnight from mosquitoes 3–7 days post blood meal. Eggs were washed with 70% ethanol and salt solution prior to transferring to the trays. All stages developed at 28° C and 80% humidity. Hatched adults were transferred into cages and fed with sugar and salt solution soaked into cotton pads. After infectious blood meal (chapter 2.2.3.4), mosquitoes were transferred to the insectary incubators (21° C, 80% humidity).

2.2.3 Cell biology

2.2.3.1 Cultivation of HuH7 cells

Human hepatoma cells (HuH7) were cultured in a complete culture medium in a cell culture incubator (5% CO_2, 37° C) and handled in a sterile cell culture hood. Cells were grown to confluency and then washed with serum-free HBSS medium, trypsinized, washed with complete culture medium and introduced into a culture flask (10–30% confluency) or counted and seeded in a lab tek or 24 well plate (chapter 2.2.3.6).

2.2.4 Microscopy and image processing

All imaging was done using Widefield light microscope Axiovert 25 or Confocal spinning disc microscope Nikon Eclipse TI-E. All microscopy samples to be compared were analysed with the same acquisition conditions. Data were processed in FIJI (contrast and brightness adjustment, assigning of artificial colours) and in some cases in AutoQuant X3 (deconvolution).

2.2.5 Statistical analysis

Experiments were performed in biological triplicates unless stated otherwise. All statistical analysis was performed in GraphPad Prism. T-test was used to compare two data sets with n > 50

and normal distribution. Mann-Whitney (a non-parametric t-test) was used to compare two sets of data with $n < 6$. Significance was concluded if $p < 0.05$.

3 Results

Ferlin-like protein (FLP) is conserved in *Plasmodium* but also other apicomplexans. Evidence from our laboratory shows that *P. falciparum* FLP might be a promising immune target [161]. Transcripts of *flp* are highly upregulated in irradiated sporozoites used for vaccination (Frank *et al.*, unpublished) and antibodies from malaria semi-immune adults bind to FLP (Heiss *et al.*, unpublished).

In this study, we focused on FLP function in the murine malaria parasite *Plasmodium berghei*. Function of ferlins in unicellular organisms is completely unknown. Our three main aims were to investigate expression during the life cycle, localization in the parasite and depletion phenotype.

Preliminary data from our laboratory showed that FLP interacted in the yeast-two-hybrid system with UIS4, a liver-specific PVM-resident protein (Sabine Fraschka, master thesis). Based on this data, we expected to detect *flp* expression during the liver stage and potentially localizing to the PVM. PVM is a highly dynamic structure [173] and in order to capture the dynamics of FLP localization, our main aim was to tag it fluorescently for *in vivo* imaging. Christina Schulte-Huxel (master thesis) and Roland Frank (unpublished) made the first attempts to knock *flp* out. Their attempts were not successful, indicating that FLP might play an essential role during the asexual blood stage (the only permissive stage for transgenic manipulations). Based on this evidence, we planned several parallel approaches to deplete FLP, namely gene knock-out, protein truncation, conditional knock down and promoter swapping.

3.1 Expression and localization study

An important question when studying a protein from a parasite with a complex life cycle is the identification of stages of interest for the study. We aimed at analysing the expression profile of *flp* during the life cycle on both the transcript (chapter 3.1.1) and protein levels (chapters 3.1.2 and 3.1.4). Important hints for studying a gene function can be gained from its subcellular localization. In order to analyse localization of FLP during the parasite life cycle, we set out two aims, preparation of polyclonal antibody targeting the protein directly (chapter 3.1.2) and endogenous fusion of the protein to a tag (chapters 3.1.3 and 3.1.4).

3.1.1 Transcriptional profiling

To gain an idea about *flp* expression dynamics during the parasite life cycle, we isolated RNA from accessible life cycle stages and used quantitative PCR (qPCR) to assess *flp* transcript abundance.

Ferlin, the second member of the ferlin protein family in *P. berghei*, is topologically highly similar to FLP and might therefore fulfil redundant functions. To gain a full picture about ferlin family transcriptional levels, we also analysed ferlin transcript abundance. The profile (Fig. 3.1) revealed that both genes are expressed in relatively high levels during the asexual blood stages. Interestingly, *flp* but not *ferlin* transcription peaks during the gametocyte stage. Mosquito stages have rather low *flp* transcript levels, suggesting that the gene does likely not play a role during parasite development in the vector, while *ferlin* transcripts were present. In contrast, the liver stage, especially at later time points of intrahepatic development, shows highly abundant *flp* and *ferlin* levels. This indicates that both *flp* and *ferlin* are functionally involved during the asexual blood stages, which is in agreement with our own data (chapter 3.2.1) and a recent screening of *P. berghei* genes [174]. Additionally, the profile identifies the gametocyte and liver stages for possible *flp* functional role.

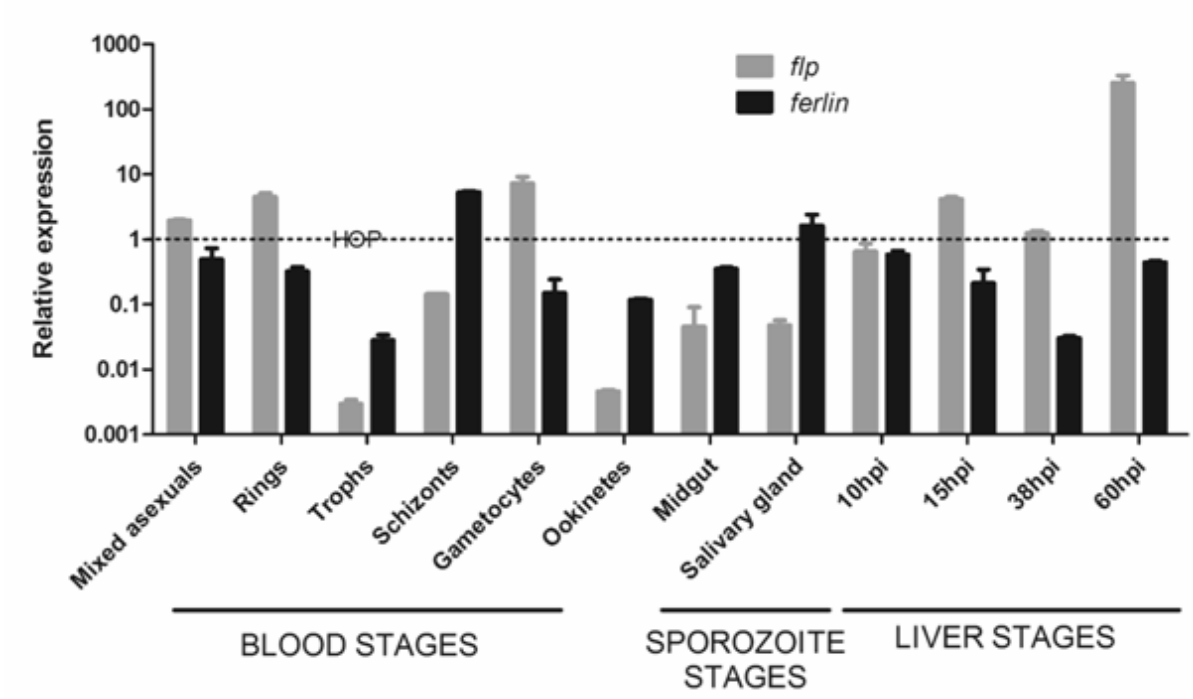

Figure 3.1 Transcriptional profile of *flp* and *ferlin* during the parasite life cycle. Transcripts of both genes are detected in asexual blood stages and liver stages. *Flp* transcription peaks in the gametocyte stage. *Ferlin* is additionally detected in mosquito stages. RNA was isolated from accessible life cycle stages, retro-transcribed into cDNA and used for qPCR. Liver stages were cultured *in vitro* (HuH7 cells). *HOP* was used as housekeeping gene for all stages (dashed line). Profiles were calculated using comparative Ct method. Pooled results from 3 biological replicates are plotted as mean ± SEM.

3.1.2 Preparation of antibody

Although the transcriptional profiling was useful for the identification of stages of interest for the *flp* study, post-transcriptional and translational regulations can lead to discrepancies in transcript and protein abundance. Also, assessing localization, which can reveal important hints regarding protein function, is dependent on protein visualization. We first aimed at visualizing FLP with a polyclonal antibody directed against recombinantly expressed parts of FLP in *E. coli*.

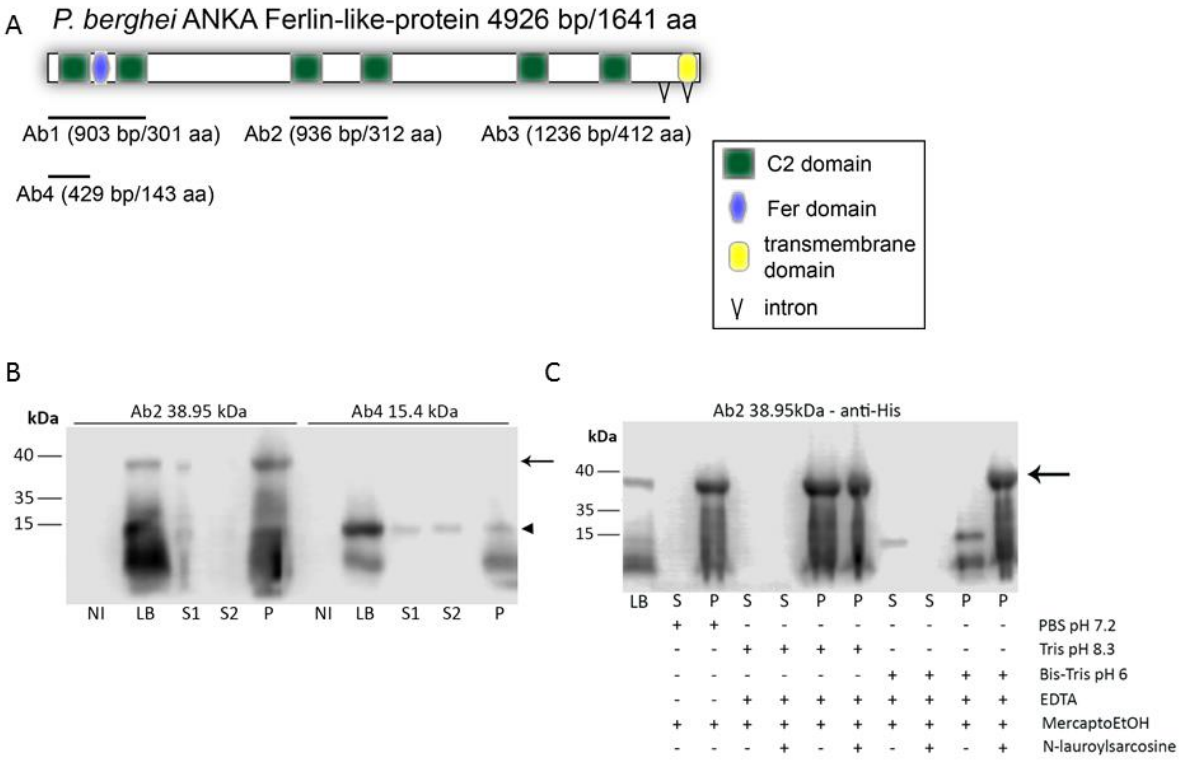

Figure 3.2 Recombinant proteins based on FLP parts are not soluble. A) Schematic of FLP topology with marked fragments designed for recombinant expression in *E. coli*. **B)** His-tag detection of recombinant proteins (Ab2 – 38.95 kDa, arrow and Ab4 – 15.4 kDa, arrowhead) in a Western blot of bacterial lysates generated with standard lysis buffers. Recombinant proteins can mostly be detected in the insoluble (pellet, P) fraction. S = soluble fraction of the lysate, LB = bacteria directly lysed in Laemmli buffer, NI = not induced control bacteria. **C)** His-tag detection of recombinant protein (Ab2 – 38.95 kDa, arrow) in a Western blot of bacterial lysates generated with a panel of lysis buffers. Recombinant protein can only be detected in the insoluble fractions (pellet, P). S = soluble fraction of the lysate, LB = bacteria directly lysed in Laemmli buffer.

Being a large transmembrane protein, the entire FLP sequence is very challenging to be cloned and expressed recombinantly. Instead, together with Marcel Deponte, we designed four fragments based on structural predictions within the FLP sequence (Fig. 3.2A). The fragments

length ranging from 429 to 1236 bp seemed suitable for cloning and expression. Fragments Ab1, Ab2 and Ab4 were PCR amplified from genomic DNA and successfully cloned into pET28a vector, which allows for fusion to a cleavable N-terminal His tag. Fragment Ab3 corresponds to an *flp* region, which harbours an intron (Fig. 3.2A). Attempts to PCR amplify this fragment from cDNA were not successful. The three plasmids were transfected into the BL21DE bacteria, which express recombinant proteins upon IPTG induction. Expression of fragments Ab2 and Ab4 was detected using the anti-His tag antibody (Fig. 3.2B), while fragment Ab1 expression was not detected (data not shown). Using the standard lysis conditions, almost all the recombinant protein was detected in the insoluble part of the lysate (Fig. 3.2). We tried to optimize several conditions including the IPTG concentration or incubation temperature during expression. We also designed four alternative lysis buffers in order to optimize solubilization of the recombinant protein. Neither of the optimization, however, led to solubilization of the recombinant protein (Fig. 3.2.C and data not shown).

3.1.3 Fluorescent tagging

An alternative approach for protein visualization is a fusion of the protein of interest to a tag, which can be visualized. In order to minimize the risk of artefacts, we used endogenous tagging of FLP and maintained expression of the fusion protein under the endogenous promoter. Other ferlin homologues typically act in membrane rearrangements [112,119,123,125,149,151]. To make *in vivo* tracking of FLP in similar highly dynamic processes possible, we used fluorescent tagging in our initial approach.

3.1.3.1 *flp::gfp* parasite line

The first method of choice for fluorescent protein tagging is usually C-terminal endogenous fusion to a GFP tag. We constructed a vector for double-crossover homologous recombination strategy for fusion of *gfp* to the 3'end of *flp* (Fig. 3.3A). Two independent transfections did not result in any detectable integration of the vector as shown by PCR genotyping (Fig. 3.3B). The lack of integration can be explained by interference of the fusion with FLP function during the asexual blood stage cycle, by a non-permissible *flp* locus for genetic manipulation or by technical issues.

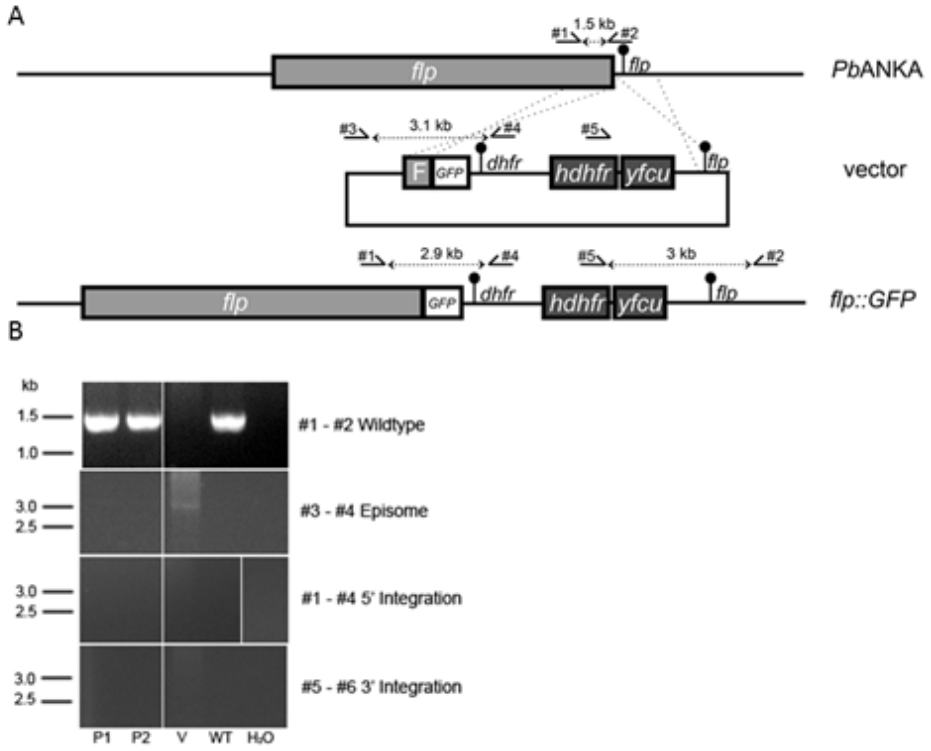

Figure 3.3 *flp* is refractory to endogenous C-terminal tagging with *gfp*. A) Double-crossover strategy was used to target the *flp* locus for homologous recombination. After successful integration, *flp* sequence lacks the stop codon and is fused to *gfp* sequence (which lacks the start codon). Primers used for genotyping bind to sites indicated by arrows. All primer sequences are listed in chapter 2.1.6.2. B) Genotyping with PCR shows that WT locus was maintained in two independently-generated parental lines (P1 and P2) and no integration was observed. Vector used for transfection (V), wildtype parasites (WT) and water (H_2O) were used as controls.

3.1.3.2 *gfp::flp* parasite line

Our next attempt to fluorescently tag FLP targeted the N-terminus of the protein. We prepared a vector for single-crossover strategy that introduced the *gfp* tag at the 5'end of the *flp* gene along with the *flp* promoter (Fig. 3.4A). Successful integration introduced the *gfp* tag and an HA tag (not depicted in the scheme) in front of the *flp* gene (Fig 3.4B). Analysis of cDNA from the parasite confirmed that the *gfp::flp* fusion gene was transcribed (Fig. 3.4C).

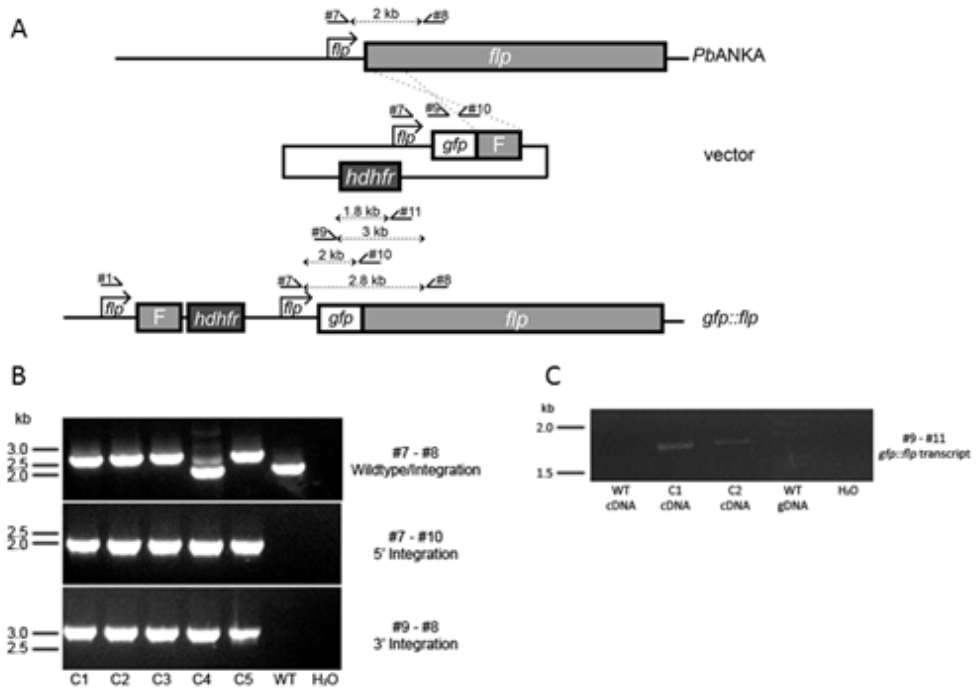

Figure 3.4 Endogenous N-terminal tagging of *flp* with *gfp*. A) Single-crossover strategy was used to target the *flp* locus. After successful integration, *flp* sequence lacks the start codon and is fused to *gfp* sequence (which lacks the stop codon) at the 5' end. Primers used for genotyping bind to sites indicated by arrows. All primer sequences are listed in chapter 2.1.6.2. **B)** Genotyping with PCR shows that four out of five clonal lines (C1 – C3 and C5) completely lack the wildtype locus and successfully integrated the vector. Vector used for transfection (V), wildtype parasites (WT) and water (H_2O) were used as controls. **C)** PCR using cDNA from two clones (C1 and C3) shows that both parasite lines synthesize the fusion transcript. cDNA and gDNA from wildtype parasites (WT) and water (H_2O) were used as controls.

Using the C1 line, we detected the fusion protein at the expected size of 211kDa on Western blot of mixed blood stages with anti-HA antibody, although we were not able to detect it in the same sample with GFP antibody (Fig. 3.5A). Only background fluorescence was detected live in the *gfp::flp* parasites (data not shown) as well as after fixation and staining with anti -GFP antibody (Fig. 3.5B). Interestingly, *gfp::flp* parasites failed to transmit to *Anopheles* mosquitoes, with extremely limited numbers of midgut sporozoites and no salivary gland sporozoites observed (Fig. 3.5C). After closer examination, we identified the transmission failure as an impaired gametocyte egress phenotype (Fig. 3.5D) with activated gametocyte trapped inside the host red blood cell and sterile. This phenotype will be further discussed in chapter 3.3. The protein fusion had a detrimental impact on the parasite viability in the host-to-vector transmission with no obvious

effect in the asexual stage. However, the high risk that the fusion protein is not properly localized and/or expressed made us stop the analysis of this line.

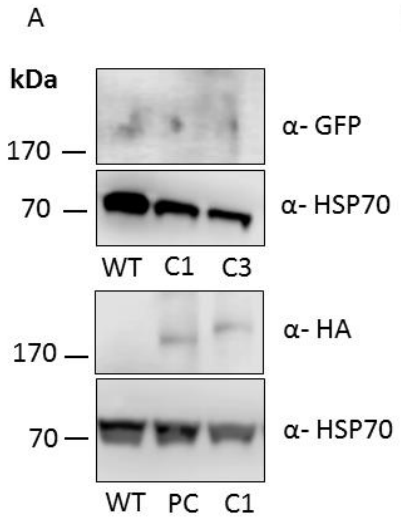

C

		Midgut sporozoites per female mosquito (n)	Salivary gland sporozoites per female mosquito (n)
WT	Cage 1	12300 (36)	11200 (39)
	Cage 2	11000 (32)	9500 (42)
	Cage 3	7000 (36)	8700 (52)
gfp::flp	Cage 1	12 (38)	0 (39)
	Cage 2	110 (39)	0 (39)
	Cage 3	180 (37)	0 (43)

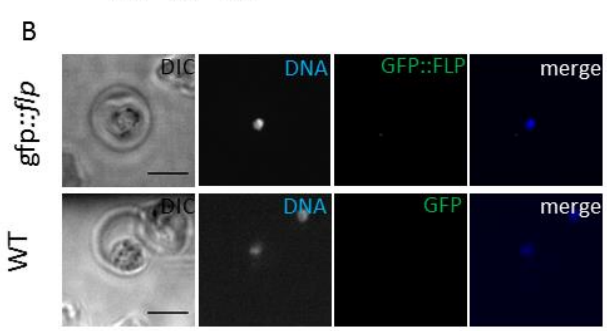

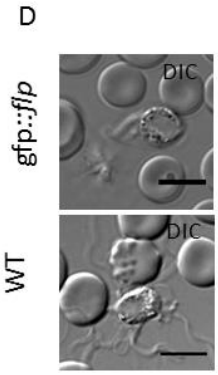

Figure 3.5 *gfp::flp* parasites arrest at the host-to-vector transmission. A) GFP::FLP fusion protein cannot be detected on Western blot with the anti-GFP antibody, but is detected with the anti-HA antibody at the expected size (211 kDa) in the clonal *gfp::flp* line (C1 and C3). Schizonts were lysed in RIPA buffer and loaded on a gradient BisTris gel. *flp::HA* schizonts (PC, 186 kDa, chapter 3.1.4.1) and wildtype schizonts (WT) were used as controls. HSP70 was used as a loading control. **B)** GFP::FLP fusion protein cannot be detected with anti-GFP antibody in fixed mixed blood stages. Parasites were fixed in 4% PFA/PBS and stained for GFP (green). DNA was stained with Hoechst (blue). Confocal images, scale bar 5 µm. **C)** *gfp::flp* parasites do not develop after transmission to the mosquito vector. Only very limited numbers of sporozoites were observed in the midguts (14 days post feed) and no sporozoites were observed in the salivary glands (17-21 days post feed). n represents number of mosquitoes analysed. D) *gfp::flp* gametocytes fail to egress from the red blood cell after gametocyte activation, resulting in aberrant exflagellation with bundled flagella. Gametocytes were activated by drop in temperature on a glass slides and imaged live. Wide field images, scale bar 5 µm.

3.1.3.3 *flp::iLOV* parasite line

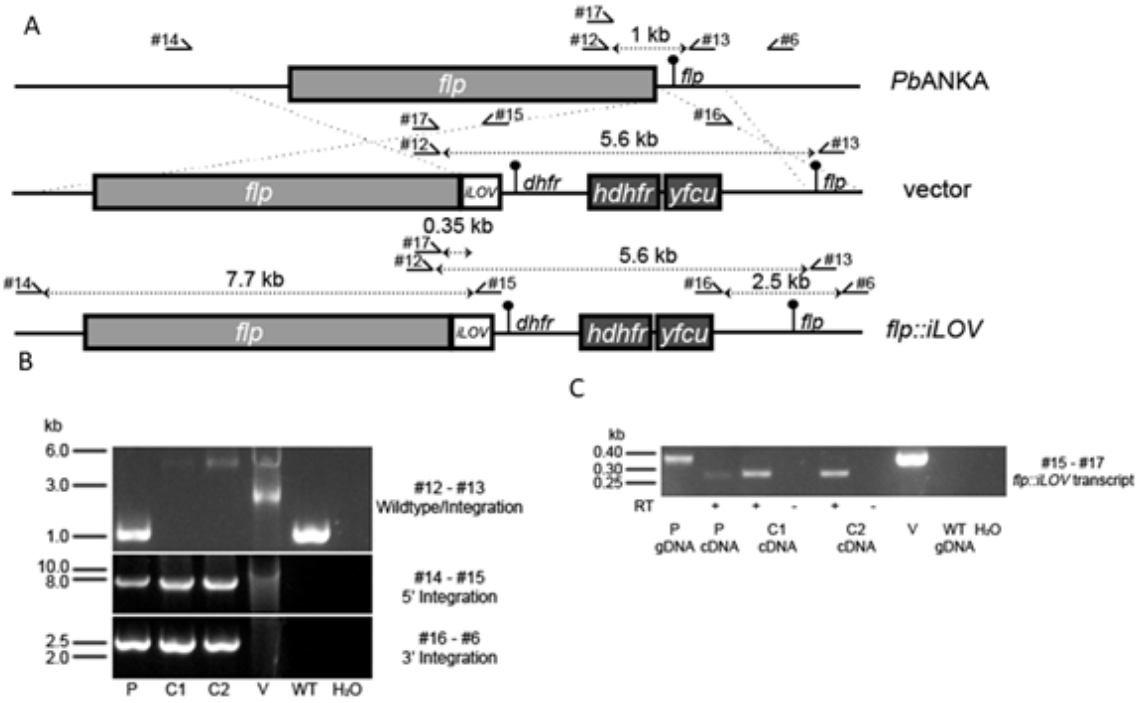

Figure 3.6 Endogenous C-terminal tagging of *flp* with *iLOV*. A) Double-crossover strategy (PlasmoGEM vector) was used to target the *flp* locus. After successful integration, *flp* sequence lacks the stop codon and is fused to *iLOV* sequence (which lacks the start codon) at the 3' end. Primers used for genotyping bind to sites indicated by arrows. All primer sequences are listed in chapter 2.1.6.2. **B)** Genotyping with PCR shows successful integration in the parental line (P). Both clonal lines (C1, C2) lack the wildtype locus and successfully integrated the vector. Vector used for transfection (V), wildtype parasites (WT) and water (H_2O) were used as controls. **C)** PCR using cDNA from the clones (C1 and C2) shows that both parasite lines synthesize the fusion transcript (transcript is shorter due to the presence of 100bp transcript at the 3'end of the gene). cDNA and gDNA from parental line (P) and wildtype parasites (WT), cDNA synthesized without reverse transcriptase (RT) and water (H_2O) were used as controls.

The *flp* gene function has proven to be very sensitive for tagging of the gene with *gfp* from both the 5' and 3' ends. Given the advantage of fluorescent tagging for *in vivo* tracking of the protein dynamics, we designed a third strategy for FLP fluorescent tagging. We tagged FLP C-terminally with a small fluorescent protein iLOV. iLOV is a relatively novel and seldom used fluorescent protein of only 10 kDa (less than half of the size of GFP), which outperforms GFP in stability and other aspects [167]. We used intermediate tagging vector from PlasmoGEM [171,172] for insertion of the iLOV tagging cassette via Gateway cloning. Resulting vector was used to target the *flp* locus via double-crossover strategy homologous recombination and endogenously insert the

iLOV tag (Fig. 3.6A). Successful integration in the parental and two clonal lines was confirmed by PCR (Fig. 3.6B) as well as production of *flp::iLOV* fusion transcript (Fig. 3.6C) by the parasite.

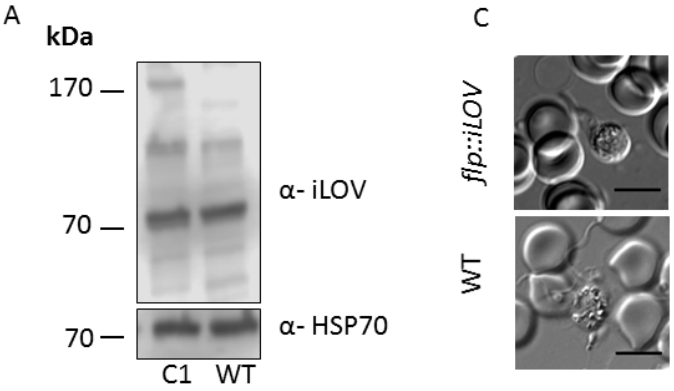

B

		Ookinetes *in vitro*		Ookinetes *in vivo* (n)	Oocyst-positive midgut (n)	Mid. spz per female mosquito (n)	Sal.gl. spz per female mosquito (n)	Mice positive after bite back
WT	Culture 1	Yes	Cage 1	ND	100 % (10)	20900 (25)	14700 (110)	ND
	Culture 2	Yes	Cage 2	Yes (10)	70 % (10)	15000 (18)	11000 (47)	3/3
	Culture 3	Yes	Cage 3	Yes (12)	92 % (12)	25000 (18)	11500 (52)	ND
flp::iLOV	Culture 1	None	Cage 1	ND	0 % (10)	0 (19)	0 (73)	ND
	Culture 2	None	Cage 2	None (12)	0 % (11)	0 (22)	0 (38)	0/3
	Culture 3	None	Cage 3	None (11)	0 % (11)	0 (22)	0 (48)	ND

Figure 3.7 *flp::iLOV* parasites arrest at the host-to-vector transmission. A) A band corresponding to the FLP::iLOV fusion protein (190 kDa) can be detected on Western blot with the iLOV antibody. However, given the low specificity of the antibody, this result should be considered with caution. Mixed blood stages were lysed in RIPA buffer and loaded on a gradient BisTris gel. Wildtype parasites (WT) were used as a control. HSP70 was used as a loading control. **B)** *flp::iLOV* parasites do not develop beyond the gametocyte stage *in vitro* nor *in vivo*. No ookinetes were observed in three independent cultures set up with *flp::iLOV* parasites. No *flp::iLOV* ookinetes were observed in midguts 20 hours after transmission to the mosquito vector. In agreement with that, no further developmental stages were observed either, specifically oocysts (10-14 days post feed) midgut sporozoites (Mid. spz 14 days post feed) and salivary gland sporozoites (Sal. gl. spz, 17-21 days post feed). **C)** *flp::iLOV* gametocytes fail to egress from the red blood cell after gametocyte activation, resulting in aberrant exflagellation with bundled flagella. Gametocytes were activated by drop in temperature on a glass slides and imaged live. Wide field images, scale bar 5 µm.

Using the clonal line, we were not able to detect a fluorescent signal in the *flp::iLOV* live parasites (data not shown). Flavin monophosphate (FMN) is a cofactor of flavin-based fluorescent proteins like iLOV [175]. Since the natural FMN concentration in the parasite is not known, we supplemented infected mice with riboflavin (a precursor of FMN) in the drinking water. However, despite this optimization, no fluorescent signal was detected (data not shown). Analysis of *flp::iLOV* parasite lysates on Western blot revealed a band at the expected size of 190 kDa (Fig. 3.7A). However, considering the high number of unspecific bands, this result has to be considered with caution. Interestingly, similarly to the *gfp::flp* parasite line, *flp::iLOV* parasites were not able to transmit to the mosquito vector due to an egress impairment during gametogenesis (Fig. 3.7.B and C). Unlike the *gfp::flp* line, *flp::iLOV* parasites arrested completely at the gametocyte stage with no ookinetes, oocysts or sporozoites observed *in vitro* or *in vivo* (Fig. 3.7B). This indicates that the smaller fluorescent tag at the C-terminus does not interfere with FLP function in the asexual blood cycle, but still hampers the function necessary for gamete egress.

3.1.4 Tagging with a small tag

Since even one of the smallest fluorescent tags interfered with the protein function, we decided to use fusion with a non-fluorescent small tag in order to visualize FLP.

3.1.4.1 *flp::HA* parasite line

We used final tagging vector from PlasmoGEM [171,172] for C-terminal tagging of FLP with a triple HA-tag. PlasmoGEM vectors, apart from their high efficiency, offer the possibility to recycle the selection cassette via 5' fluorocytosine selection (Fig. 3.8A) [169]. Vectors have successfully integrated via double-crossover strategy and no wildtype locus was observed in the clonal lines based both on *Pb*ANKA (*flp::HA*, Fig. 3.8B) and 820cl1m1cl1 (*flp::HA*^{820}, Fig. 3.8C) backgrounds. Using the 5'fluorocytosine selection, we obtained clonal lines that recycled the selection cassette (Fig. 3.8B and C) and were therefore available for further modifications.

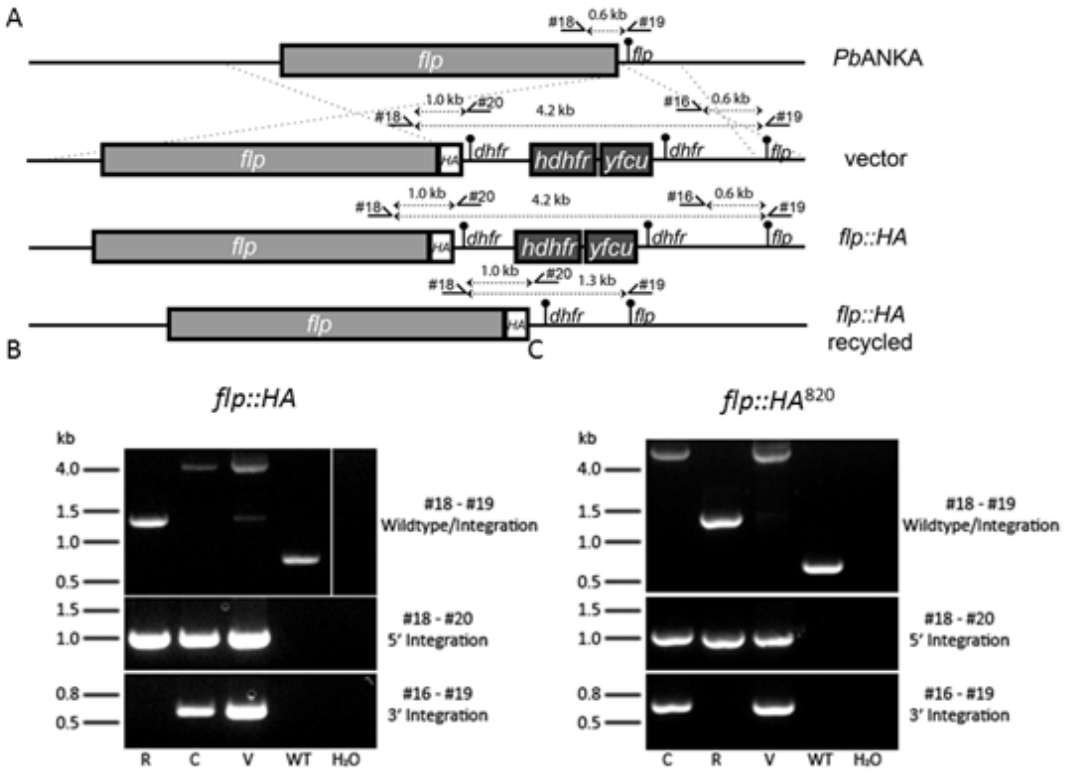

Figure 3.8 Endogenous C-terminal tagging of *flp* with HA tag. A) Double-crossover strategy (PlasmoGEM vector) was used to target the *flp* locus. After successful integration, *flp* sequence lacks the stop codon and is fused to triple HA tag at the 3' end. Duplicated 3'UTR of *dhfr* can be used for recycling of the selection cassette using 5' fluorocytosine selection. Primers used for genotyping bind to sites indicated by arrows. All primer sequences are listed in chapter 2.1.6.2. **B)** Transfection into *Pb*ANKA background. Genotyping with PCR shows successful integration of the vector and lack of the wildtype locus in the clonal (C) and recycled (R) lines. Recycled line has additionally lost the selection cassette. Vector used for transfection (V), wildtype parasites (WT) and water (H_2O) were used as controls. **C)** Transfection into 820cl1m1cl1 line. Genotyping with PCR shows successful integration of the vector and lack of the wildtype locus in the clonal (C) and recycled (R) lines. Recycled line has additionally lost the selection cassette. Vector used for transfection (V), wildtype parasites (WT, line 820cl1m1cl1) and water (H_2O) were used as controls.

Using the *flp::HA* recycled clonal line, we detected the fusion protein of expected size on a Western blot of the schizont-enriched and gametocyte-enriched samples (Fig. 3.9A). This expression matched the transcriptional data from chapter 3.1.1. Using immunofluorescent

staining, we detected the FLP::HA fusion protein in schizonts and gametocytes. In both cases, the signal showed speckled pattern distributed randomly in the cytoplasm (Fig. 3.9B). This pattern is typical for localization into vesicles, which is in agreement with localization of other ferlin orthologues [123,125,133,153]. In the gametocyte stage, egress vesicles carry proteases and other proteins necessary for the gametocyte egress [57–62,64]. A typical feature of egress vesicles is the relocalization to the cell periphery after gametocyte activation. Interestingly, after gametocyte activation, FLP::HA-labelled vesicles localized to the cell periphery (Fig. 39B), suggesting a role for these vesicles in egress.

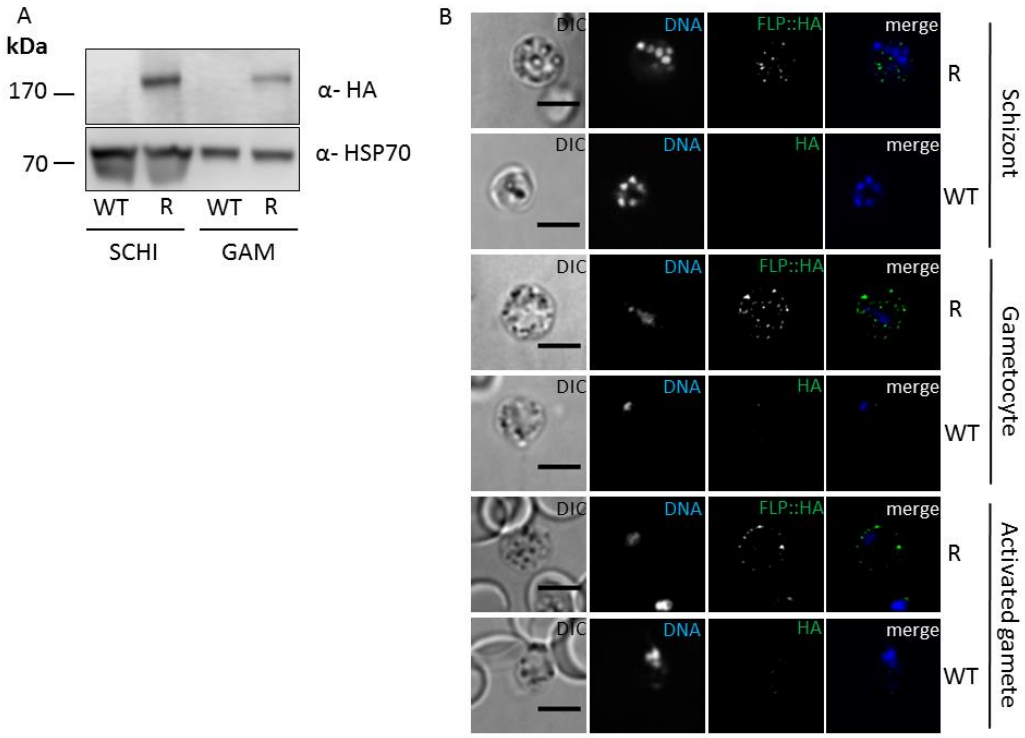

Figure 3.9 FLP::HA is expressed in asexual and sexual blood stages. A) FLP::HA fusion protein can be detected by Western blot with the anti-HA antibody at the expected size (186 kDa) in the schizont- (SCHI) and gametocyte- (GAM) enriched blood stage samples of the clonal recycled *flp::HA* line (R). Parasites were lysed in RIPA buffer and loaded on a gradient BisTris gel. Wildtype parasites (WT) were used as control. HSP70 was used as a loading control. **B)** FLP::HA fusion protein can be detected with HA antibody in fixed schizonts, gametocytes and activated gametes. Parasites were fixed in 4% PFA/PBS and stained for HA (green). To obtain activated gametes, gametocytes were incubated in ookinete medium at room temperature for 15 minutes prior to fixation. DNA was stained with Hoechst (blue). Confocal images, scale bar 5 µm.

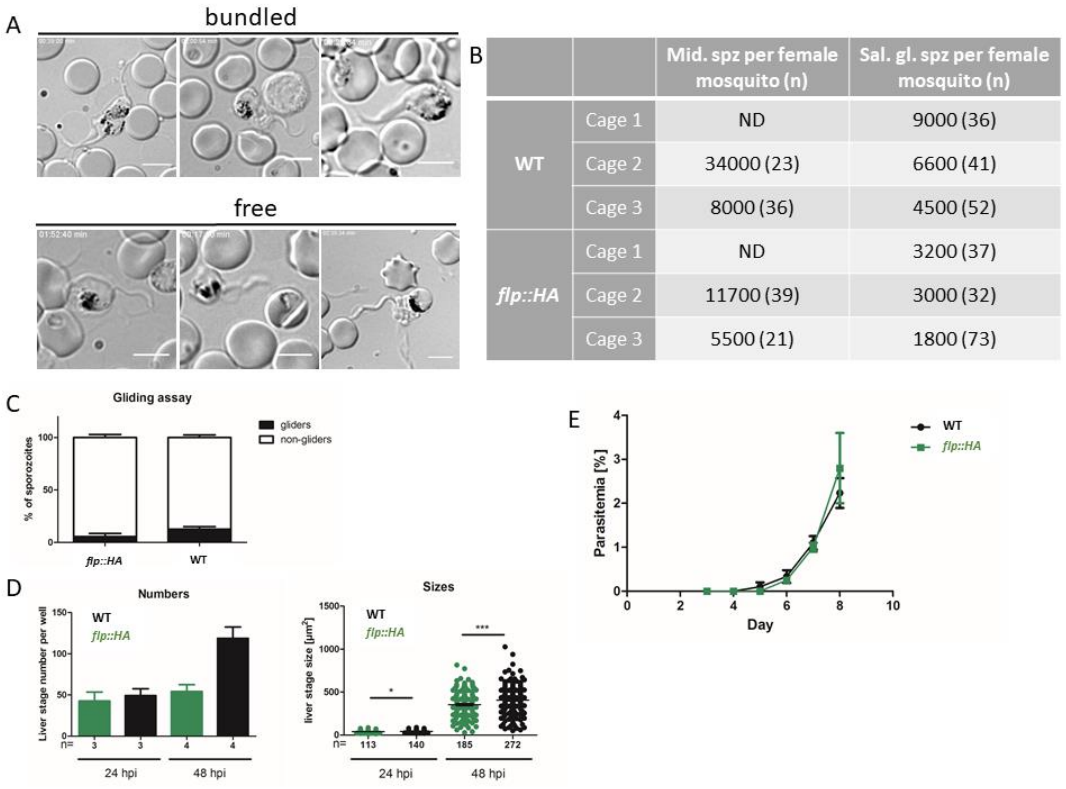

		Mid. spz per female mosquito (n)	Sal. gl. spz per female mosquito (n)
WT	Cage 1	ND	9000 (36)
	Cage 2	34000 (23)	6600 (41)
	Cage 3	8000 (36)	4500 (52)
flp::HA	Cage 1	ND	3200 (37)
	Cage 2	11700 (39)	3000 (32)
	Cage 3	5500 (21)	1800 (73)

Figure 3.10 *flp::HA* parasites progress through life cycle despite minor gametocyte egress and liver development impairments. A) Similarly to *gfp::flp* and *flp::iLOV, flp::HA* gametocytes transiently fail to egress from the RBC after gametocyte activation, resulting in aberrant exflagellation with bundled flagella. Observed phenotype was ranging from bundled flagella (upper panel, prominent at early time points after activation) to free flagella (lower panel, predominant at later time points). Gametocytes were activated by drop in temperature on a glass slides and imaged live. Wide field images, scale bar 5 µm. **B)** *flp::HA* parasites produce reduced numbers of both midgut sporozoites (Mid. spz 14 days post feed) and salivary gland sporozoites (Sal. gl. spz, 17-21 days post feed). n represents number of mosquitoes analysed. ND = not determined **C)** *flp::HA* sporozoites show no significant impairment in gliding compared to wildtype sporozoites. Isolated sporozoites were allowed to glide on a glass slide for 30 minutes and their trails were stained with antibodies and quantified. Data are pooled from 2 biological replicates as mean ± SEM. **D)** Liver stages of *flp::HA* cultured *in vitro* (using HuH7 cells) are significantly smaller than wildtype and show tendency to slightly lower numbers. Data pooled from 2 independent experiments are plotted as mean ± SEM. Statistical analysis: t-test. **E)** C57BL/6 mice (n = 3) injected intravenously with 10 000 *flp::HA* sporozoites show similar parasitaemia curve as wildtype sporozoite-injected mice. Parasitaemia was followed by daily Giemsa smears until day 8 post injection (when wildtype controls died of ECM). Data are plotted as mean ± SEM.

Given the obvious interference of fluorescent tags fused to the C-terminus with FLP function with the asexual development (chapter 3.1.3.1) and gametocyte egress (chapter 3.1.3.3), we were wondering if the HA tag had any negative impact on FLP (the triple HA tag adds about 8kDa to the protein size, only 2 kDa less than iLOV). We first examined the male exflagellation by microscopy. Indeed, exflagellating *flp::HA* gametes showed an intermediate phenotype (Fig. 3.10A) with some gametes with bundled flagella (where egress did not proceed normally, present mainly at early timepoints after activation) and some gametes with free flagella (predominant at later time points). This moderate egress impairment was mostly transient, as bundling of flagella became scarce at later time points (a phenomenon never observed in the case of *gfp::flp* and *flp::iLOV* lines). This egress delay translated into reduced sporozoite numbers during the mosquito development (Fig. 3.10B). The *flp::HA* sporozoites showed no defect in gliding (Fig. 3.10C). *In vitro* liver stage development revealed a reduction in numbers of *flp::HA* parasites at 48 hpi (Fig. 3.10D) and a moderate reduction in liver stage sizes at both 24 hpi and 48 hpi (3.10D). However, this mild phenotype observed *in vitro* did not correspond to the *in vivo* situation. C57BL/6 mice injected with *flp::HA* sporozoites showed prepatency and parasite growth in the blood comparable to wildtype parasites (Fig. 3.10E). Altogether, tagging of the C-terminus of FLP does interfere with FLP function. However, this interference is dependent on the size of the used tag with the 8 kDa HA tag leaving only very minor damage to the parasite.

3.1.4.1.1 *flp::HA*^{820} parasite line

The abundance of FLP in gametocytes on both the transcript (Fig. 3.1) and protein (Fig. 3.9) levels made us wonder about sex-specific expression and localization. In order to study the FLP specifically in male and female gametocytes, respectively, we generated the *flp::HA*^{820} line. This line is based on the parental 820cl1m1cl1 line, which expresses fluorescent markers (RFP and GFP) under sex-specific promoters, allowing to distinguish the two gametocyte sexes [61]. We obtained a clonal line and recycled the selection cassette (Fig. 3.8C). Gametocytes of the *flp::HA*^{820} line were fixed and stained with anti-HA antibody and a secondary antibody with Alexa 488 or 546 (selected not to overlap with the gender-specific marker of the gender analysed). Both male and female gametocyte showed similar levels and localization pattern of FLP::HA (Fig. 3.11), indicating that the protein plays a gender-independent function in the gametocyte stage.

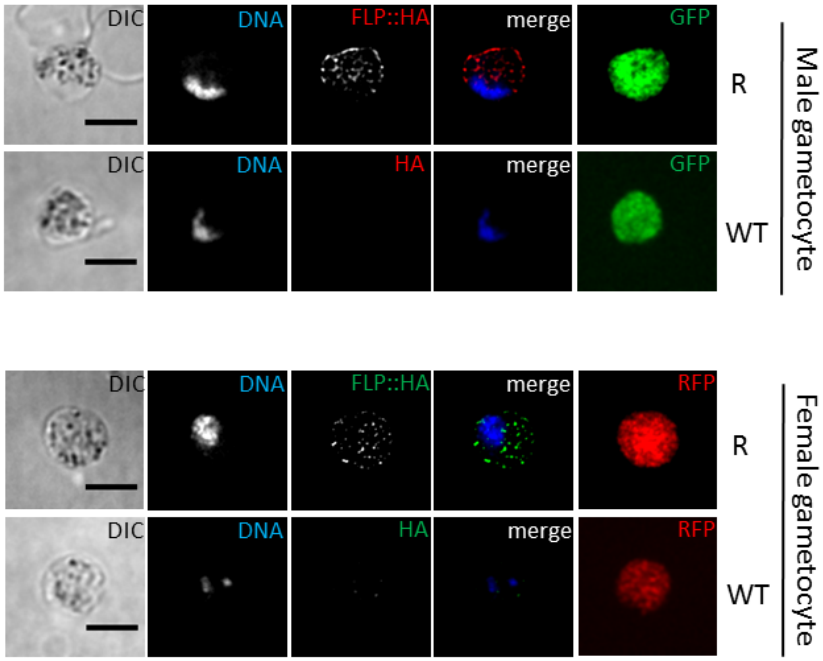

Figure 3.11 FLP::HA is expressed and localized equally in male and female gametocytes. FLP::HA fusion protein can be detected with anti-HA antibody in fixed male gametocytes (distinguished by expression of GFP marker in green) and female gametocytes (distinguished by expression of RFP marker in red) of the recycled *flp::HA*^{820} line (R). Gametocytes of the line 820cl1m1cl1 (WT) were used as negative controls. Gametocytes were fixed in 4% PFA/PBS and stained for HA (red or green). DNA was stained with Hoechst (blue). Confocal images, scale bar 5 µm.

3.1.5 3' RACE

The sensitivity of *flp* to tagging made us wonder about the correct annotation of the gene. The sequence of *flp* contains two introns near the 3'end end of the sequence (Fig. 3.12A). Additionally, downstream, very close to the 3' end of *flp*, another gene is located on the complementary strand, with overlapping 3'UTR with *flp*. In case *flp* was spliced in a different manner than had been predicted or if alternative splicing was present, we may have altered *flp* expression by fusing a C-terminal tag to the incorrect end of the sequence. We used 3'RACE to check the sequence of *flp* transcript, including the splicing of introns. Given the restriction of the *flp::iLOV* phenotype to the gametocyte stage, we analysed both the asexual blood stage and gametocyte-enriched samples to account for stage-specific differences. Isolated RNA was used for cDNA synthesis with a polyT primer and a gene specific primer annealing upstream of the two introns (Fig. 3.12A). To enhance specificity, we performed a nested PCR using a primer annealing to an adapter within the polyT primer and a gene specific primer annealing in between the two introns (Fig. 3.12A). The resulting

bands showed similar pattern for both the mixed blood stages and gametocyte-enriched samples (Fig. 3.12B) and indicated that the polyA signal was located about 100 bp downstream from the stop codon. Four bands were isolated from the gel and cloned into pGEM vector and subsequently sequenced. All samples confirmed the correct splicing of both introns in the way the gene is annotated in PlasmoDB and the presence of polyA signal at position 118 downstream of the gene (data not shown). This indicates that sensitivity of FLP for tagging is likely not originating from transcriptional aberrations.

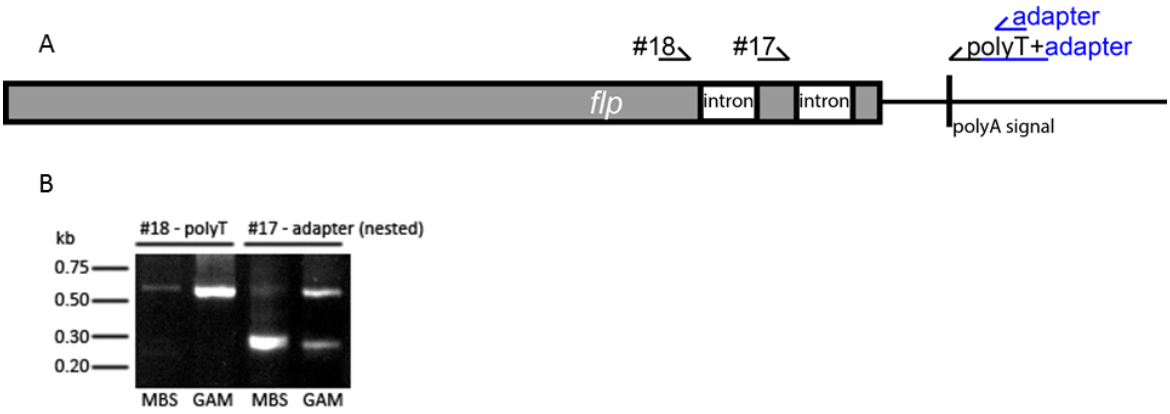

Figure 3.12 3'RACE shows that *flp* transcript is spliced as annotated. A) 3' end of *flp* contains two annotated introns. Primers annealing upstream of the introns and in between them in combination with polyT and adapter primers, respectively, were used for 3'RACE. All primer sequences are listed in chapter 2.1.6.2. **B)** PCR products are approximately 100 bp longer than the expected size until the stop codon, indicating that the polyA signal is located that far downstream of the stop codon. Both mixed blood stages (MBS) and gametocyte (GAM) band patterns look alike.

3.2 Phenotype analysis of transgenic parasites with altered *flp* expression

3.2.1 Knock-out

Knock-out (KO) is the first method of choice for functional studies in *Plasmodium*. In *P. berghei* about 45 % of genes were shown to be essential (during the asexual blood stage), a very high proportion compared to other organisms [174]. Approaches for studying essential genes in *Plasmodium* are still rather scarce but development of new methods is rapidly increasing.

3.2.1.1 *Δflp* parasite line

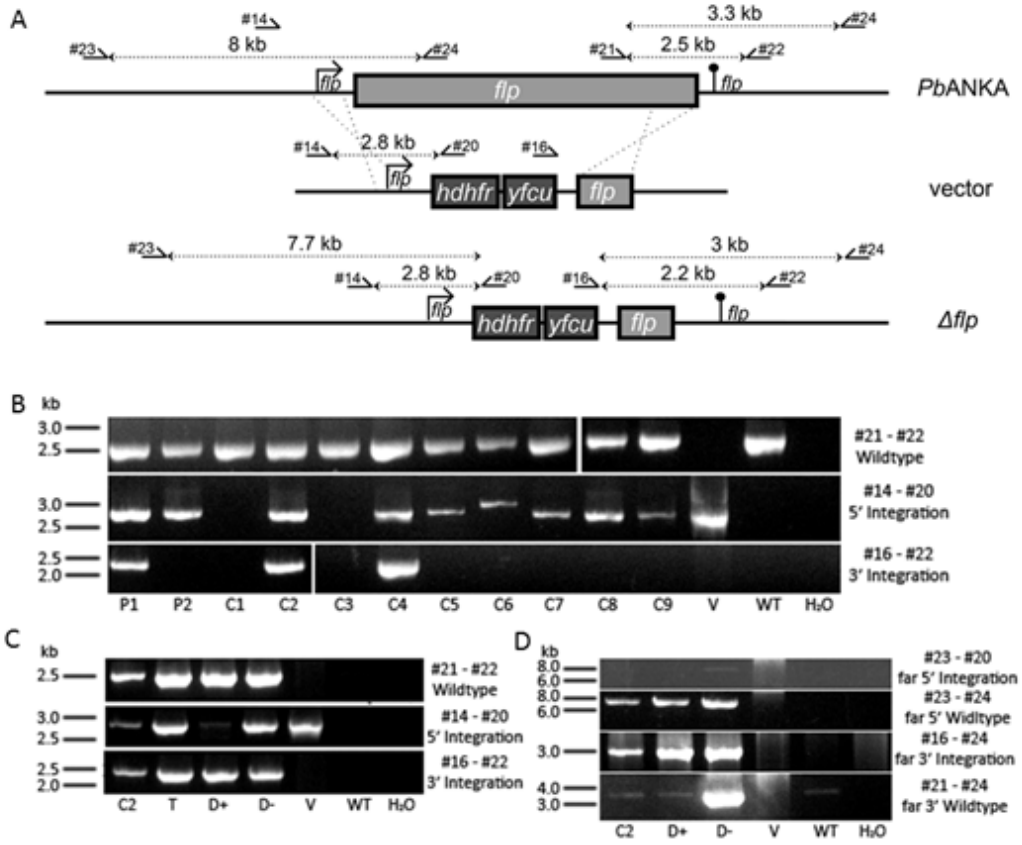

Figure 3.13 The *flp* locus is refractory to deletion. A) Double-crossover strategy (PlasmoGEM vector) was used to target the *flp* locus. After successful integration, most of the *flp* sequence is deleted. Primers used for genotyping bind to sites indicated by arrows. All primer sequences are listed in chapter 2.1.6.2. **B)** Genotyping with PCR shows successful integration in parental lines (P1-P2) and two out of nine clonal lines (C2, C4). None of the parasite population lacks the wildtype locus. Vector used for transfection (V), wildtype parasites (WT) and water (H_2O) were used as controls. **C)** Genotyping with PCR shows that not only the parasites under continuous drug pressure (clonal line C2, transfer parasites T and drug-selected parasites D+) but also parasites grown for over one week with no drug pressure (D-) kept both the integration and the wildtype loci. Vector used for transfection (V), wildtype parasites (WT) and water (H_2O) were used as controls. **D)** Genotyping with PCR shows that not only the parasites under continuous drug pressure (clonal line C2 and drug-selected parasites D+) but also parasites grown for over one week with no drug pressure (D-) kept both the integration locus expanding almost 8 kb upstream and 3 kb downstream of the selection cassette along with the wildtype locus expanding 8 kb upstream and over 3 kb downstream from the *flp* gene. Vector used for transfection (V), wildtype parasites (WT) and water (H_2O) were used as controls.

We used a final KO vector from PlasmoGEM [171,172] to generate *Δflp* parasites (Fig. 3.13A). Although the vector has integrated successfully in two parental lines (P1 and P2) and also in two lines obtained after limiting dilution (referred to as clonal lines, C2 and C4), these parasites never lost the wildtype locus (Fig. 3.13B). This indicated that disruption of the *flp* locus was not viable for the parasites and that FLP likely played indispensable function during the asexual blood stage cycle. This result was recently confirmed by a high-throughput screen of PlasmoGEM knock-out vectors, in which *flp* was classified as an essential gene [174].

Interestingly, two clonal lines (C2 and C4) did harbour the integration locus along with the wildtype locus (Fig. 3.13B). This might be explained by co-existence of wildtype parasite population along with the *Δflp* parasite population (maintained by the selection pressure of Pyrimethamine) and potentially their mutual help in survival. During the limiting dilutions, however, parasites are not exposed to the drug pressure and it was therefore unclear how the *Δflp* population would have been maintained. To test whether the integration and wildtype signals originated from different parasite populations or rather from parasites harbouring the two loci in a single genome, we first tested growth for extended time period (over a week) with and without drug pressure. Surprisingly, both populations identically maintained the integration signal along with the wildtype one (Fig. 3.13C). This strongly argues against co-existence of two parasite populations and suggests a duplication of the *flp* locus (one remaining intact and the other one integrating the vector) in the parasite genome. To get a better idea about the potential duplication, we genotyped the integration and wildtype loci with primers annealing further upstream and downstream from the *flp* locus. Both wildtype and integration loci extending further up- and downstream were detected by PCR (Fig. 3.13D), indicating that if part of the genome has duplicated, this sequence must have covered over 12 kb.

3.2.2 Truncation of terminal domains

flp is refractory to gene deletion as well as to tagging with large proteins. From the phenotypes caused by the deletion and tagging, it became clear that FLP fulfils functions both in the asexual and sexual blood stages. To shed more light on which parts of the protein are indispensable for these functions, we deleted N- and C-terminal domains of the protein, respectively. We chose the terminal domains for technical reasons as well as for their assumed functional importance.

3.2.2.1 Δflp_{C2A} parasite line

The first C2 domain (C2A) was shown to carry the main functional role in many ferlins [113]. We used a single cross-over strategy to delete the C2A domain of FLP, while keeping the partially overlapping FerI domain intact, reintroducing the start codon and the *flp* promoter (Fig. 3.14A).

Although the transfected parasites (parental line, P) showed weak positive signal for integration, this integration was lost after limiting dilution with all clonal lines (C1 – C6) only containing the wildtype *flp* locus (Fig. 3.14B). An independent second transfection resulted in an identical result (data not shown). This indicates that the C2A domain of FLP is necessary for the asexual blood stage cycle and probably fulfils an indispensable role.

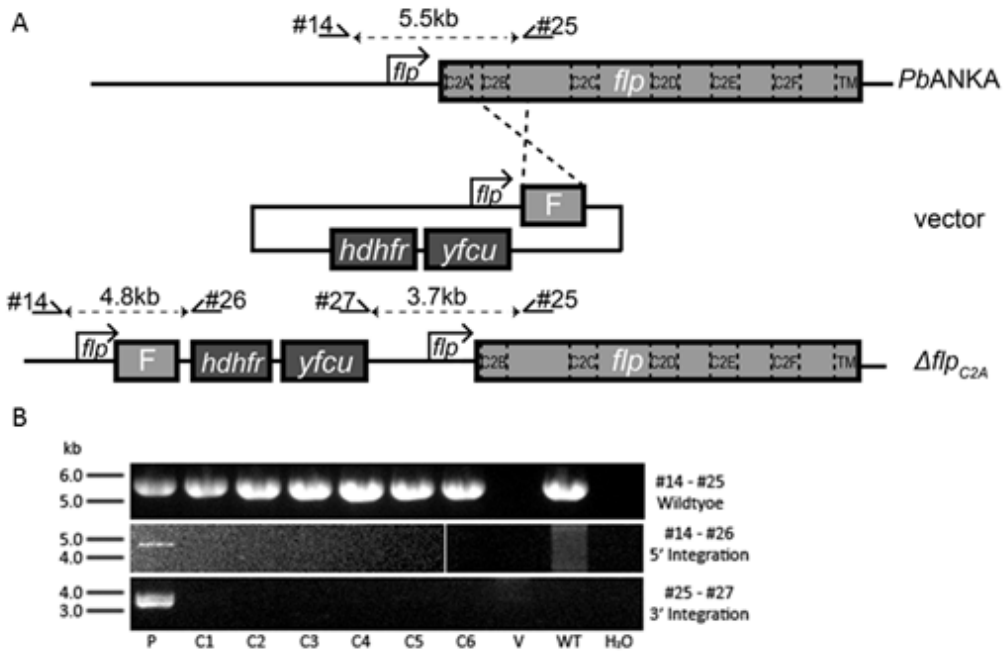

Figure 3.14 *flp* is refractory to deletion of the N-terminal C2 domain. A) Single-crossover strategy was used to target the *flp* locus. After successful integration, *flp* sequence lacks the N-terminal C2 domain and a new start codon is introduced. Primers used for genotyping bind to sites indicated by arrows. All primer sequences are listed in chapter 2.1.6.2. **B)** Genotyping with PCR shows that WT locus was maintained in the parental (P) as well as in clonal lines (C1 – C6). Weak integration-specific bands were observed in the parental line but were lost from all the clonal lines. Vector used for transfection (V), wildtype parasites (WT) and water (H_2O) were used as controls.

3.2.2.2 Δflp_{TM} parasite line

Truncation of the transmembrane domain (TM) might lead to mislocalization of FLP and potentially interfere with its function. We used a double-crossover strategy to delete the C-terminal TM domain, reintroduce the stop codon and 3'UTR of *dhfr* (3.15A). Despite two independent transfections (and two additional ones with b3D.DT^H.^D vector backbone, data not shown) we did not observe any integration of the vector into the transfected parasites' genome (3.15B). This indicates that deletion of FLP TM domain is lethal for the parasite. This data, together

with no integration yielded for *flp::gfp* line (chapter 3.1.3.1), suggest that the C-terminal part of FLP is especially highly sensitive to genetic manipulations.

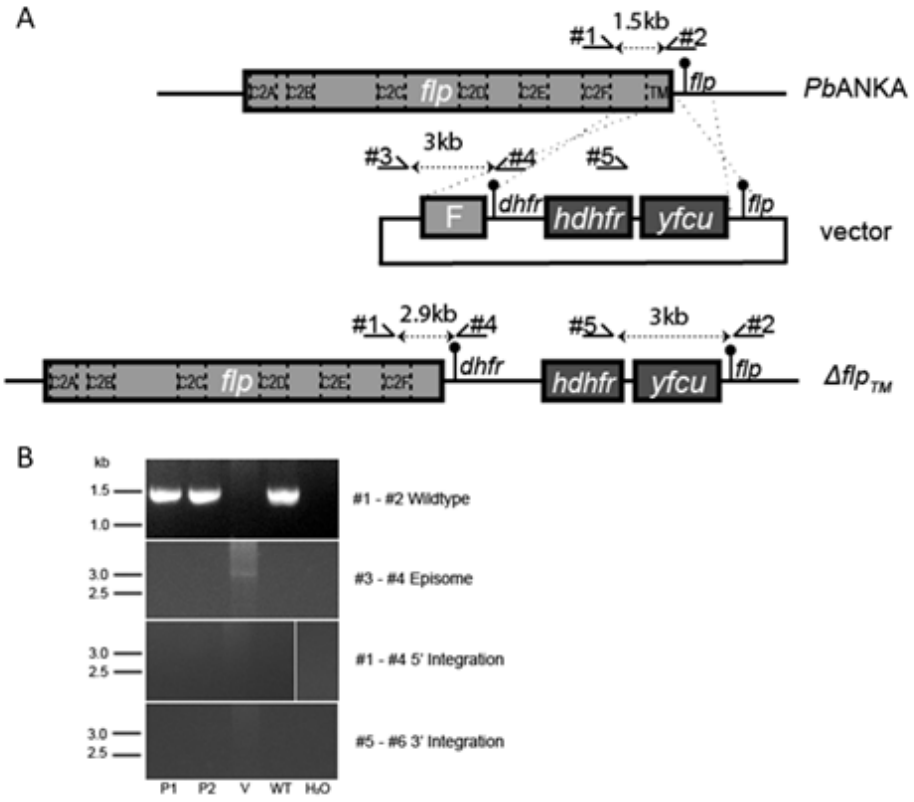

Figure 3.15 *flp* is refractory to deletion of C-terminal transmembrane domain. A) Double-crossover strategy was used to target the *flp* locus. After successful integration, *flp* sequence lacks the C-terminal transmembrane domain and a new stop codon is introduced. Primers used for genotyping bind to sites indicated by arrows. All primer sequences are listed in chapter 2.1.6.2. **B)** Genotyping with PCR shows that WT locus was maintained in two independently-generated parental lines (P1 and P2) and no integration was observed. Vector used for transfection (V), wildtype parasites (WT) and water (H_2O) were used as controls.

3.2.3 Auxin-inducible degron system

About 45 % of genes in *Plasmodium berghei* are essential for the blood stage [174], leaving them inapproachable by knock-out studies. To address function of these proteins, several fast-acting inducible systems were developed in the recent years [176]. These systems are typically based on the use of small molecules and target the gene expression either at the transcript (glms system [177]) or at the protein level (de)stabilization (DD-domain [178] or auxin-inducible degron system, AID). The AID system exploits plant proteins, expressing transgenic SCF complex (Skp1, Cullin 1

and F box protein ubiquitin ligase) and an F box protein TIR1. In this background, the protein of interest is tagged C-terminally with auxin-inducible degron (AID). Upon addition of auxin, TIR1 recruits the tagged protein for ubiquitination by SCF and subsequent degradation by proteasome [179]. The system was recently adapted for *P. berghei* and showed promising results in depletion of calcineurin, an essential gene [103].

3.2.3.1 *flp::AID* parasite line

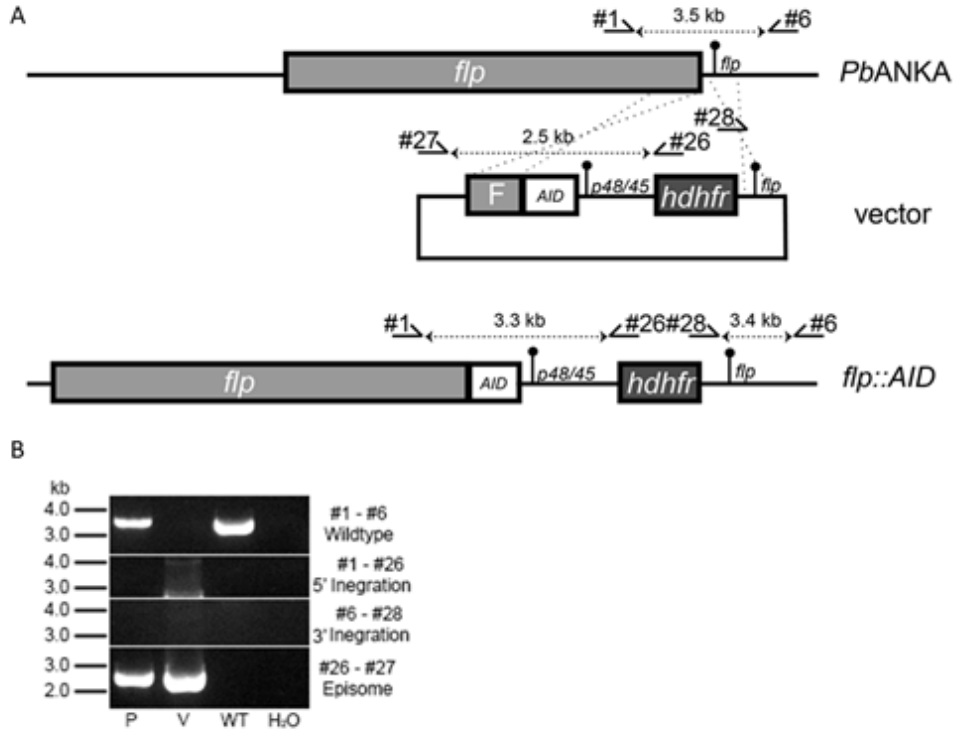

Figure 3.16 *flp* is refractory to endogenous C-terminal tagging with AID tag. A) Double-crossover strategy was used to target the *flp* locus. After successful integration, *flp* sequence lacks the stop codon and is fused to AID sequence (which lacks the start codon). Primers used for genotyping bind to sites indicated by arrows. All primer sequences are listed in chapter 2.1.6.2. **B)** Genotyping with PCR shows that wildtype locus along with the episome were maintained in the parental line (P) and no integration was observed. Vector used for transfection (V), wildtype parasites (WT) and water (H_2O) were used as controls.

We used the AID system to address FLP function by rapid depletion during the asexual blood stage and beyond. The *Pb*ANKA-based transgenic line expressing SCF and TIR1 as well as the backbone plasmid for AID tagging was a kind gift from Nisha Philip and Andrew Waters. We used double-crossover strategy to tag *flp* with AID endogenously (Fig. 3.16A). After transfection, no integration of the vector, only the wildtype locus and episome were detected (Fig. 3.16B). This was

reminiscent of the transfection result for C-terminal GFP tagging (chapter 3.1.3.1), where no integration was observed either. Given the large size of the tag (27.7 kDa), comparable to the GFP size, it seems likely that the AID tag interferes with FLP function.

3.2.4 Promoter swapping

Swapping of promoters can be used to study essential genes in other than the asexual blood stage. The exact promoter sequence as well as enhancer and silencer sequences are largely unknown in *Plasmodium*. However, using an assumed promoter (around 1.5 kb of 5'UTR) of a gene with a known transcription profile has been successfully used to change the transcriptional profile of genes of interest [49,60,180–182]. In this chapter, we used 5' UTR regions of several genes and integrated them upstream of the *flp* gene (with added Kozak sequence in case this was not part of the sequence used). These sequences will be referred to as promoters. In all but one case their suitability for promoter swapping was reported previously.

3.2.4.1 Δflp_{ook} parasite line

Based on the transcriptional profile (chapter 3.1.1) the liver stage was of primary importance for the functional study of FLP. The promoter of *ama1* was the first one used for promoter swapping and therefore its sequence suitable for swapping was known. The promoter was previously used to shut down expression during the ookinete stage [180]. Based on the transcriptional profile (Fig. 3.1), depletion in ookinete stage should not have any effect on *flp* as its transcription is extremely low in this stage. *ama1* expression is also undetectable during the early liver stage [183], we therefore used this promoter to address *flp* function during the liver stage. We used a single cross-over strategy to exchange the endogenous *flp* with the *ama1* promoter (Fig. 3.17A). After successful integration, *flp* was under the control of *ama1* promoter (Fig. 3.17B) as shown by the altered *flp* transcription profile that resembled the one of *ama1* (3.17C). This data set shows that the *flp* locus is suitable for promoter swapping and its transcription profile can be manipulated.

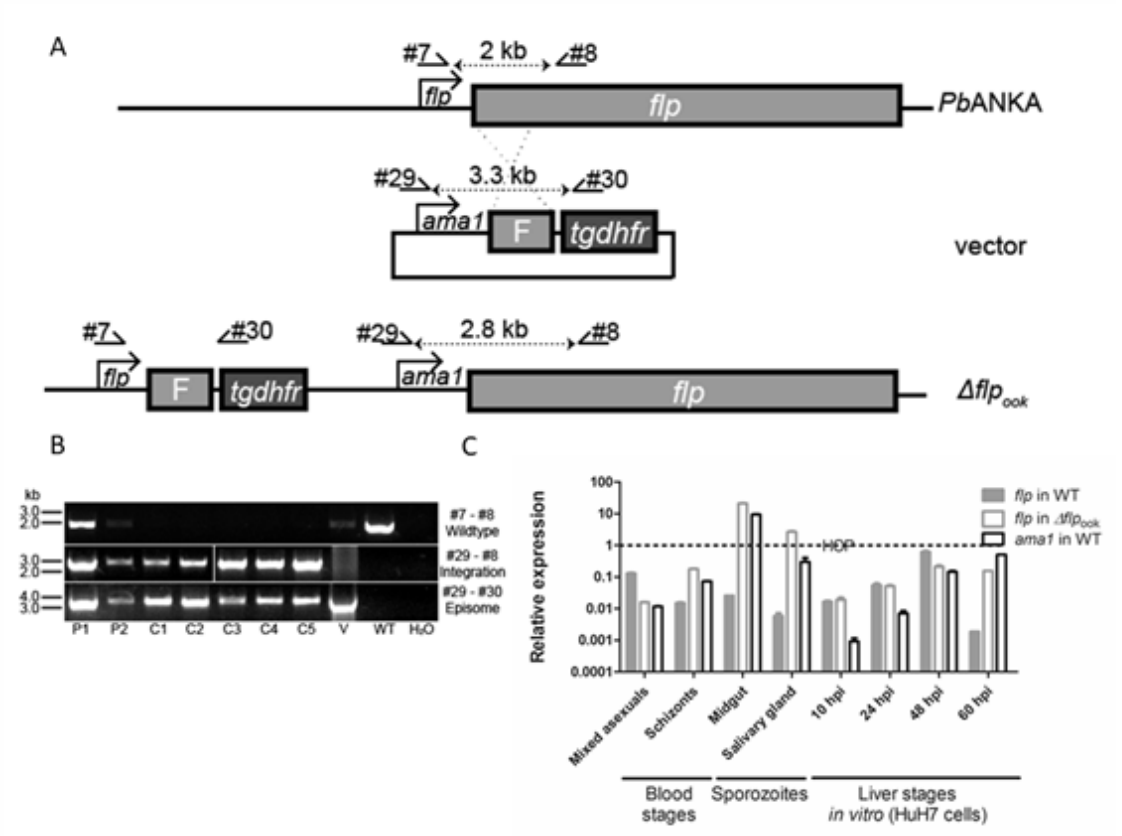

Figure 3.17 *flp* under the control of *ama1* promoter changes its transcriptional profile. A) Single-crossover strategy was used to target the *flp* locus. After successful integration, *flp* promoter sequence is located further upstream and *ama1* promoter is located in front of *flp*. Primers used for genotyping bind to sites indicated by arrows. All primer sequences are listed in chapter 2.1.6.2. **B)** Genotyping with PCR shows that WT locus was maintained only in the parental lines (P1 - P2) but is not present in the clones (C1 – C5). Integration-specific bands were observed in the parental as well as clonal lines. Vector used for transfection (V), wildtype parasites (WT) and water (H_2O) were used as controls. **C)** qPCR profiling shows that after the promoter exchange, *flp* transcriptional profile resembles the one of *ama1*. HOP was used as housekeeping gene for all stages (dashed line). Data were calculated using the comparative C_T method. Data are plotted as mean ± SEM.

We were not able to observe any phenotype of the *Δflp$_{ook}$* clonal line distinct from the wildtype case in either sporozoite numbers, sporozoite gliding, invasion into hepatocytes and liver stage or blood stage development (Fig. 3.18). The reason for this might be residual expression of *flp* in the *Δflp$_{ook}$* early liver stage (Fig. 3.17C), which might be sufficient to maintain FLP function. At the same time, the transcription of *flp* peaks at late time points of the liver development, when *ama1* expression is on again and therefore also the *Δflp$_{ook}$* line expressed *flp* (Fig. 3.17C).

A		Mid. spz per female mosquito (n)	Sal. gl. spz per female mosquito (n)
WT	Cage 1	32000 (26)	22000 (92)
	Cage 2	21000 (28)	11600 (43)
	Cage 3	18000 (33)	11000 (50)
Δflp$_{ook}$	Cage 1	11000 (21)	5600 (37)
	Cage 2	7000 (31)	4000 (32)
	Cage 3	21000 (41)	14000 (73)

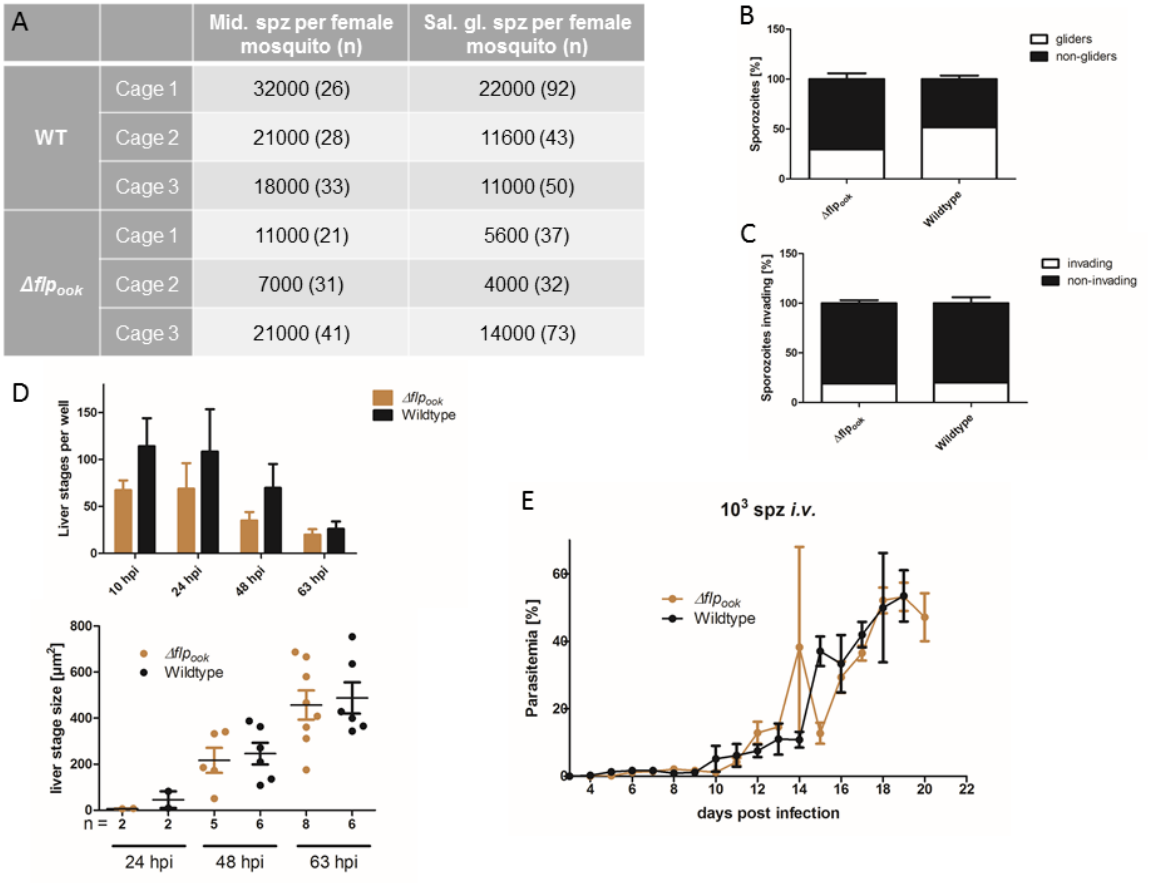

Figure 3.18 *Δflp*$_{ook}$ parasites progress through life cycle with no significant difference compared to wildtype. A) *Δflp*$_{ook}$ parasites produce comparable numbers of both midgut sporozoites (Mid. spz, 14 days post feed) and salivary gland sporozoites (Sal. gl. spz, 17-21 days post feed) to wildtype. n represents number of female mosquitoes analysed. **B)** Sporozoites of the *Δflp*$_{ook}$ line show no significant impairment in gliding compared to wildtype sporozoites. Isolated sporozoites were allowed to glide on a glass slide for 30 minutes and their trails were stained with antibodies and quantified. Data pooled from two experiments are plotted as mean ± SEM. **C)** Sporozoites of the *Δflp*$_{ook}$ line show the same capacity to invade HuH7 cells *in vitro* as wildtype sporozoites. Sporozoites were allowed to invade for 2 hours, fixed, stained and invaded and non-invaded parasites were quantified. Data pooled from two experiments are plotted as mean ± SEM. **D)** Liver stages of *Δflp*$_{ook}$ cultured *in vitro* (HuH7 cells) are not different in numbers or sizes compared to wildtype. Data pooled from two experiments are plotted as mean ± SEM. **E)** C57BL/6 mice (n = 6) injected with 10 000 *Δflp*$_{ook}$ sporozoites *i.v.* show similar parasitaemia curve as wildtype sporozoite-injected mice. Parasitaemia was followed by daily Giemsa smears. Pooled data are plotted as mean ± SEM.

3.2.4.2 *Δflp$_{spz}$* parasite line

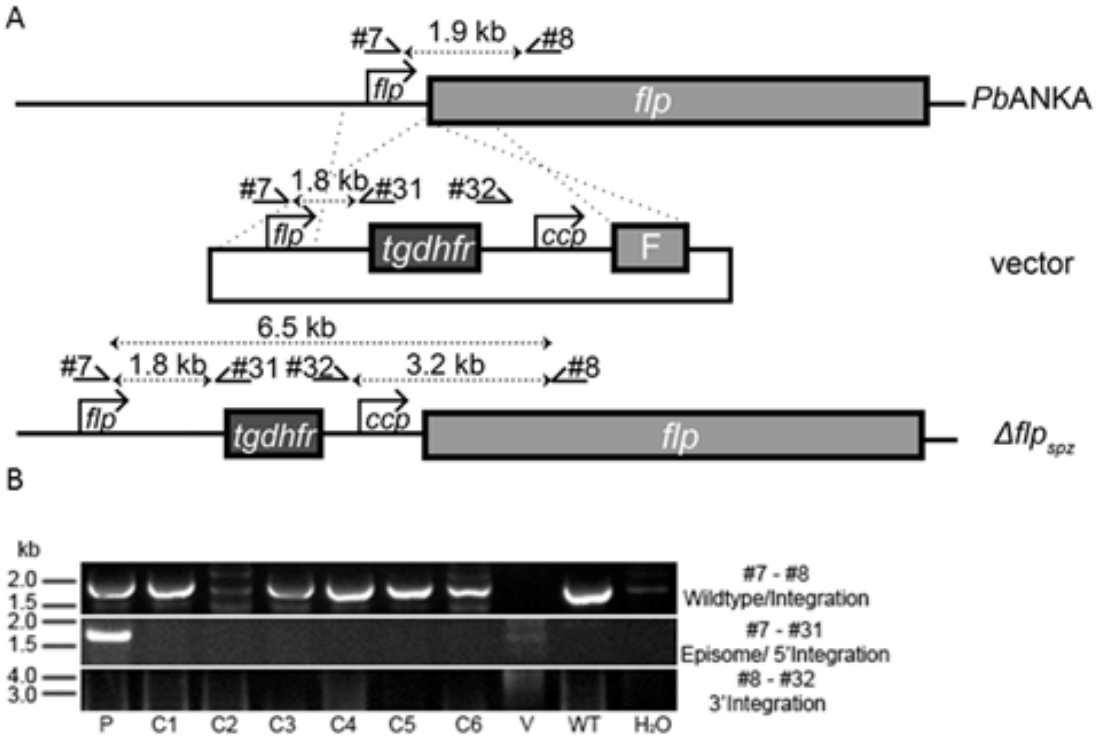

Figure 3.19 *flp* under the control of *ccp* promoter is lethal for the parasite. A) Double-crossover strategy was used to target the *flp* locus. After successful integration, *flp* promoter sequence is shifted further upstream and *flp* is under the control of *ccp* promoter. Primers used for genotyping bind to sites indicated by arrows. All primer sequences are listed in chapter 2.1.6.2. **B)** Genotyping with PCR shows that WT locus was maintained in the parental (P) as well as in clonal lines (C1 – C6). Weak integration-specific bands were observed in the parental line but were lost from all the clonal lines. Vector used for transfection (V), wildtype parasites (WT) and water (H_2O) were used as controls.

Another promoter that had been used previously and had potential to be turned off during the liver stage is the *ccp* promoter. It was used to maintain expression in gametocyte and ookinete stages and shut it down during the sporozoite stage [60]. *flp* transcription seems rather low in the sporozoite stage (Fig. 3.1), so no phenotype was expected there. The *ccp* genes function specifically during the transmission to mosquito and their expression is very low in other stages [184], which makes them good candidates for liver stage depletion via promoter swapping. We used a double cross-over strategy to exchange the endogenous *flp* promoter with *ccp* promoter (Fig. 3.19A). Although the integration of the vector was observed in the parental line, all the parasites obtained after limiting dilution maintained the wildtype *flp* locus (Fig. 3.19B). A similar result was obtained from another independent transfection (data not shown). After closer examination of the published transcriptional profile of *ccp*, it turned out that its expression during

asexual blood stages is very low [184]. The *pat* gene (used previously for the *ccp* promoter swap) [60] is not essential during the asexual blood stage and so the low expression did not affect the parasites. The lack of integration of this weak promoter further confirms the essentiality of FLP function during the asexual blood stage.

3.2.4.3 Δflp_{liver} parasite line

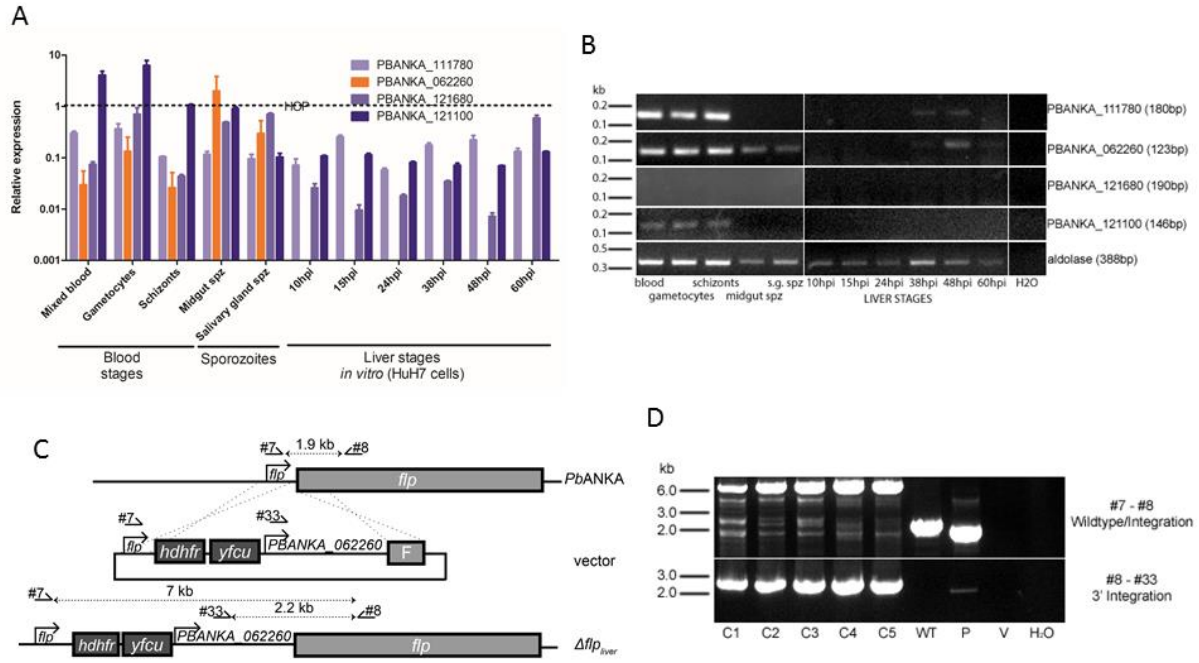

Figure 3.20 PBANKA_062250 promoter is off in the liver but its activity is likely too low in the blood stage. A) qPCR profiling shows that out of four candidates, all are transcribed during blood and sporozoite stages. During the liver stage only PBANKA_062260 showed no detectable transcript. HOP was used as housekeeping gene for all stages (dashed line). Data were calculated using the comparative C_T method. All primer sequences are listed in chapter 2.1.6.2. **B)** RT-PCR profiling shows that out of four candidates, none is detectably transcribed during the liver stage. Three candidates show detectable transcription during the blood stage but only PBANKA_062260 showed detectable transcript in the mosquito stages. Aldolase was used as housekeeping gene for all stages. All primer sequences are listed in chapter 2.1.6.2. **C)** Double-crossover strategy was used to target the *flp* locus. After successful integration, *flp* promoter sequence is located further upstream and PBANKA_062260 promoter is located in front of *flp*. Primers used for genotyping bind to sites indicated by arrows. All primer sequences are listed in chapter 2.1.6.2. **D)** Genotyping with PCR shows integration-specific bands in both the parental (P) and clonal lines. Although the clonal lines show strong integration bands, all the lines maintained residual wildtype locus. Vector used for transfection (V), wildtype parasites (WT) and water (H_2O) were used as controls.

After the failure of the two indirect approaches to deplete *flp* expression in the liver stage, we screened potential candidate genes, expression of which is maintained in the blood stage but shuts down during the liver stage. This is generally a rare expression profile given that the liver stage serves in many aspects as preparation for the blood stage cycle and to our knowledge, there are so far no genes with such profile described for *P. berghei.* We analysed a transcriptional screening performed in *P. yoellii* instead [162]. Searching for genes with the highest ratio between blood stage and liver stage transcription, we selected four candidates, which had known homologues in *P. berghei* and their 5'UTR was gene-free. We analysed the transcription profiles of the *P. berghei* homologues using qPCR (Fig. 3.20A) and RT-PCR (Fig. 3.20B). Based on strong transcription (detectable by RT-PCR) during the blood and sporozoite stages and lack of transcriptional activity in liver stages, we decided to use the promoter of PBANKA_062260.

We used a double-crossover strategy to introduce the PBANKA_062260 promoter upstream of *flp* (Fig. 3.20C). Although both parental and clonal lines integrated the vector, none of the parasite populations was free of the wildtype *flp* locus (Fig. 3.20D). This is similar to *Δflp* integration, suggesting that the Δflp_{liver} parasites are not viable in the asexual blood stage. This could be explained by low promoter activity (similarly to the *ccp* promoter, chapter 3.2.4.2). Transcription of *flp* and PBANKA_062260 in wildtype parasites were not compared directly but the normalized levels indicate about 100 times lower transcription activity for PBANKA_062260 compared to *flp* (Fig. 3.1 and 3.19A).

3.2.4.4 Δflp_{gam} parasite line

Two indicators pointed towards functional involvement of FLP in the gametocyte stage. First, *flp* transcript and also the protein were abundant in the gametocyte stage (Fig. 3.1 and 3.9) and the protein localization changed during gametogenesis (Fig. 3.9). Second, tagging with GFP at the N-terminus and iLOV at the C-terminus of FLP interfered with successful continuation of the life cycle.

To study FLP function specifically during the gametocyte stage, we used promoter swapping strategy with the *clag* promoter. This promoter was repeatedly used previously for a similar purpose, hence its sequence and transcriptional profile was known [49,182,185]. We used a double-crossover strategy to exchange the endogenous *flp* promoter with the one of *clag* (Fig. 3.21A). We have successfully generated a clonal line Δflp_{gam} (Fig. 3.21B) and an independent clonal line (Fig. 3.21C) as well as a $\Delta flp_{gam}{}^{820}$ line in the 820cl1m1cl1 background (Fig. 3.21D, further used in chapter 3.3.2). We used qPCR to assess changes in *flp* transcriptional levels. Indeed, *flp* transcriptional profile in the Δflp_{gam} line was altered and resembled the one of *clag* (Fig. 3.21E).

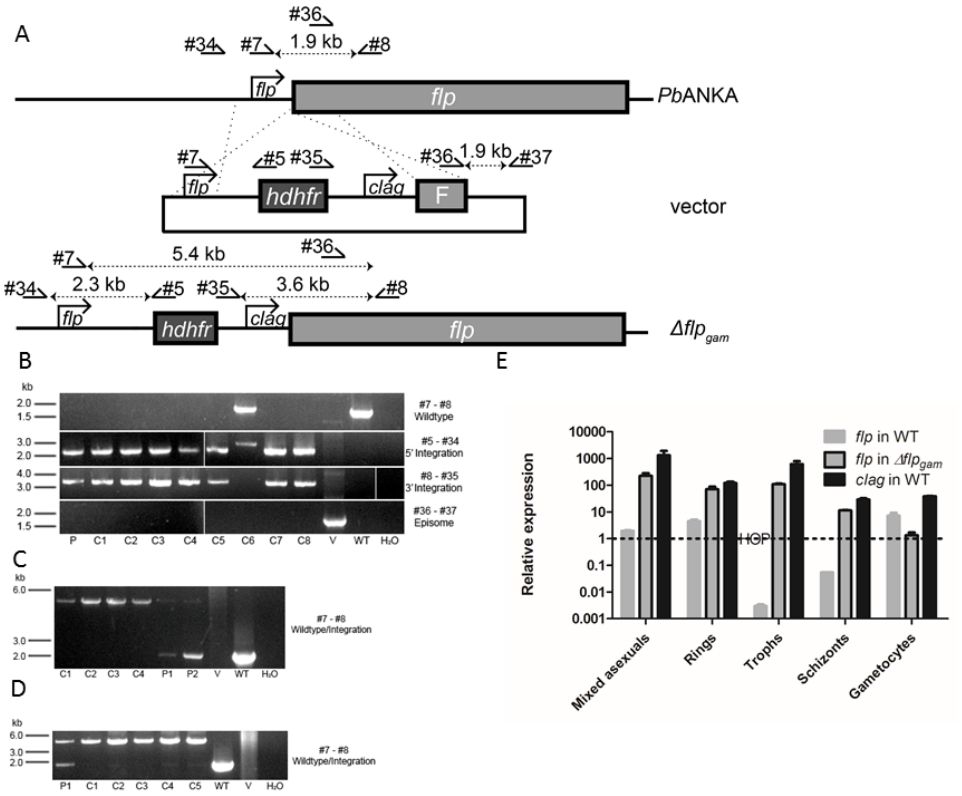

Figure 3.21 *flp* under the control of *clag* promoter changes transcriptional profile. A) Double-crossover strategy was used to target the *flp* locus. After successful integration, *flp* promoter sequence is located further upstream and *clag* promoter is located in front of *flp*. Primers used for genotyping bind to sites indicated by arrows. All primer sequences are listed in chapter 2.1.6.2. **B)** Genotyping with PCR shows that WT locus was maintained only in the parental line (P) and one clone (C6) but is not present in seven clones (C1 – C5 and C7 – C8). Integration-specific bands were observed in the parental and clonal lines. Vector used for transfection (V), wildtype parasites (WT) and water (H_2O) were used as controls. **C)** Second independent clone was generated in *Pb*ANKA background. Genotyping with PCR shows that WT locus was maintained only in the parental line (P) but is not present in four clones (C1 – C4). Integration-specific bands were observed in the parental as well as clonal lines. Vector used for transfection (V), wildtype parasites (WT) and water (H_2O) were used as controls. **D)** Third independent clone was generated in the 820cl1m1cl1 background. Genotyping with PCR shows that WT locus was maintained only in the parental line (P) but is not present in four clones (C1 – C5). Integration-specific bands were observed in the parental as well as clonal lines. Vector used for transfection (V), wildtype parasites (WT) and water (H_2O) were used as controls. **E)** qPCR profiling shows that after the promoter exchange, *flp* transcriptional profile resembles the one of *clag*. HOP was used as housekeeping gene for all stages (dashed line). Data were calculated using the comparative C_T method. All primer sequences are listed in chapter 2.1.6.2.

Transcript levels do not always correspond to protein levels. In order to see whether FLP was depleted in the *Δflp*$_{gam}$ gametocytes on the protein level, we generated *Δflp::HA*$_{gam}$ line, in which the *flp* promoter was exchanged with the *clag* promoter in the background of recycled *flp::HA* line (generated in chapter 3.1.4.1) (Fig. 3.22A). We obtained several clonal lines (Fig. 3.22B), in which *flp* expression was altered – the protein became highly abundant in the schizont stage and was absent in the gametocyte stage (Fig. 3.22C).

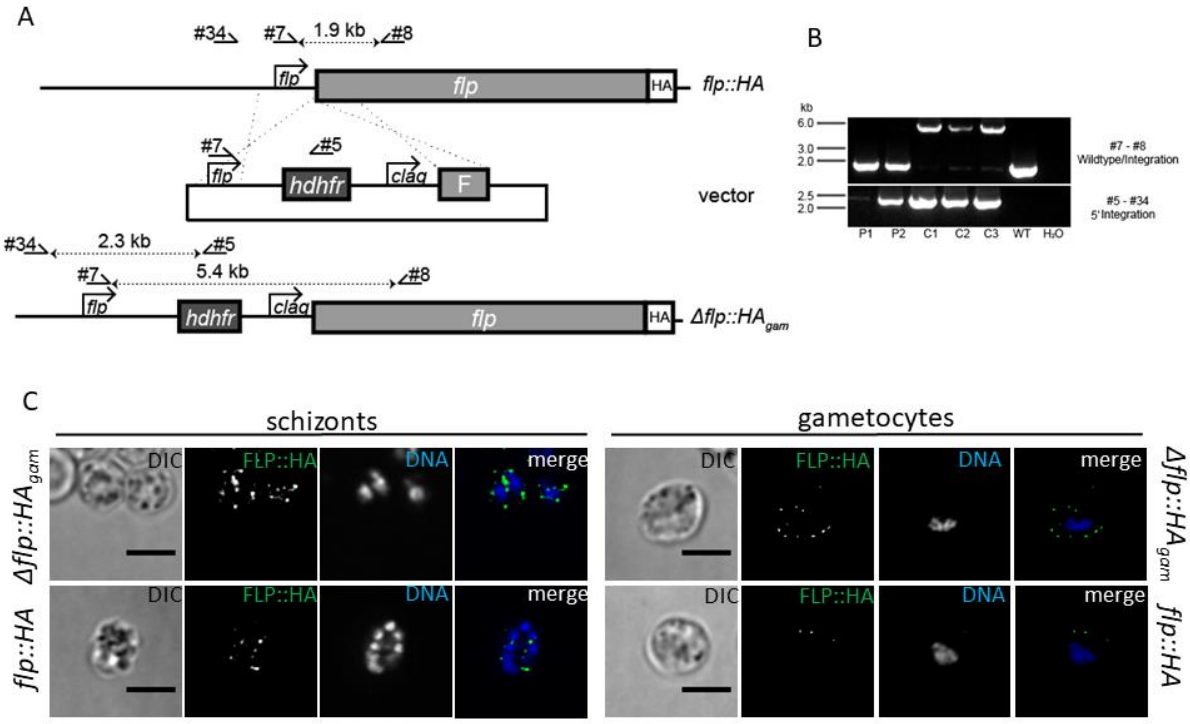

Figure 3.22 *flp* under the control of *clag* promoter changes expression profile. A) Double-crossover strategy was used to target the *flp* locus. After successful integration, *flp* promoter sequence is located further upstream and *clag* promoter is located in front of *flp*. Primers used for genotyping bind to sites indicated by arrows. All primer sequences are listed in chapter 2.1.6.2. **B)** Genotyping with PCR shows that WT locus was maintained only in the parental lines (P1 – P2) but is not present in the clones (C1 – C3). Integration-specific bands were observed in the parental as well as clonal lines. Wildtype parasites (WT) and water (H_2O) were used as controls. **C)** FLP::HA fusion protein can be detected with anti-HA antibody in fixed *flp::HA* schizonts, under the control of *clag* promoter the FLP::HA protein is much more abundant. In *flp::HA* gametocytes, the fusion protein FLP::HA protein can be readily detected but under the control of *clag* promoter expression is not detected. Parasites were fixed in 4% PFA/PBS and stained for HA (green). DNA was stained with Hoechst (blue). Confocal images, scale bar 5 µm.

A	*Pb*ANKA	*Δflp*$_{gam}$	*Δflp*$_{gam}$ clone 2	820cl1m1cl1	*Δflp*$_{gam}^{820}$
Ookinetes *In vitro*/*In vivo*	Yes	None	None	Yes	None
Oocysts-positive midguts	51 % ± 18 %	0 %	0 %	19 % ± 4 %	0 %
Midgut sporozoites (per female mosquito)	14000 ± 3960	0	0	5200 ± 4200	0
Salivary gland sporozoites (per female mosquito)	7600 ± 4400	0	0	2100 ± 70	0
Vector-to-host transmission (BS-positive mice)	3/3	0/3	ND	ND	ND

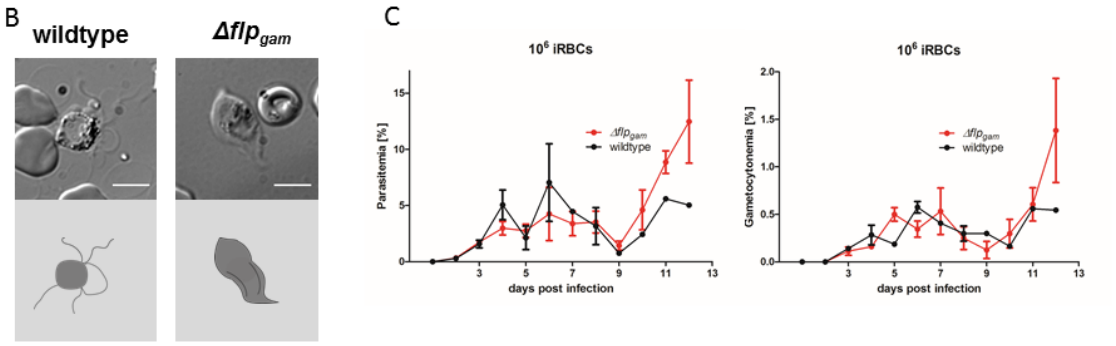

Figure 3.23 *Δflp*$_{gam}$ parasites arrest at the host-to-vector transmission. A) *Δflp*$_{gam}$ parasites do not develop beyond the gametocyte stage *in vitro* nor *in vivo*. No ookinetes were observed in three independent cultures set up with *Δflp*$_{gam}$ parasites. No *Δflp*$_{gam}$ ookinetes were observed in midguts 20 hours after transmission to the mosquito vector. In agreement with that, no further developmental stages were observed either, specifically oocysts (10-14 days post feed) midgut sporozoites (14 days post feed) and salivary gland sporozoites (17-21 days post feed). Data are pooled from three independent experiments and plotted as mean ± SEM. ND = not determined **B)** Similarly to *gfp::flp* and *flp::iLOV, Δflp*$_{gam}$ gametocytes fail to egress from the RBC after gametocyte activation, resulting in aberrant exflagellation with bundled flagella. Gametocytes were activated by drop in temperature on a glass slides and imaged live. Wide field images, scale bar 5 µm. **C)** Parasite growth and gametocytogenesis are comparable between wildtype and *Δflp*$_{gam}$ line. C57BL/6 mice (n = 3) were injected with 10^6 iRBCs *i.v.* and parasitaemia and gametocytemia were followed by daily Giemsa smears until day 12. Pooled data are plotted as mean ± SEM.

Having established the lines that lacked FLP in the gametocyte stage, the obvious question was whether these lines would show similar phenotype to *gfp::flp* and *flp::iLOV*. Indeed, a complete arrest of life cycle was observed both *in vitro* and after mosquito feeding (Fig. 3.23A). This

phenotype was again underlined by impaired exflagellation with bundled flagella (Fig. 3.23B). The highly upregulated expression of *flp* in the asexual blood stages of the *Δflp*$_{gam}$ line (Fig. 3.21E and 3.22C) might affect parasite growth. We injected C57BL/6 mice with infected red blood cells (iRBCs) and followed parasitaemia and gametocytemia (Fig. 3.23C) to assess any effects of *flp* overexpression. No difference to wildtype in parasite growth or gametocyte production was observed (Fig. 3.23C), neither any obvious changes in parasite morphology (data not shown).

3.3 Role of FLP in host-to-vector transmission

Fluorescent FLP tagging and its gametocyte-specific depletion showed that the protein plays an indispensable role in gametogenesis, specifically in the egress of microgametes. Microgametes lacking FLP remained trapped in the host erythrocyte, beating in the restricted area for long time periods (30 mins post activation was latest time point analysed, data not shown). Clearly, FLP was critical for the parasite transmission to the mosquito vector as the lack of FLP led to a complete arrest of life cycle with no mosquito-specific stages observed *in vitro* nor *in vivo*.

3.3.1 Calcium dependency

Ferlins, as proteins with multiple C2 domains, typically mediate calcium-dependent functions. FLP is a typical ferlin in its topology and it therefore seems plausible that its function is calcium-mediated. The process of gametogenesis is tightly regulated by calcium. Several pathways are regulated simultaneously by a single calcium peak [42], leaving investigation of individual pathways very challenging. Egress from surrounding membranes - a part of gametogenesis, is also calcium-dependent [53]. A study addressing impact of small molecules on gametocyte egress [53] reported a failed egress with bundling flagella, a phenotype similar to that caused by FLP absence, as a result of 1,10-phenanthroline treatment. 1,10-phenanthroline is a zinc chelator and its impact made authors speculate on the involvement of metalloproteases in the process of egress. However, 1,10-phenanthroline at high concentrations (which were needed for the effect) also chelates calcium. Although calcium typically peaks in concentration for a very short period of time, gametocyte egress consists of a time sequence of events [54]. This made us wonder if we could separate the individual pathways in gametogenesis and find conditions in which calcium chelation would lead to a similar phenotype as the one caused by FLP absence.

BAPTA-AM added at	no preincubation	preincubation at 37°C
0 min	exflagellation	no exflagellation
0.5 min	exflagellation	ND
1 min	exflagellation	no exflagellation
2 min	exflagellation	no exflagellation
5 min	exflagellation	exflagellation
8 min	exflagellation	exflagellation
15 min	exflagellation	exflagellation
Not added	exflagellation	exflagellation
DMSO added	exflagellation	exflagellation

Table 3.1 Exflagellation of wildtype gametocytes is abolished by BAPTA-AM at early time points after gametocyte activation. Blood with high gametocytonemia was collected and incubated in ookinete medium (no preincubation) or first pre-incubated in RPMI medium at 37^{o}C. Addition of BAPTA-AM without preincubation had no negative effect on exflagellation. After pre-incubation, addition of BAPTA-AM at later time points did not interfere with exflagellation, addition at early time points interfered with exflagellation. However, no intermediate phenotype was observed. Addition of DMSO (vehicle) and no treatment were used as controls. ND = not determined.

We used the membrane-permeable chelator BAPTA-AM used previously to study calcium involvement in gametogenesis [57,73]. We collected blood from a mouse with high gametocytonemia, incubated it in ookinete medium (mimicking the mosquito environment) for 15-20 minutes and analysed exflagellation by light microscopy. When blood was added to ookinete medium immediately after collecting and BAPTA-AM was added at any time point, all samples exflagellated (Table 3.1). This showed that the short manipulation time was long enough to trigger calcium-dependent pathways before BAPTA-AM was added. We optimized the assay with a pre-incubation step at 37° C in RPMI medium (mimicking the mammalian host environment) before mixing the blood with ookinete medium and BAPTA-AM to achieve more precise regulation of activation. In this approach, addition of BAPTA-AM at later time points (5 mins and later) as well as addition of DMSO (the BAPTA-AM solute) did not hinder exflagellation. In contrast, addition of BAPTA-AM at 0, 1 and 2 minutes after activation by ookinete medium, respectively,

led to a complete abolishment of exflagellation (Table 3.1). Addition of BAPTA-AM between 2 and 5 mins after activation led to inconsistent outcomes. However, the outcome was always either a population of exflagellating or not exflagellating parasites with no intermediate phenotype observed. This indicates that impairment of pathways leading to the flagella bundling cannot be mimicked by calcium chelation *in vitro*.

Another possibility to address calcium dependency of FLP would be interfering with calcium binding to the protein by mutation of involved residues. Calcium binds into negatively charged pockets in the C2 domains, which consist of several aspartates [91,114]. However, with no structural information on the C2 domains of Plasmodial ferlins, finding these pockets based on relatively low evolutionary sequence conservation is almost impossible. The first C2 domains (C2A) generally carry the main functional activity in ferlins [113]. Our attempts to delete the first C2 domain were unsuccessful (chapter 3.2.2.1), indicating that this domain is necessary for FLP function during the asexual blood stage and its function therefore cannot be easily addressed in the parasite.

3.3.2 Female fertility status

While the *Δflp*$_{gam}$ male gametes were clearly impaired with all observed flagella trapped inside the RBC during exflagellation (Fig. 3.23B), female fertility status in the absence of FLP remained unclear. Similar phenotypes underlined by impaired egress were previously linked both to processes common for both gametocyte sexes [59,61,64] and specific for male gametocytes [62]. To address the female fertility status in the absence of FLP, we made use of the *Δflp*$_{gam}^{820}$ line (generated in chapter 3.2.4.4), which expresses red fluorescent protein in female gametocytes, gametes, zygotes and ookinetes [61]. We used this line for a cross-fertilization assay (Fig. 3.24A) with GFPcon [163], a line that expresses cytosolic GFP in all stages. Briefly, equal amounts of gametocytes from both lines were mixed in an ookinete culture. In case that the *Δflp*$_{gam}^{820}$ macrogametes were fertile, they would get fertilized by GFPcon microgametes and red ookinetes would be produced (Fig. 3.24A). While mixing of the two parental lines (820cl1m1cl1 and GFPcon) led to production of both red and green ookinetes in a ratio of about 1:1 (Fig. 3.24B), mixing of *Δflp*$_{gam}^{820}$ with GFP con led to production of significantly reduced amount of red ookinetes, indicating that *Δflp*$_{gam}^{820}$ female macrogametes are impaired in their fertilization capacity, likely due to an egress impairment.

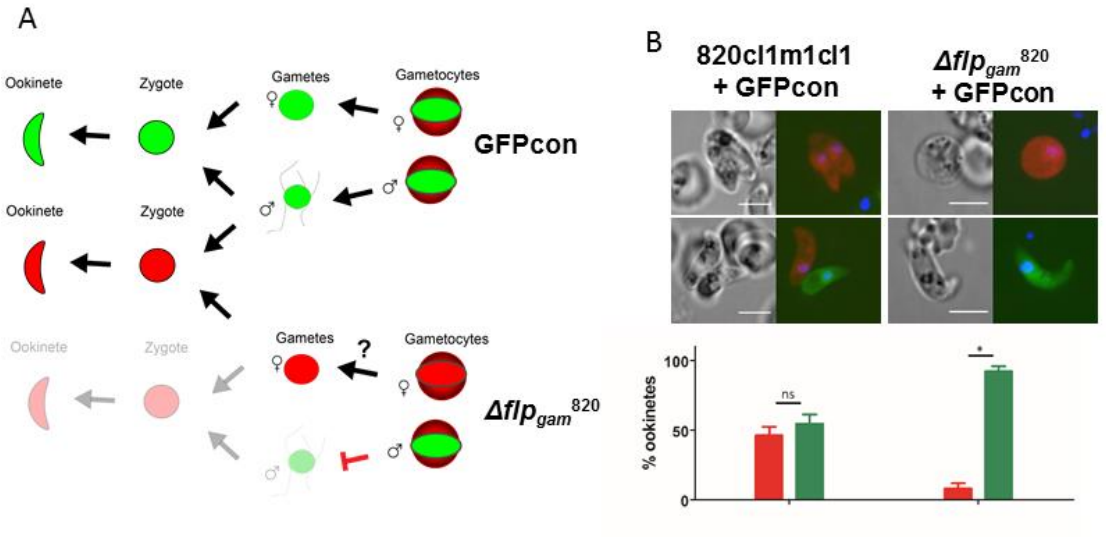

Figure 3.24 Female *Δflp*$_{gam}^{820}$ gametocytes are impaired in fertility. A) Schematic of the cross-fertilization experiment between *Δflp*$_{gam}^{820}$ and GFPcon. While GFPcon expresses GFP in all stages, *Δflp*$_{gam}^{820}$ expresses RFP in female gametocytes, gametes, zygotes and ookinetes. In case the *Δflp*$_{gam}^{820}$ macrogametes were fertile, the product of cross-fertilization between *Δflp*$_{gam}^{820}$ macrogamete and GFPcon microgamete would be a red ookinete. **B)** Ookinete cultures with equal amounts of gametocytes from each line were set up and 50 random ookinetes per experiment were analysed for fluorescent marker (GFP or RFP) presence, ratios were plotted in a bar chart. While cross-fertilization of parental lines produces both red and green ookinetes, cross-fertilization of FLP-lacking gametocytes (*Δflp*$_{gam}^{820}$) with fully fertile green gametocytes (GFPcon) produces significantly less red ookinetes. DNA was stained with Hoechst (blue). Confocal images, scale bar 5 µm. Data pooled from five experiments are plotted as mean ± SEM. Statistical analysis: Mann-Whitney test.

3.3.3 Egress failure

By comparing the gametocyte impairment caused by the absence of FLP with similar published phenotypes, we speculated that the parasites remained trapped inside the host RBC. The gametocyte needs to disrupt two surrounding membranes in order to egress – red blood cell membrane (RBCM) and parasitophorous vacuole membrane (PVM). The previously published phenotypes underlined by impaired egress were linked to defects of rupture of both these membranes – PVM rupture impairment underlies most of these defects [59–61,64], but also RBCM rupture defect can result in an aberrant exflagellation [62].

In order to address the status of membrane rupture in activated gametocytes lacking FLP, we used antibodies against markers of the two membranes, i.e. TER-119 (RBCM marker) and SEP1 (PVM marker, [166]). Activated gametes were fixed and stained for the membrane marker and for tubulin (staining flagella) to distinguish microgametes that had triggered the process of gametogenesis (Fig. 3.25). While in the wildtype case, over half of the tubulin-positive microgametes were free of RBCM, gametes lacking FLP were all trapped inside an intact RBCM, which was often expanded along the flagella (Fig. 3.25A). The PVM was lyzed in over 80 % of tubulin-positive wildtype microgametes, while about two thirds of gametes lacking FLP were still inside an intact PVM and the rest was surrounded by a damaged PVM (Fig. 3.25B).

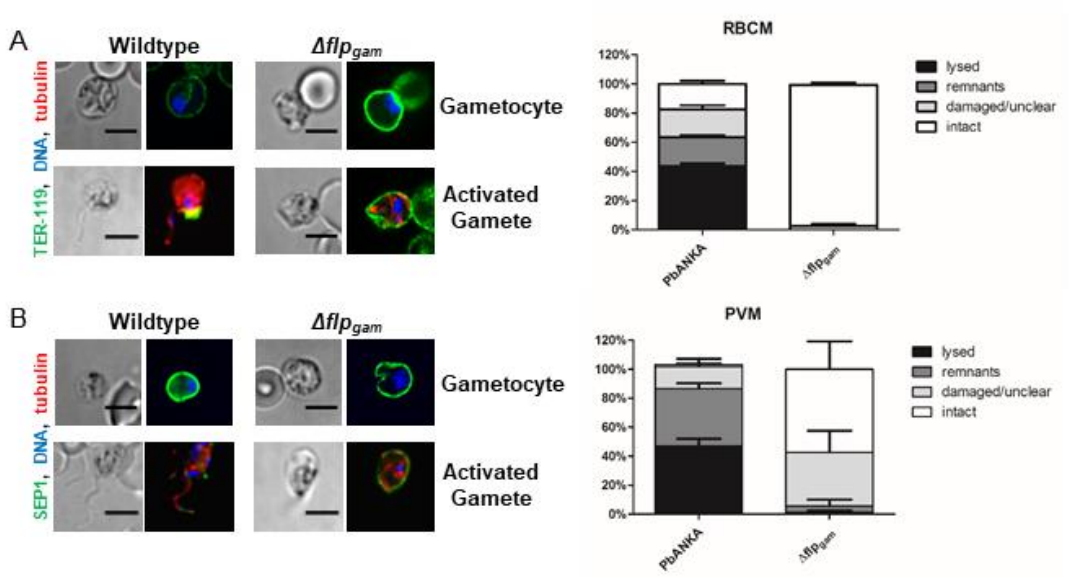

Figure 3.25 *Δflp*$_{gam}$ microgametes fail to disrupt the RBCM and PVM. A) While wildtype flagellated gametes mostly egress from the RBCM, *Δflp*$_{gam}$ flagellated microgametes remain trapped inside the RBCM. Gametocytes were activated in ookinete medium for 20 minutes, fixed in 4% PFA/PBS and stained for TER-119 (RBCM marker, green) and tubulin (flagella, red). DNA was stained with Hoechst (blue). Confocal images, scale bar 5 µm. 50 images of random tubulin-positive microgametes per experiment (n = 3) were used to quantify the membrane condition and plotted in bar plot. Pooled data are plotted as mean ± SEM. **B)** While wildtype flagellated gametes egress from the PVM, *Δflp*$_{gam}$ flagellated microgametes remain trapped inside. Gametocytes were activated in ookinete medium for 20 minutes, fixed in 4% PFA/PBS and stained for SEP1 (PVM marker, green) and tubulin (flagella, red). DNA was stained with Hoechst (blue). Confocal images, scale bar 5 µm. 50 images of random tubulin-positive microgametes per experiment (n = 3) were used to quantify the membrane condition and plotted in bar plot. Pooled data are plotted as mean ± SEM.

3.3.4 Rescue of the egress defect with detergent lysis

Gametocytes that lacked FLP were clearly trapped inside the RBCM and PVM, which likely caused the transmission failure. In order to study whether this was the only impairment caused by FLP absence, we used mild detergent lysis to release gametes from the surrounding membranes (similarly to a published assay [62]). *Δflp*$_{gam}$ gametocytes treated with 0.002% digitonin at the time of activation showed normal-looking exflagellation with free flagella (Fig. 3.26A), which got released from the residual body. This effect was not observed if digitonin was added at later time points, when exflagellation has already started (data not shown), a similar observation was made before [62]. In ookinete cultures with 0.002% digitonin in the medium the *Δflp*$_{gam}$ line produced ookinetes with normal morphology (in contrast to untreated cultures where no ookinetes but large number of unfertilized female gametes was observed, Fig. 3.26B).

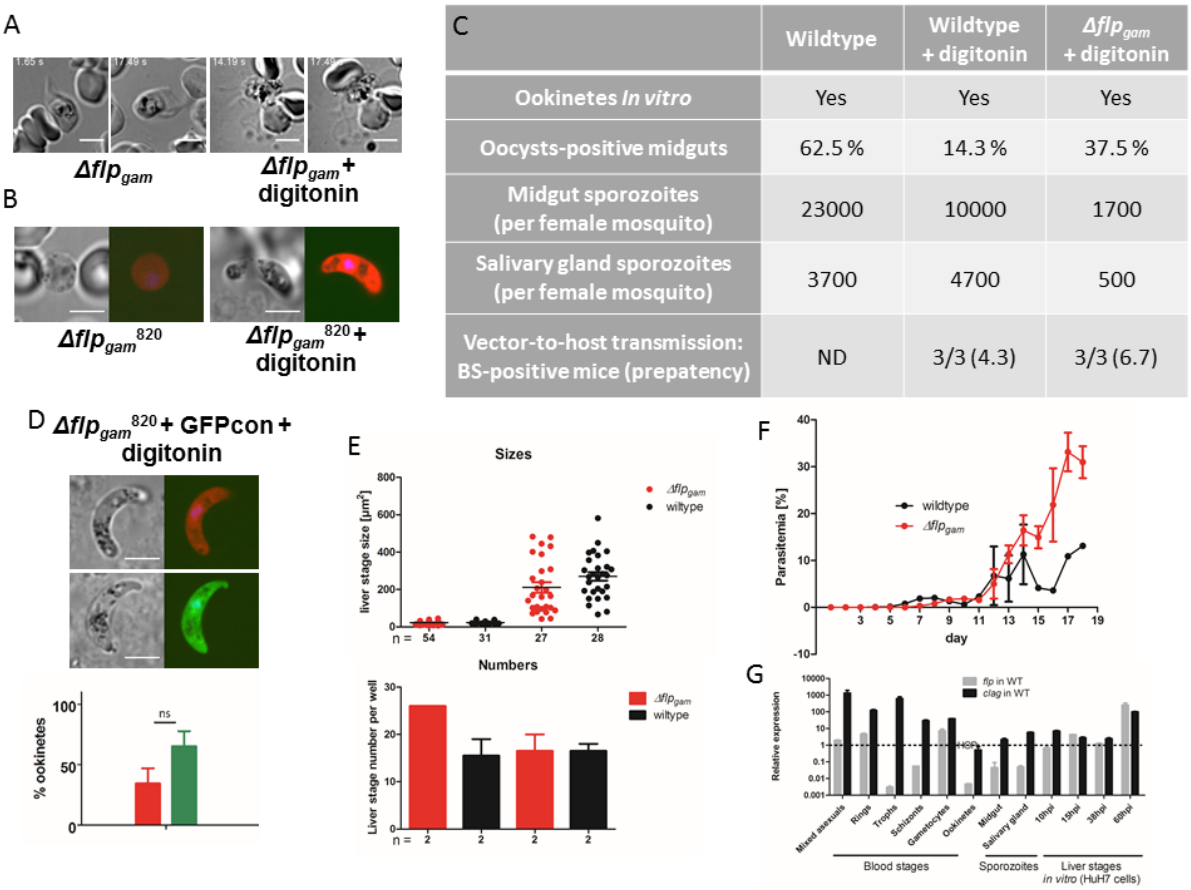

C	Wildtype	Wildtype + digitonin	*Δflp*$_{gam}$ + digitonin
Ookinetes *In vitro*	Yes	Yes	Yes
Oocysts-positive midguts	62.5 %	14.3 %	37.5 %
Midgut sporozoites (per female mosquito)	23000	10000	1700
Salivary gland sporozoites (per female mosquito)	3700	4700	500
Vector-to-host transmission: BS-positive mice (prepatency)	ND	3/3 (4.3)	3/3 (6.7)

Figure 3.26 *Δflp*$_{gam}$ parasites rescued by detergent lysis *in vitro* progress through life cycle. A) While *Δflp*$_{gam}$ gametocytes show exflagellation impairment with bundled flagella, after digitonin treatment, free flagella are recovered. Gametocytes were activated by drop in temperature and 5 µl of ookinete medium (with or without 0.002% digitonin) on a glass slides and imaged live. Wide field images, scale bar 5 µm. **B)** *Δflp*$_{gam}^{820}$ do not produce ookinetes and many unfertilized female gametes can be observed in ookinete cultures. After digitonin is added, *Δflp*$_{gam}^{820}$ ookinetes with normal morphology are observed. **C)** *Δflp*$_{gam}$ ookinetes can develop into subsequent stages after transmission to *Anopheles* mosquitoes. Digitonin-treated parasites produce reduced numbers of both midgut sporozoites (14 days post feed) and salivary gland sporozoites (17-21 days post feed), probably due to toxic effects of the detergent. Isolated sporozoites were used to inject C57BL/6 mice (n = 3) and all mice developed blood stage parasitaemia. Prepatency is depicted in days. **D)** Ookinete cultures with equal amounts of gametocytes from each line were set up as in fig. 3.24. While in cross-fertilization of FLP-lacking gametocytes with fully fertile green gametocytes produces significantly less red ookinetes (Fig. 3.24B), after digitonin treatment, red ookinetes are produced again. DNA was stained with Hoechst (blue). Confocal images, scale bar 5 µm. Pooled data from 5 experiments are plotted as mean ± SEM. Statistical analysis: Mann-Whitney test. **E)** Liver stages of *Δflp*$_{gam}$ cultured *in vitro* (using HuH7 cells) are comparable to wildtype in both sizes and numbers. Data are plotted as mean ± SEM. **F)** C57BL/6 mice (n = 3) injected with 10 000 *Δflp*$_{gam}$ sporozoites *i.v.* show similar parasitaemia curve as wildtype sporozoite-injected mice. Parasitaemia was followed by daily Giemsa smears until day 8 post infection (when wildtype controls died by ECM). Data are plotted as mean ± SEM. **F)** qPCR profiling shows that *flp* transcriptional profile resembles the one of *clag* during the liver stage. HOP was used as housekeeping gene for all stages (dashed line). Data were calculated using the comparative C_T method. Data are plotted as mean ± SEM. All primer sequences are listed in chapter 2.1.6.2.

Ookinetes from digitonin-treated cultures were used for feeding of *Anopheles* mosquitoes and oocyst as well as both sporozoite populations developed (Fig. 3.26C). We repeated cross-fertilization of *Δflp*$_{gam}^{820}$ and GFPcon line (used in chapter 3.3.2). After digitonin treatment, this cross-fertilization produced comparable numbers of red and green ookinetes (Fig.3.26D). Isolated sporozoites (from ookinete-fed *Anopheli*, Fig. 3.26C) were used to infect HuH7 cells. Analysis of *in vitro* liver stages did not show significant differences to wildtype in sizes or numbers (Fig. 3.26E). Isolated sporozoites were also injected into C57BL/6 mice and all mice developed parasitaemia, although *Δflp*$_{gam}$ sporozoite-injected mice showed a delay in prepatency compared to wildtype sporozoite-injected mice (Fig. 3.26C). The growth of parasites in the mice did not show any

difference to wildtype (Fig. 3.26F). The lack of phenotype during the liver stage was a bit surprising, but transcriptional profiling of *clag* and *flp* showed that the profiles of the two genes are somewhat comparable during the liver stage (Fig. 3.16G). This indicates that *flp* expression in the Δflp_{gam} line is probably comparable to wildtype levels during the liver stages and no phenotypes are to be expected.

3.3.5 Colocalization of FLP and known egress factors

FLP plays a specific role in egress of male and female gametocytes and localizes to vesicles. Vesicles carrying egress molecules play a fundamental role in gametocyte egress. The marker of osmiophilic bodies, the first reported egress vesicles, is the protein G377, which also takes part in their biogenesis [57,58]. We investigated colocalization between G377::mCherry and FLP::HA using a double mutant transgenic line, an approach employed previously to colocalize G377 and PAT, another egress molecule [60]. We used the recycled *flp::HA* line (chapter 3.1.4.1) and a single-crossover strategy to insert an endogenous mCherry tag at the 3'end of *g377* (Fig.3.27A). Successful integration was verified by PCR genotyping (Fig. 3.27B). We fixed gametocytes of the double mutant and checked for localization of the mCherry and HA-tag. Although both fusion proteins localized to speckles indicating vesicular localization, these speckles clearly did not colocalize (Fig. 3.27C). The G377 protein expression is restricted to female gametocytes [36,57,58]. FLP is expressed in both male and female gametocytes (Fig. 3.11), which suggests that vesicles occupied by FLP should be different to the female-specific G377-positive OBs. Another protein known to occupy egress vesicles but not colocalizing with G377-positive OBs is PPLP2 [62]. We again investigated a double mutant line for colocalization between PPLP2::mCherry and FLP::HA. We used a single-crossover strategy to insert an endogenous mCherry tag at the 3'end of *pplp2* in the *flp::HA* background (Fig.3.27D). Successful integration was verified by PCR genotyping (Fig. 3.27E). In fixed gametocytes, both fusion proteins localized to speckles indicating vesicular localization, but clearly did not colocalize (Fig. 3.27F). This indicates that although FLP is an indispensable player in gametocyte egress, it occupies a distinct subset of vesicles than do G377 and PPLP2.

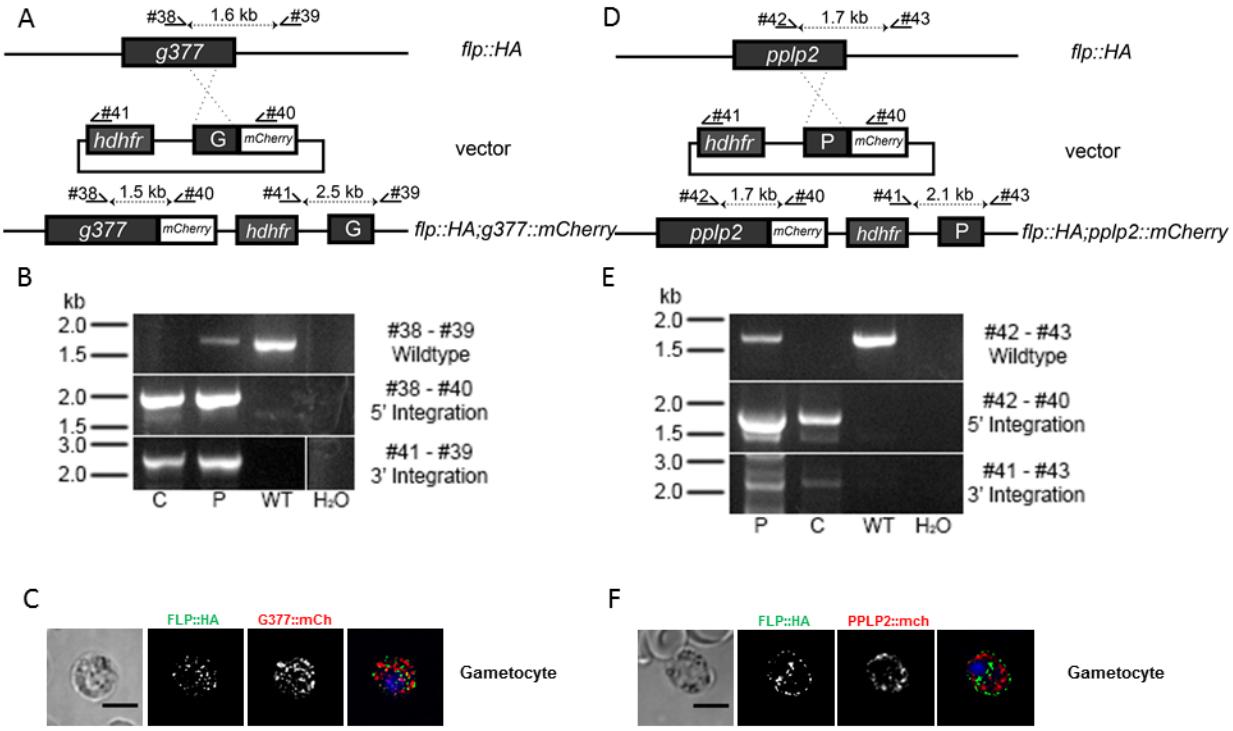

Figure 3.27 Colocalization of FLP::HA with egress molecules G377 and PPLP2. A) Single-crossover strategy was used to target the *g377* locus. After successful integration, *g377* sequence lacks the stop codon and is fused to *mCherry* sequence at the 3' end. Primers used for genotyping bind to sites indicated by arrows. All primer sequences are listed in chapter 2.1.6.2. **B)** Genotyping with PCR shows successful integration in the parental line (P). Both clonal lines (C1, C2) completely lack the wildtype locus and successfully integrated the vector. Vector used for transfection (V), wildtype parasites (WT) and water (H_2O) were used as controls. **C)** FLP::HA fusion protein detected with HA antibody (green) does not colocalize with G377::mCherry (red). Gametocytes were fixed in 4% PFA/PBS. DNA was stained with Hoechst (blue). Confocal images, scale bar 5 µm. **D)** Single-crossover strategy was used to target the *pplp2* locus. After successful integration, *pplp2* sequence lacks the stop codon and is fused to *mCherry* sequence at the 3' end. Primers used for genotyping bind to sites indicated by arrows. All primer sequences are listed in chapter 2.1.6.2. **E)** Genotyping with PCR shows successful integration in the parental line (P). Both clonal lines (C1, C2) completely lack the wildtype locus and successfully integrated the vector. Vector used for transfection (V), wildtype parasites (WT) and water (H_2O) were used as controls. **F)** FLP::HA fusion protein detected with HA antibody (green) does not colocalize with PPLP2::mCherry (red). Gametocytes were fixed in 4% PFA/PBS. DNA was stained with Hoechst (blue). Confocal images, scale bar 5 µm.

4 Discussion

Ferlins are well established important players in several secretory pathways, not very different from SNAREs [119,125,127,131,133,186]. Their function is dependent on calcium and takes part in regulation of vesicle fusion [112,116–119], although other roles were assigned to ferlins as well [118,120,126,148,154]. The molecular pathways, including interaction partners, were only deciphered for mammalian ferlins [127,129,135,136,141,154]. Especially human ferlins have been in the focus of active research as their mutation causes severe conditions (such as deafness and muscular dystrophy) [121,132,187]. Human ferlins, due to their involvement in growth factors signalling [143–145,147,148,155], have also become the focus of cancer research. Much less data was reported about invertebrate ferlins. However, two ferlins from invertabrates (Fer 1 from *C. elegans* and Misfire from *D. melanogaster*), play a critical role in fertility [112,153,157,188]. This originally named the whole family of proteins – fertility factors or ferlins. Mammalian ferlins have not been linked to fertility to date. However, also in mammals, ferlin transcripts were found in testis [188].

4.1 *flp* expression peaks in the gametocyte stage and late liver stage

To identify stages in which FLP function can be anticipated, we first analysed *flp* expression levels during the life cycle. We used qPCR to determine expression of *flp* and *ferlin* in all accessible stages of the parasite (Fig. 3.1). Based on the interaction between FLP and a liver-specific protein UIS4, which was previously identified in our laboratory (Sabine Fraschka, master thesis), we expected *flp* expression during the liver stage. Indeed, the highest abundance of *flp* transcript was detected at the late liver stage, with a gradual rise throughout liver development.

Both *flp* and *ferlin* transcripts were abundant in the asexual blood stage (Fig. 3.1), which matched the essential role proposed for both genes (chapter 3.2.1, preliminary data from our laboratory and [174]). Similarly, during the liver stage, both gene transcripts were detected in high levels. We identified two stages, in which *flp* and *ferlin* pattern differed – the gametocyte stage and mosquito stages. Purification of the gametocyte stage is challenging and asexual blood stage contamination cannot be avoided [189]. Therefore, each result has to be considered biased towards the mixed asexual stages. Despite that, both genes show significantly different level compared to the asexual blood stage (Fig. 3.1). *flp* expression on the transcript level peaks in the gametocyte, while ferlin transcript is not abundant. During the mosquito stages, *ferlin* expression is detected while *flp*

transcript is not abundant. This suggests that only one ferlin gene is active in both the gametocyte and sporozoite stages.

4.2 *flp* is highly sensitive to genetic manipulations

The *Plasmodium* life cycle consist of a number of stages that subsequently develop in the mammalian host and the mosquito vector during the period of several weeks (Fig. 1.1). Only one exception in the cycle allows for cultivation and multiplication of parasite material - the asexual blood stage cycle (Fig. 1.1). The blood stage cycle lasts 48 hours and produces over 20 merozoites in each iRBC, which allows for selection methods. This is the reason why, to date, only the asexual blood stage is permissive for transgenesis followed by selection of transfected parasites [24]. This leaves genetic manipulations that are lethal for the parasite during the asexual blood stage challenging or even impossible to study. Interestingly, this is the case for a large number of gene manipulations [174] and *flp* is one of the sensitive genes. Given the restriction of transgenic manipulations, the lethality of given gene manipulation will translate into failure to generate transfected parasites. The transfection itself as well as the homologous recombination and subsequent selection process are a multistep and complex procedure. The simple lack of transfected parasites can therefore be assigned to the failure of any of the steps and lethality of the manipulation cannot be reliably concluded. However, failure of multiple attempts (typically three), complemented with an independent approach (different vector background etc.) are usually considered as a strong argument against the viability of the given manipulation for the parasite in the malaria field. To confirm that the genetic locus is permissive to manipulation *per se*, a knock-in strategy, in which the wildtype locus is inserted should serve as control.

FLP deletion by knock-out is not viable for the parasite as shown by several independent approaches by us (chapter 3.2.1, Christina Schulte-Huxel, Roland Frank) and an independent screening [174]. Interestingly, integration of the *flp* KO vector was detected in some parasite populations, but wildtype population was always present as well (Fig. 3.12). By further analysis, we showed that both the wildtype and *flp*-KO loci are maintained in the population even without drug pressure. At the same time, no clear duplication of genomic regions could be detected (Fig. 3.12). This shows that the presence of *flp*-KO locus is conditioned by the presence of the wildtype *flp* locus in the same parasite population or, more likely, in the very same parasite. However, more detailed analysis including the detection of duplicated regions with FISH probes is needed to address the molecular basis. FLP function during asexual blood stage development remains unknown and its investigation would require an inducible system. Inducible systems for *Plasmodium* are still rather scarce and mostly require tagging of the protein of interest [176]. Since

endogenous tagging has proven to be detrimental in the case of FLP (discussed below), the recently developed inducible systems will probably not be applicable to study its function.

All the other manipulations performed in this study need to be considered with caution as independent approaches performed at other times or other laboratories are missing. However, most of the results originate from several biological replicates. The number of independent non-viable lines collectively represents a strong argument supporting *flp* as a very sensitive gene for genetic manipulations (Fig. 4.1). The conclusion of five transgenic manipulations (chapters 3.1.3.1, 3.1.3.2, 3.1.3.3 and 3.2.3.1) is that FLP cannot be endogenously tagged with large proteins and its terminal domains cannot be deleted (chapters 3.2.2.1 and 3.2.2.2). Especially the C-terminus of the protein seems to be very sensitive, as no integration was detected for vectors truncating the C-terminal transmembrane domain (two vector backbones were used in four transfections, chapter 3.2.2.2) and for tagging of FLP with a large tag (GFP and AID, chapters 3.1.3.1 and 3.2.3.1, respectively). Small fluorescent protein iLOV was fused successfully to FLP (chapter 3.1.3.3) but interfered with its function in host-to-vector transmission. FLP tagged with HA tag was viable throughout the life cycle, although a minor phenotype at host-to-vector transmission was observed (chapter 3.1.4.1). The N-terminus of FLP was sensitive to the truncation of the first C2 domain (chapter 3.2.2.1). Similarly to *Δflp*, Δflp_{C2A} parasites were detected in the population but the wildtype locus was never lost. N-terminal fusion of FLP to a GFP tag (chapter 3.1.3.2) interfered with host-to-vector transmission. Interestingly, both FLP::iLOV and GFP::FLP interfered with FLP function in the gametocyte stage and showed similar phenotype to depletion of FLP – impaired egress with disrupted transmission (Fig. 3.5, 3.7 and 3.23). While *flp::iLOV* (and the FLP-depleted Δflp_{gam} line) underwent a complete arrest of life cycle, *gfp::flp* parasites could transmit an extremely reduced number of parasites, as detected by the presence of a few sporozoites in the midgut (Fig. 3.5). Likely due to the highly limited numbers, these parasites did not overcome the upcoming bottleneck of midgut-to-salivary gland migration and no sporozoites were observed in the salivary glands. Phenotypes underlined by impaired egress that result in partial block of transmission were observed before [59,61,62]. These phenotypes were reported in KO studies, indicating that the deleted genes played important but not crucial roles in the process of egress. We have shown that FLP plays and indispensable role in egress (Fig. 3.23). Therefore, the only likely explanation of the development of several *gfp::flp* midgut sporozoites is only partial interference of the tag with FLP function.

Surprisingly, neither GFP nor iLOV fluorescence was detected in either of the lines. FLP protein levels in the asexual blood stage are likely very low (Fig. 3.9) and that may prevent the detection of the fusion proteins live. Using Western blot, we successfully detected the GFP::FLP fusion

protein with anti-HA antibody (HA tag was used as a linker between GFP and FLP) but not with anti-GFP antibody. This suggests that GFP antibody did not efficiently detect the fusion protein and it explains why IFA on fixed parasites was not successful with this antibody (Fig. 3.4). Anti-iLOV antibody detected a band corresponding to FLP::iLOV on a Western blot (Fig. 3.6), although many unspecific bands were present. The anti-iLOV antibody does not detect native protein and so it could not be used for IFA [167]. In conclusion, low FLP levels together with suboptimal antibodies prevented the detection of fluorescently tagged FLP during the asexual blood stage. A set of antibodies and proper controls with similar (low) levels of iLOV and GFP proteins, respectively, would be needed for optimization of detection procedures.

The only tag, fusion of which to FLP did not abolish transmission of the parasite, was the small HA tag (Fig. 4.1). However, *flp::HA* line showed a transient egress impairment and slower liver stage development *in vitro* (Fig. 3.10). This indicates that FLP::HA cannot fulfil its function completely due to the very small tag. The localization determined using the tagged line (Fig. 3.9) has to be, therefore, considered with caution. Three main points argue against mislocalization of tagged FLP – first, mislocalized proteins do usually not localize to distinct speckles (the case of FLP::HA) but are degraded, localize to uneven aggregates or show no particular localization in the cell. Second, FLP::HA localizes to vesicles, which matches very well with ferlin orthologues from a number of organisms [112,117,123,125,133]. Third, although the HA tagging caused a delay in egress, the *flp::HA* parasites were viable throughout the life cycle (Fig. 3.10). This, in contrast to *gfp::flp* and *flp::iLOV* parasites, which completely fail to transmit (Fig. 3.5 and 3.7), indicates that FLP::HA must be functional and likely largely properly localized. However, cases in which mislocalized tagged protein was functionally completely intact were reported [190]. The biggest risk of mislocalization is represented by dimerizing fluorescent proteins from the GFP family. Dimerization of YFP underlined the mislocalization mentioned above [190]. Dimerization of GFP might contribute to the interference with FLP::GFP and GFP::FLP functions. No dimerization or oligomerization was reported for the HA tag and iLOV was shown to stay monomeric in solution [191]. This suggests that it is rather direct interference with FLP function than the mislocalization that causes egress impairment observed in *flp::iLOV* and transiently in *flp::HA*. Although we were not able to address FLP role during the liver stage in this study, based on the high transcript abundance (Fig. 3.1), its function can be anticipated. Also, *flp::HA* line was impaired during the liver stage *in vitro*, indicating that HA tag (and potentially other tags) might interfere with FLP function in the liver stage.

Interestingly, *gfp::flp* and *flp::iLOV* lines showed no effect on the asexual blood stage development but interfered with FLP function in the gametocyte stage. These two stages differ in the

surrounding environment – mammalian host and mosquito vector differ by almost 15° C in temperature. Temperature sensitive mutations are known from yeast and they were observed in the case of ferlins as well. *C. elegans* Fer1 mutations are temperature sensitive [112] and also four mutation of human otoferlin are temperature dependent, leading to a more severe phenotype at elevated temperature [124]. However, proving that the change in temperature causes defects to the tagged FLP would require thorough biochemical analysis.

Using transfection of additional copies of the genes, C-terminal tagging of five human ferlins led to no obvious phenotype in ferlin behaviour or the viability of the cells in cell culture [123]. However, to our knowledge, no endogenous tagging was reported for any ferlin member to date. This may indicate that the detrimental effects of endogenous tagging are a common feature of the protein family.

FLP depletion by KO was not possible (Fig. 3.13) and its sensitivity to tagging prevented conditional depletion with the AID system (Fig. 3.16). As an alternative approach, we used promoter swapping. The first generated line, Δflp_{ook}, proved that the 5'UTR of *flp* was genetically accessible and, more importantly, that *flp* transcriptional profile can be manipulated (Fig. 3.17). However, no difference to wildtype was detected in the Δflp_{ook} line (Fig. 3.18), which indicates that FLP does not play a role in the ookinete stage, as was expected from the transcriptional profile (Fig. 3.1). What remains unclear is the role of FLP in the early liver stage. *Ama1* expression is very low in this stage [183], but residual expression of *flp* under the *ama1* promoter was detected (Fig. 3.17). The lack of phenotype can hence be explained by the lack of FLP function in the early liver stage or by a function that can be fulfilled by very low amount of the protein.

Generation of two other lines with promoter swapping was not feasible, namely Δflp_{spz} (*ccp* promoter) and Δflp_{liver} (PBANKA_062260 promoter). In the case of *ccp* promoter, transcriptional data point towards very low expression during the asexual blood stage, during which FLP plays an essential function. The fact that integration of the *ccp* promoter was observed but wildtype population was never lost (Fig. 3.19) reproduces the phenotype observed for the *Δflp* line (Fig. 3.13). This further argues for the too low expression of FLP in the asexual blood stage as the reason why Δflp_{spz} could not be generated. A similar story is the generation of the Δflp_{liver} line. Based on similarities with the Δflp_{spz} line mentioned above, the suboptimal expression levels during the asexual blood cycle seem to be the most likely explanation for the failure of generation of this line. However, since the promoter of PBANKA_062260 was never used before, its sequence is not known and it is possible that the 1.5 kb of its 5'UTR is not acting as a promoter. In such case, this line would resemble the *Δflp* line and in either case would not be viable.

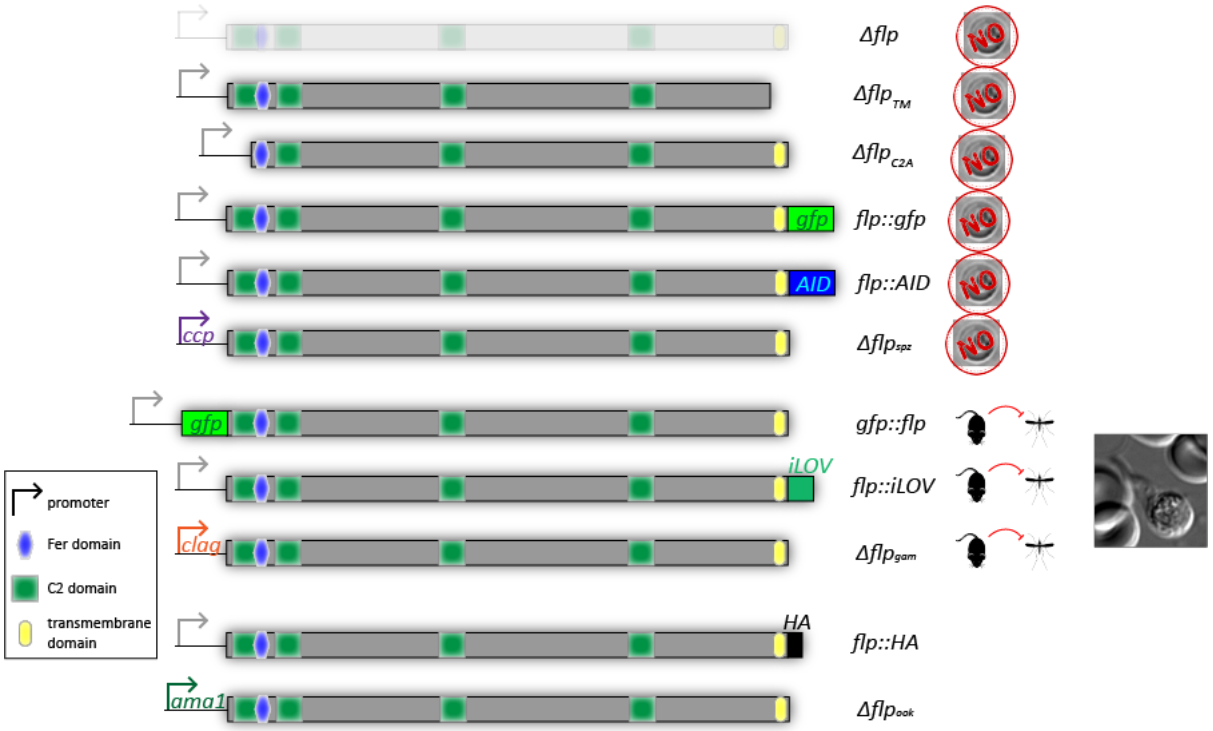

Figure 4.1 FLP is sensitive to genetic manipulations. All parasite transgenesis is taking place during the asexual blood stage, leaving manipulations lethal for this stage impossible to establish. *flp* is refractory to gene knock-out (*Δflp*). Truncations of both N-terminal C2A domain (Δflp_{C2A}) and C-terminal TM domain (Δflp_{TM}) are not viable for the parasite. Tagging of FLP shows different degree of interference depending on the size and location of the tag. C-terminus is more sensitive, with GFP tag (*flp::gfp*) and AID tag (*flp::AID*) lethal and iLOV (*flp::iLOV*) interfering with FLP function in gametogenesis leading to arrest at host-to-vector transmission. Promoter swapping using a weak asexual blood stage promoter (*ccp*. Δflp_{spz}) was lethal for the parasite. Promoter inactive in the gametocyte stage (*clag*. Δflp_{gam}) abolished host-to-vector transmission. Promoter inactive in the ookinete stage (*ama1*. Δflp_{ook}) had no effect on the viability. The *flp* gene locus is permissive for genetic manipulations as shown by successful transgenesis at both the 5'end (Δflp_{ook}) and the 3'end (*flp::HA*). Tagging might interfere with functions of the terminal domains – the first C2 domain and the transmembrane domain.

The promoter swap approach was not successful for FLP depletion during the liver stage. This is underlined by the fact that expression profile covering all stages but the liver stage is very rare. The liver stage fulfils a preparation role for the blood stage and finding a gene that is off in that stage but abundantly expressed during the asexual blood cycle is very unlikely. An alternative approach with the use of more than one promoter, specific for individual stages, might support

parasite development through the blood and mosquito stages and shut *flp* expression down in the liver stage. However, this approach would require cloning of the whole gene, which is almost impossible due to its size. Alternatively, a conditional KO with FLP/FRT system [192] could be used to excise the *flp* locus from the genome in the beginning of the liver stage.

Depletion of FLP in the gametocyte stage by promoter swapping worked very well as shown by the reduction in transcript and protein levels (Fig 3.21 and 3.22). *Clag* expression is much higher than *flp* expression during the asexual blood stage, which led to overexpression of *flp* about hundred-fold in the Δflp_{gam} line (Fig. 3.21 and 3.22). Surprisingly, this overexpression did not translate into a phenotype, as both parasite growth and gametocyte development remained comparable to wildtype in the Δflp_{gam} line (Fig. 3.22). This indicates that FLP fulfils functions, which are not hampered by high abundance of the protein. Depletion study should be complemented by a genetic rescue to exclude possible artefacts. Similarity with the role and the evolutionary conservation between FLP and Fer-1 from *C. elegans* made us additionally consider complementation with that gene. In both cases, cloning was not successful despite many attempts, likely due to the extremely large size of the genes and the AT-rich genome of *Plasmodium*.

The failure of transgenesis in *Plasmodium* can be underlined by the resistance of the genetic locus to manipulations. However, this option cannot be considered in the case of FLP. First, both the 5'end and the 3'end were successfully modified without impact on parasite viability. The 5'UTR of *flp* was replaced by *ama1* promoter with no harm to the parasite (Fig. 3.18). At the 3'end, HA tag was fused to FLP, which resulted in a viable line (Fig. 3.10). An explanation for the failure of C-terminal tagging could be an alternative splicing or alternative end of the gene. Our 3'RACE analysis showed that during both the asexual blood stage and the gametocyte stage, *flp* transcript is spliced and terminated exactly as annotated (Fig. 3.12). This overall suggests that it is indeed an interference with FLP function that prevents fusion to tags or truncation of the gene. The explanation for that is suggested by the domain assignment (Fig. 4.1). The C-terminus is occupied by the TM domain (with a single C-terminal amino acid outside of the membrane). This structure and topology is reminiscent of SNARE proteins, which rely on the very short C-terminus during co-translational insertion into membranes and C-terminal tagging is not possible. Similarly to SNARE, C-terminal tagging of FLP might interfere with insertion of the protein into membranes. The N-terminus of FLP is occupied by the first C2 domain, which was shown to carry the most important functions in many ferlin homologues [113] and a tag might compromise its function. Usually, interference of tags with protein functions can be prevented by a linker of several amino acids between the tag and the protein. We used a linker of at least 10 amino acids for all the tagged

lines. However, the function of FLP was still compromised. Overall it is very difficult to conclude what underlies the failure to generate tagged line. The impact of tagging cannot be reliably predicted even for proteins with clear domain topology and known functions. With no function assigned to FLP domains, the design and troubleshooting of tagging strategies is more a guessing.

Given the tendency that smaller tags translated into better viability of the parasite, other small tags could be fused to the less sensitive N-terminus of FLP to confirm its localization pattern determined using the *flp::HA* line (Fig. 3.9). The ideal option would be to use a fluorescent tag, to capture dynamics of the protein. One option might be the tetra-cysteine tags FlAsH and ReAsh, one of the smallest available tags that can react with fluorescent dyes *in vivo* [193]. However, this tagging approach is generally prone to high background as all cysteine-rich proteins (which are common in *Plasmodium*) coordinate the dye. The tag was used once in *Plasmodium* so far and although the visualization of the protein of interest was successful it was not perfect and complementary approaches had to be used to confirm the data [194].

The usual approach to confirm protein subcellular localization is antibody staining. We tried to express recombinant parts of the FLP protein and use it for immunization of rodents and generation of polyclonal antibody (chapter 3.1.2). Although two out of four recombinant proteins were successfully expressed, they were not soluble and extensive optimizations did not help. The insoluble recombinant protein could be purified under denaturing conditions and used for immunization. However, this approach fundamentally increases the risk of future off-targeting of the polyclonal antibody. Another alternative is the commercial generation of anti-peptide antibodies offered by several companies. Apart from the high cost of the procedure, experience with these antibodies in the malaria field is generally not good.

4.3 FLP is necessary for host-to-vector transmission

Ferlins are established mediators of calcium-induced membrane fusion and regulated exocytosis in higher eukaryotes. We showed for the first time that an evolutionarily ancient member of the ferlin protein family is critical for fertility in a protozoan. Specifically FLP is necessary for egress of both male and female gametes from the host RBC (3.24 and 3.25) and life cycle progression in the mosquito vector (Fig. 3.23).

Vesicular localization is typical for the ferlin protein family [117,125,132,153]. Using the *flp::HA* line, we detected FLP in speckles, indicating vesicular localization, in both asexual and sexual blood stages (Fig. 3.9). These vesicles relocalized to the cell surface in the process of gametogenesis (Fig. 3.9), suggesting localization to egress vesicles, e.g. osmiophilic bodies [56,58] or egress vesicles

containing PPLP2 [62,63], GEST [59], PAT [60] or MTRAP [64,66]. Indeed, we observed an egress defect after gametocyte-specific depletion of FLP - gametes lacking FLP failed to egress from the host RBC (Fig. 3.24).

While the RBCM was clearly intact around activated *Δflp*$_{gam}$ microgametes (Fig. 3.24), the rupture of the PVM could not be completely excluded or confirmed from our data. The FLP-lacking gametes were still decorated by the PVM marker SEP1 after activation (Fig. 3.24), but the signal was less prominent than in non-activated gametocytes and the PVM often appeared damaged. This is reminiscent of starting PVM vacuolisation, an early step of gamete egress defined in a recent study [54]. The explanation for this membrane appearance could be an incomplete lysis or a blocked release of PVM remnants due to the presence of the RBCM (these remnants readily dissolve in the activated wildtype gametes, Fig. 3.24). However, the appearance of a completely lysed PVM trapped inside the intact RBCM (as reported for PPLP2 knock-out [62]) appears substantially different to our observation [54], suggesting that PVM egress is indeed impaired in the *Δflp*$_{gam}$ parasites. Partially successful PVM lysis in the activated gametes lacking FLP could be explained by the reported observation that the PVM can rupture in the absence of calcium [53]. As discussed in chapter 4.4, FLP likely functions downstream of the calcium signalling and therefore an additional pathway that is FLP- and calcium-independent might initiate PVM rupture.

Similar egress impairment phenotypes were reported in a number of studies [53,59–62,64,66]. All of the proteins underlying these phenotypes localize to vesicular structures, similarly to FLP (Fig. 3.9). In several cases, these vesicles were identified as OBs by co-localization with the marker proteins G377 or MDV1/PEG3 [59–61]. While we detected FLP expression in both male and female gametocytes (Fig. 3.11) with similar abundance and localization of the protein, we could not observe obvious co-localization with G377- or PPLP2-containing vesicles (Fig. 3.27). Interestingly, while depletion of GEST and MDV1/PEG3 (egress factors localizing to G377-positive OBs) only leads to partial arrest of the life cycle at host-to-vector transmission [59,61], FLP-depleted parasites failed to transmit completely (Fig. 3.23), demonstrating the essential role of the protein in this process. This is reminiscent of PAT and MTRAP, two recently described egress factors, depletion of which leads to a complete life-cycle arrest during transmission [60,64,64,66,66]. MTRAP localizes to egress vesicles but does not colocalize with G377 in *P. falciparum* [64] nor with MDV1/PEG3 in *P. berghei* [64,66]. This indicates that gametocyte egress molecules cluster into different combinations and occupy different subsets of vesicles. From published data it appears that some subsets have a smaller impact on gametocyte egress than others with partial redundancy. While MDV1/PEG3, PPLP2, G377 and GEST KO show severe but incomplete block of transmission [57–59,61–63], respectively, PAT [60], MTRAP [64,66] and FLP are critical for

transmission. PAT was previously shown to occupy vesicles together with female-specific G377 and male-specific PPLP2 [60]. This indicates that PAT is present in several subsets of vesicles, likely underlying its necessary role (Fig. 4.2). MTRAP and FLP do not colocalize with G377, respectively (Fig. 3.27, [64]), MTRAP does not colocalize with MDV1/PEG3 [64] and FLP with PPLP2 (Fig. 3.27). Both proteins localize to vesicles that are essential for gametocyte egress and their colocalization was not analysed, so we speculate that FLP and MTRAP might occupy the same or similar subset of vesicles (Fig. 4.2).

Due to the lack of a marker protein defining the FLP-containing vesicles, we were not able to address the precise time and localization of the egress defect caused by FLP absence. Based on data from other ferlin orthologues, a function in vesicular exocytosis seems most likely, with impaired fusion of egress vesicles in Δflp_{gam} parasites possibly causing the observed phenotype. Alternatively, FLP could play a role in the trafficking of egress vesicles to the cell periphery, as mediating of vesicular trafficking via interaction within protein complexes was reported to be an additional function of dysferlin [152].

In vitro, Δflp_{gam} female gametocytes were strongly impaired in fertility as shown by cross fertilization experiments. Some of the Δflp_{gam} macrogametes got fertilized by fertile microgametes as shown by the presence of a few red ookinetes (Fig. 3.24). This could be explained by physical forces exerted by the motile microgametes, leading to fertilization of non-egressed macrogametes. An alternative explanation of the dramatically reduced fertilization capacity in macrogametes, other than an egress defect, seems highly unlikely as the Δflp_{gam} life cycle progression as well as macrogamete fertilization can be rescued by chemical membrane lysis (Fig. 3.26).

Although the transmission of FLP-depleted parasites was completely abolished, the trapped gametes were fully fertile as transmission could be rescued by chemical membrane lysis (Fig. 3.26). This is in agreement with the function of other ferlins important for fertility since ferlin-lacking sperm cells were unable to fuse vesicles or lyse a surrounding membrane, but otherwise developed normally [153,157]. While *C. elegans*, *D. melanogaster* and *P. berghei* ferlins are critically needed for fertility, no mammalian ferlin was reported to play similar roles to date. However, ferlin transcripts were detected in testis and male germ line of mice and colts [195,196]. Otoferlin-specific antibody also detected the protein in murine testis [125]. This might indicate that the ancient role of ferlins was to some degree maintained in evolution, although more specialized roles for ferlins developed.

4.4 FLP as a candidate for calcium-dependent mediator of egress

While we were not able to answer whether FLP function is calcium-dependent in this study, many ferlins were shown to be critically dependent on calcium signalling [112,117,118,125,132]. The C2 domain, the most characteristic feature of ferlins, is a well described calcium- and phospholipid-binding unit of about 130 amino acids, which typically confers calcium-dependent functions to proteins that harbour it, e.g. synaptotagmins [91]. Egress in the related apicomplexan parasite *Toxoplasma gondii* is dependent on a C2 domain-containing protein DOC2, which mediates exocytosis in a calcium-dependent fashion [82]. In *Plasmodium*, the only egress factor with calcium binding domain suggested to date is CDPK1, a calcium-dependent protein kinase. CDPK1 plays multiple roles in transmission and subsequent ookinete development. However, its role in egress was suggested based on the delayed egress of CDPK1-depleted gametocytes [49]. Although the reason for the delay is not clear, it is unlikely that CDPK1 mediates egress of the essential egress vesicles, as CDPK1-KO gametes eventually egress [49]. Given the dependence of *Plasmodium* gamete egress on calcium signalling and the presence of six C2 domains in the FLP sequence, it seems likely that its functions during this process is indeed regulated by calcium. FLP may even represent the missing link between calcium signalling and gamete egress (Fig. 4.2). However, more experiments are needed to confirm or disprove this hypothetical link. This remains a major challenge due to the essentiality of FLP during the asexual blood stage on the one hand, and several pathways being simultaneously triggered by calcium during gametogenesis on the other.

Several pathways are regulated by a single transient peak in calcium in the beginning of gametogenesis (Fig. 4.2) [73]. It is therefore challenging to track the dependency of individual pathways on calcium. Chelation is known to inhibit exflagellation [73]. We chelated calcium at different time points after induction of gametogenesis with the aim to trigger CDPK pathways but prevent FLP functions. However, no intermediate outcomes resembling the absence of FLP were observed (Table 3.1), indicating that the whole pathway is regulated simultaneously and/or is irreversible by chelation once calcium has bound its targets.

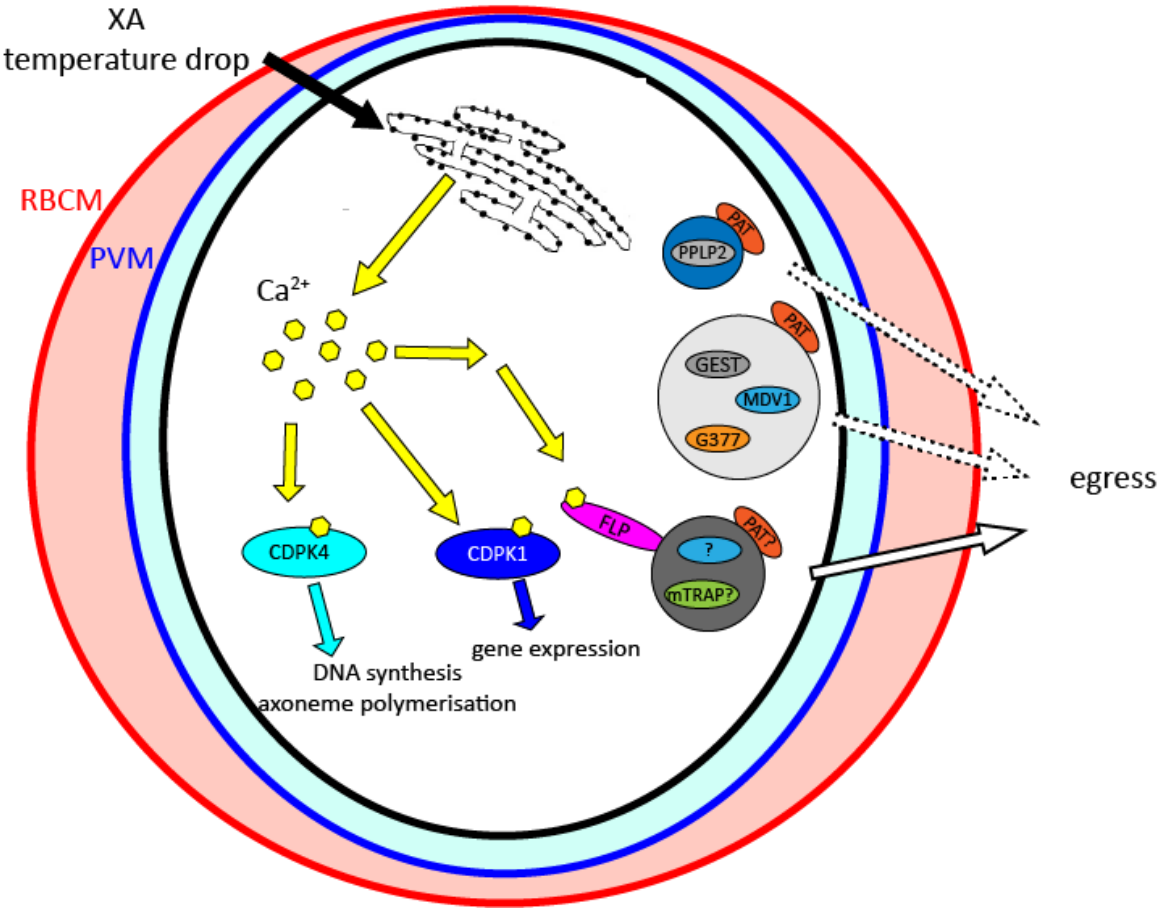

Figure 4.2 Revised model of gametogenesis regulated by calcium. In response to the drop in temperature and presence of the xanthurenic acid, signal transduction is triggered that results in calcium release from the endoplasmic reticulum. Calcium mediates several pathways. Activation of CDPK4 and CDPK1 lead to flagella assembly and mitosis in microgametocytes and to changes in gene expression, respectively. Calcium mediates egress of gametocytes via exocytosis of egress vesicles. These vesicles carry different sets of cargo proteins (shown is a suggestion of individual subsets based on published data) and have different importance for the gametocyte egress. The molecular player necessary for translation of the calcium signal into the exocytosis of vesicle is currently not known and we propose FLP as a potential candidate.

Egress of asexual and sexual blood stages of *Plasmodium* differs in many points. For example, gamete egress is triggered in response to the sudden and profound changes in the extracellular environment, while asexual parasites emerge when they reach maturity. While many of the described gamete egress factors can be knocked-out and have therefore no critical function during the asexual development [58–64,66], *flp* is refractory to gene deletion (Fig. 3.13). Its localization

in the schizont stage (Fig. 3.9) appears similar to the staining of exonemes, vesicles carrying the egress protease SUB1 in the asexual blood stage [69,74]. It is therefore tempting to speculate that FLP plays a role in egress of blood stage merozoites, perhaps even extending its role to the egress of liver stage merozoites as suggested by the high *flp* transcript abundance in the late liver stage (Fig 3.1). Host cell egress of intraerythrocytic sexual and blood-stage parasites, as well as intra-hepatic liver-stage merozoites do share common features [26]; for example the inside-out model is currently accepted for the egress of all three parasite stages with PVM rupture preceding that of the RBCM [21,53,70]. Furthermore, a sharp increase of calcium levels has been reported in all three cases [72–74] and some common players such as proteases from the SERA family, SUB1, falcipain-1/berghepain-1, plasmepsins IX and X can be found [52,53,66,69,74–81]).

4.5 Conclusion

In conclusion, we present the first characterization of an apicomplexan ferlin protein that functions in fertility. Progression of life cycle is critically dependent on FLP with both male and female gametes remaining trapped inside the host RBC and sterile when FLP is depleted. FLP localization to vesicles is in very good agreement with data from other ferlin orthologues, which allows speculating on calcium-dependency of FLP function and its potential role in exocytosis of its resident vesicles. Our data establish FLP as a critical factor for *Plasmodium* gamete egress with a potential hypothetical function in the egress of other parasite stages.

Further experiments shall address the dependency of FLP function on calcium as well as its functions in the asexual blood and liver stages. Given the restrictions in *flp* manipulations, novel techniques able to overcome the essentiality during asexual blood stage, allowing for tracking of individual pathways in a complex signalling transduction and visualizing of proteins live with minimal impact on their function will likely be needed to answer the questions. Although *flp* sensitivity to manipulations is extraordinary, many other essential genes can be found in the *Plasmodium* genome. There is a strong request for novel techniques and many people work on the development. After detailed analysis, FLP might be established not only as a promising immune target but also as a multi-stage essential (egress) factor.

5 References

1. Laveran A (1881) The pathology of malaria. *Lancet* **2**: 840–841.

2. Ross R (1897) Observations on a condition necessary to the transformation of the malaria crescent. *British Medical Journal* **1**: 251.

3. Han YS, Thompson J, Kafatos FC, Barillas-Mury C (2000) Molecular interactions between Anopheles stephensi midgut cells and Plasmodium berghei: the time bomb theory of ookinete invasion of mosquitoes. *The EMBO journal* **19**: 6030–6040.

4. Sinden RE, Dawes EJ, Alavi Y, Waldock J, Finney O, Mendoza J, Butcher GA, Andrews L, Hill AV, Gilbert SC, et al. (2007) Progression of Plasmodium berghei through Anopheles stephensi is density-dependent. *PLoS Pathog* **3**: e195.

5. Kariu T, Yuda M, Yano K, Chinzei Y (2002) MAEBL is essential for malarial sporozoite infection of the mosquito salivary gland. *J Exp Med* **195**: 1317–1323.

6. Al-Olayan EM, Beetsma AL, Butcher GA, Sinden RE, Hurd H (2002) Complete development of mosquito phases of the malaria parasite in vitro. *Science* **295**: 677–679.

7. Ménard R, Sultan AA, Cortes C, Altszuler R, Van Dijk MR, Janse CJ, Waters AP, Nussenzweig RS, Nussenzweig V (1997) Circumsporozoite protein is required for development of malaria sporozoites in mosquitoes. *Nature* **385**: 336.

8. Vanderberg J, Rhodin J (1967) Differentiation of nuclear and cytoplasmic fine structure during sporogonic development of Plasmodium berghei. *The Journal of cell biology* **32**: C7.

9. Sinden R, Garnham P (1973) A comparative study on the ultrastructure of Plasmodium sporozoites within the oocyst and salivary glands, with particular reference to the incidence of the micropore. *Transactions of the Royal Society of Tropical Medicine and Hygiene* **67**: 631–634.

10. Klug D, Frischknecht F (2017) Motility precedes egress of malaria parasites from oocysts. *Elife* **6**:

11. Aly AS, Matuschewski K (2005) A malarial cysteine protease is necessary for Plasmodium sporozoite egress from oocysts. *Journal of Experimental Medicine* **202**: 225–230.

12. Wang Q, Fujioka H, Nussenzweig V (2005) Exit of Plasmodium sporozoites from oocysts is an active process that involves the circumsporozoite protein. *PLoS Pathog* **1**: e9.

13. Sinden R, Matuschewski K (2005) The sporozoite. In, *Molecular Approaches to Malaria* pp 169–190. American Society of Microbiology.

14. Hillyer JF, Barreau C, Vernick KD (2007) Efficiency of salivary gland invasion by malaria sporozoites is controlled by rapid sporozoite destruction in the mosquito haemocoel. *Int J Parasitol* **37**: 673–681.

15. Pimenta PF, Touray M, Miller L (1994) The journey of malaria sporozoites in the mosquito salivary gland. *Journal of Eukaryotic Microbiology* **41**: 608–624.

16. Matsuoka H, Yoshida S, Hirai M, Ishii A (2002) A rodent malaria, Plasmodium berghei, is experimentally transmitted to mice by merely probing of infective mosquito, Anopheles stephensi. *Parasitology international* **51**: 17–23.

17. Amino R, Thiberge S, Martin B, Celli S, Shorte S, Frischknecht F, Ménard R (2006) Quantitative imaging of Plasmodium transmission from mosquito to mammal. *Nat Med* **12**: 220–224.

18. Frevert U, Engelmann S, Zougbédé S, Stange J, Ng B, Matuschewski K, Liebes L, Yee H (2005) Intravital observation of Plasmodium berghei sporozoite infection of the liver. *PLoS Biol* **3**: e192.

19. Lingelbach K, Joiner KA (1998) The parasitophorous vacuole membrane surrounding Plasmodium and Toxoplasma: an unusual compartment in infected cells. *Journal of cell science* **111**: 1467–1475.

20. Gonzalez V, Combe A, David V, Malmquist NA, Delorme V, Leroy C, Blazquez S, Ménard R, Tardieux I (2009) Host cell entry by apicomplexa parasites requires actin polymerization in the host cell. *Cell Host Microbe* **5**: 259–272.

21. Graewe S, Rankin KE, Lehmann C, Deschermeier C, Hecht L, Froehlke U, Stanway RR, Heussler V (2011) Hostile takeover by Plasmodium: reorganization of parasite and host cell membranes during liver stage egress. *PLoS pathogens* **7**: e1002224.

22. Baer K, Klotz C, Kappe SH, Schnieder T, Frevert U (2007) Release of hepatic Plasmodium yoelii merozoites into the pulmonary microvasculature. *PLoS pathogens* **3**: e171.

23. Sturm A, Amino R, van de Sand C, Regen T, Retzlaff S, Rennenberg A, Krueger A, Pollok J-M, Menard R, Heussler VT (2006) Manipulation of host hepatocytes by the malaria parasite for delivery into liver sinusoids. *Science* **313**: 1287–1290.

24. Janse CJ, Franke-Fayard B, Mair GR, Ramesar J, Thiel C, Engelmann S, Matuschewski K, van Gemert GJ, Sauerwein RW, Waters AP (2006) High efficiency transfection of Plasmodium berghei facilitates novel selection procedures. *Molecular and biochemical parasitology* **145**: 60–70.

25. Arnot DE, Ronander E, Bengtsson DC (2011) The progression of the intra-erythrocytic cell cycle of Plasmodium falciparum and the role of the centriolar plaques in asynchronous mitotic division during schizogony. *International journal for parasitology* **41**: 71–80.

26. Kuehn A, Pradel G (2010) The coming-out of malaria gametocytes. *J Biomed Biotechnol* **2010**: 976827.

27. Sinha A, Hughes KR, Modrzynska KK, Otto TD, Pfander C, Dickens NJ, Religa AA, Bushell E, Graham AL, Cameron R, et al. (2014) A cascade of DNA-binding proteins for sexual commitment and development in Plasmodium. *Nature* **507**:

253.

28. Lopez-Rubio J-J, Mancio-Silva L, Scherf A (2009) Genome-wide analysis of heterochromatin associates clonally variant gene regulation with perinuclear repressive centers in malaria parasites. *Cell host \& microbe* **5**: 179–190.

29. Kafsack BFC, Rovira-Graells N, Clark TG, Bancells C, Crowley VM, Campino SG, Williams AE, Drought LG, Kwiatkowski DP, Baker DA, et al. (2014) A transcriptional switch underlies commitment to sexual development in malaria parasites. *Nature* **507**: 248–252.

30. Brancucci NM, Bertschi NL, Zhu L, Niederwieser I, Chin WH, Wampfler R, Freymond C, Rottmann M, Felger I, Bozdech Z, et al. (2014) Heterochromatin protein 1 secures survival and transmission of malaria parasites. *Cell host \& microbe* **16**: 165–176.

31. Coleman BI, Skillman KM, Jiang RH, Childs LM, Altenhofen LM, Ganter M, Leung Y, Goldowitz I, Kafsack BF, Marti M, et al. (2014) A Plasmodium falciparum histone deacetylase regulates antigenic variation and gametocyte conversion. *Cell host \& microbe* **16**: 177–186.

32. Alano P (2007) Plasmodium falciparum gametocytes: still many secrets of a hidden life. *Mol Microbiol* **66**: 291–302.

33. Silvestrini F, Alano P, Williams J (2000) Commitment to the production of male and female gametocytes in the human malaria parasite Plasmodium falciparum. *Parasitology* **121**: 465–471.

34. Smith T, Lourenco P, Carter R, Walliker D, Ranford-Cartwright L (2000) Commitment to sexual differentiation in the human malaria parasite, Plasmodium falciparum. *Parasitology* **121**: 127–133.

35. Robert V, Read A, Essong J, Tchuinkam T, Mulder B, Verhave J-P, Carnevale P (1996) Effect of gametocyte sex ratio on infectivity of Plasmodium falciparum to Anopheles gambiae. *Transactions of the Royal Society of Tropical Medicine and Hygiene* **90**: 621–624.

36. Khan SM, Franke-Fayard B, Mair GR, Lasonder E, Janse CJ, Mann M, Waters AP (2005) Proteome analysis of separated male and female gametocytes reveals novel sex-specific Plasmodium biology. *Cell* **121**: 675–687.

37. Guttery DS, Roques M, Holder AA, Tewari R (2015) Commit and Transmit: Molecular Players in Plasmodium Sexual Development and Zygote Differentiation. *Trends in parasitology* **31**: 676–685.

38. Sinden R, Croll N (1975) Cytology and kinetics of microgametogenesis and fertilization in Plasmodium yoelii nigeriensis. *Parasitology* **70**: 53–65.

39. Billker O, Lindo V, Panico M, Etienne A, Paxton T, Dell A, Rogers M, Sinden R, Morris H (1998) Identification of xanthurenic acid as the putative inducer of

malaria development in the mosquito. *Nature* **392**: 289.

40. Mair GR, Lasonder E, Garver LS, Franke-Fayard BMD, Carret CK, Wiegant JCAG, Dirks RW, Dimopoulos G, Janse CJ, Waters AP (2010) Universal features of post-transcriptional gene regulation are critical for Plasmodium zygote development. *PLoS Pathog* **6**: e1000767.

41. Mair GR, Braks JA, Garver LS, Dimopoulos G, Hall N, Wiegant JC, Dirks RW, Khan SM, Janse CJ, Waters AP (2006) Translational Repression is essential for Plasmodium sexual development and mediated by a DDX6-type RNA helicase. *Science (New York, NY)* **313**: 667.

42. Brochet M, Billker O (2016) Calcium signalling in malaria parasites. *Molecular microbiology* **100**: 397–408.

43. Straschil U, Talman AM, Ferguson DJP, Bunting KA, Xu Z, Bailes E, Sinden RE, Holder AA, Smith EF, Coates JC, et al. (2010) The Armadillo repeat protein PF16 is essential for flagellar structure and function in Plasmodium male gametes. *PLoS ONE* **5**: e12901.

44. Tewari R, Dorin D, Moon R, Doerig C, Billker O (2005) An atypical mitogen-activated protein kinase controls cytokinesis and flagellar motility during male gamete formation in a malaria parasite. *Molecular microbiology* **58**: 1253–1263.

45. Marques SR, Ramakrishnan C, Carzaniga R, Blagborough AM, Delves MJ, Talman AM, Sinden RE (2015) An essential role of the basal body protein SAS-6 in Plasmodium male gamete development and malaria transmission. *Cellular microbiology* **17**: 191–206.

46. Rangarajan R, Bei AK, Jethwaney D, Maldonado P, Dorin D, Sultan AA, Doerig C (2005) A mitogen-activated protein kinase regulates male gametogenesis and transmission of the malaria parasite Plasmodium berghei. *EMBO Rep* **6**: 464–469.

47. Deligianni E, Morgan RN, Bertuccini L, Kooij TW, Laforge A, Nahar C, Poulakakis N, Schüler H, Louis C, Matuschewski K, et al. (2011) Critical role for a stage-specific actin in male exflagellation of the malaria parasite. *Cellular microbiology* **13**: 1714–1730.

48. Sinden R, Talman A, Marques S, Wass MN, Sternberg MJ (2010) The flagellum in malarial parasites. *Current opinion in microbiology* **13**: 491–500.

49. Sebastian S, Brochet M, Collins MO, Schwach F, Jones ML, Goulding D, Rayner JC, Choudhary JS, Billker O (2012) A Plasmodium calcium-dependent protein kinase controls zygote development and transmission by translationally activating repressed mRNAs. *Cell host \& microbe* **12**: 9–19.

50. Janse C, Van der Klooster P, Van der Kaay H, Van der Ploeg M, Overdulve J (1986) Rapid repeated DNA replication during microgametogenesis and DNA synthesis in young zygotes of Plasmodium berghei. *Transactions of the Royal*

Society of Tropical Medicine and Hygiene **80**: 154–157.

51. Ukaegbu UE, Zhang X, Heinberg AR, Wele M, Chen Q, Deitsch KW (2015) A unique virulence gene occupies a principal position in immune evasion by the malaria parasite plasmodium falciparum. *PLoS Genet* **11**: e1005234.

52. Blackman MJ (2008) Malarial proteases and host cell egress: an "emerging"cascade. *Cellular microbiology* **10**: 1925–1934.

53. Sologub L, Kuehn A, Kern S, Przyborski J, Schillig R, Pradel G (2011) Malaria proteases mediate inside-out egress of gametocytes from red blood cells following parasite transmission to the mosquito. *Cellular microbiology* **13**: 897–912.

54. Andreadaki M, Hanssen E, Deligianni E, Claudet C, Wengelnik K, Mollard V, McFadden GI, Abkarian M, Braun-Breton C, Siden-Kiamos I (2018) Sequential Membrane Rupture and Vesiculation during Plasmodium berghei Gametocyte Egress from the Red Blood Cell. *Scientific Reports* **8**: 3543.

55. Hale VL, Watermeyer JM, Hackett F, Vizcay-Barrena G, van Ooij C, Thomas JA, Spink MC, Harkiolaki M, Duke E, Fleck RA, et al. (2017) Parasitophorous vacuole poration precedes its rupture and rapid host erythrocyte cytoskeleton collapse in Plasmodium falciparum egress. *Proceedings of the National Academy of Sciences* **114**: 3439–3444.

56. Sinden R (1982) Gametocytogenesis of Plasmodium falciparum in vitro: an electron microscopic study. *Parasitology* **84**: 1–11.

57. Olivieri A, Bertuccini L, Deligianni E, Franke-Fayard B, Currà C, Siden-Kiamos I, Hanssen E, Grasso F, Superti F, Pace T, et al. (2015) Distinct properties of the egress-related osmiophilic bodies in male and female gametocytes of the rodent malaria parasite Plasmodium berghei. *Cellular microbiology* **17**: 355–368.

58. Koning-Ward D, Tania F, Olivieri A, Bertuccini L, Hood A, Silvestrini F, Charvalias K, Berzosa D'\iaz P, Camarda G, McElwain TF, et al. (2008) The role of osmiophilic bodies and Pfg377 expression in female gametocyte emergence and mosquito infectivity in the human malaria parasite Plasmodium falciparum. *Molecular microbiology* **67**: 278–290.

59. Talman AM, Lacroix C, Marques SR, Blagborough AM, Carzaniga R, Ménard R, Sinden RE (2011) PbGEST mediates malaria transmission to both mosquito and vertebrate host. *Molecular microbiology* **82**: 462–474.

60. Kehrer J, Singer M, Lemgruber L, Silva PA, Frischknecht F, Mair GR (2016) A Putative Small Solute Transporter Is Responsible for the Secretion of G377 and TRAP-Containing Secretory Vesicles during Plasmodium Gamete Egress and Sporozoite Motility. *PLoS Pathog* **12**: e1005734.

61. Ponzi M, Sidén-Kiamos I, Bertuccini L, Currà C, Kroeze H, Camarda G, Pace T, Franke-Fayard B, Laurentino EC, Louis C, et al. (2009) Egress of Plasmodium berghei gametes from their host erythrocyte is mediated by the MDV-1/PEG3

protein. *Cellular microbiology* **11**: 1272–1288.

62. Deligianni E, Morgan RN, Bertuccini L, Wirth CC, Silmon de Monerri NC, Spanos L, Blackman MJ, Louis C, Pradel G, Siden-Kiamos I (2013) A perforin-like protein mediates disruption of the erythrocyte membrane during egress of Plasmodium berghei male gametocytes. *Cellular microbiology* **15**: 1438–1455.

63. Wirth CC, Glushakova S, Scheuermayer M, Repnik U, Garg S, Schaack D, Kachman MM, Weißbach T, Zimmerberg J, Dandekar T, et al. (2014) Perforin-like protein PPLP2 permeabilizes the red blood cell membrane during egress of Plasmodium falciparum gametocytes. *Cellular microbiology* **16**: 709–733.

64. Bargieri DY, Thiberge S, Tay CL, Carey AF, Rantz A, Hischen F, Lorthiois A, Straschil U, Singh P, Singh S, et al. (2016) Plasmodium Merozoite TRAP Family Protein Is Essential for Vacuole Membrane Disruption and Gamete Egress from Erythrocytes. *Cell Host \& Microbe* **20**: 618–630.

65. Lal K, Delves MJ, Bromley E, Wastling JM, Tomley FM, Sinden RE (2009) Plasmodium male development gene-1 (mdv-1) is important for female sexual development and identifies a polarised plasma membrane during zygote development. *International journal for parasitology* **39**: 755–761.

66. Kehrer J, Frischknecht F, Mair GR (2016) Proteomic analysis of the Plasmodium berghei gametocyte egressome and vesicular bioID of osmiophilic body proteins identifies merozoite TRAP-like Protein (MTRAP) as an essential factor for parasite transmission. *Molecular \& Cellular Proteomics* **15**: 2852–2862.

67. Blackman MJ, Carruthers VB (2013) Recent insights into apicomplexan parasite egress provide new views to a kill. *Curr Opin Microbiol* **16**: 459–464.

68. Baum J, Gilberger T-W, Frischknecht F, Meissner M (2008) Host-cell invasion by malaria parasites: insights from Plasmodium and Toxoplasma. *Trends Parasitol* **24**: 557–563.

69. Yeoh S, O'Donnell RA, Koussis K, Dluzewski AR, Ansell KH, Osborne SA, Hackett F, Withers-Martinez C, Mitchell GH, Bannister LH, et al. (2007) Subcellular discharge of a serine protease mediates release of invasive malaria parasites from host erythrocytes. *Cell* **131**: 1072–1083.

70. Wickham ME, Culvenor JG, Cowman AF (2003) Selective inhibition of a two-step egress of malaria parasites from the host erythrocyte. *Journal of Biological Chemistry* **278**: 37658–37663.

71. Sturm A, Graewe S, Franke-Fayard B, Retzlaff S, Bolte S, Roppenser B, Aepfelbacher M, Janse C, Heussler V (2009) Alteration of the parasite plasma membrane and the parasitophorous vacuole membrane during exo-erythrocytic development of malaria parasites. *Protist* **160**: 51–63.

72. Sturm A, Amino R, Van de Sand C, Regen T, Retzlaff S, Rennenberg A, Krueger A, Pollok J-M, Menard R, Heussler VT (2006) Manipulation of host hepatocytes

by the malaria parasite for delivery into liver sinusoids. *Science* **313**: 1287–1290.

73. Billker O, Dechamps S, Tewari R, Wenig G, Franke-Fayard B, Brinkmann V (2004) Calcium and a calcium-dependent protein kinase regulate gamete formation and mosquito transmission in a malaria parasite. *Cell* **117**: 503–514.

74. Agarwal S, Singh MK, Garg S, Chitnis CE, Singh S (2013) Ca(2+) -mediated exocytosis of subtilisin-like protease 1: a key step in egress of Plasmodium falciparum merozoites. *Cell Microbiol* **15**: 910–921.

75. Pino P, Caldelari R, Mukherjee B, Vahokoski J, Klages N, Maco B, Collins CR, Blackman MJ, Kursula I, Heussler V, et al. (2017) A multistage antimalarial targets the plasmepsins IX and X essential for invasion and egress. *Science* **358**: 522–528.

76. Hopp CS, Bennett BL, Mishra S, Lehmann C, Hanson KK, Lin J, Rousseau K, Carvalho FA, van der Linden WA, Santos NC, et al. (2017) Deletion of the rodent malaria ortholog for falcipain-1 highlights differences between hepatic and blood stage merozoites. *PLoS pathogens* **13**: e1006586.

77. Nasamu AS, Glushakova S, Russo I, Vaupel B, Oksman A, Kim AS, Fremont DH, Tolia N, Beck JR, Meyers MJ, et al. (2017) Plasmepsins IX and X are essential and druggable mediators of malaria parasite egress and invasion. *Science* **358**: 518–522.

78. Schmidt-Christensen A, Sturm A, Horstmann S, Heussler VT (2008) Expression and processing of Plasmodium berghei SERA3 during liver stages. *Cellular microbiology* **10**: 1723–1734.

79. Withers-Martinez C, Strath M, Hackett F, Haire LF, Howell SA, Walker PA, Christodoulou E, Dodson GG, Blackman MJ (2014) The malaria parasite egress protease SUB1 is a calcium-dependent redox switch subtilisin. *Nature communications* **5**: 3726.

80. Tawk L, Lacroix C, Gueirard P, Kent R, Gorgette O, Thiberge S, Mercereau-Puijalon O, Ménard R, Barale J-C (2013) A key role for Plasmodium subtilisin-like SUB1 protease in egress of malaria parasites from host hepatocytes. *Journal of Biological Chemistry* **288**: 33336–33346.

81. Collins CR, Hackett F, Atid J, Tan MSY, Blackman MJ (2017) The Plasmodium falciparum pseudoprotease SERA5 regulates the kinetics and efficiency of malaria parasite egress from host erythrocytes. *PLoS pathogens* **13**: e1006453.

82. Farrell A, Thirugnanam S, Lorestani A, Dvorin JD, Eidell KP, Ferguson DJ, Anderson-White BR, Duraisingh MT, Marth GT, Gubbels M-J (2012) A DOC2 protein identified by mutational profiling is essential for apicomplexan parasite exocytosis. *Science* **335**: 218–221.

83. Kafsack BF, Pena JD, Coppens I, Ravindran S, Boothroyd JC, Carruthers VB (2009) Rapid membrane disruption by a perforin-like protein facilitates parasite

exit from host cells. *Science* **323**: 530–533.

84. Koussis K, Withers-Martinez C, Yeoh S, Child M, Hackett F, Knuepfer E, Juliano L, Woehlbier U, Bujard H, Blackman MJ (2009) A multifunctional serine protease primes the malaria parasite for red blood cell invasion. *EMBO J* **28**: 725–735.

85. Berridge MJ, Lipp P, Bootman MD (2000) The versatility and universality of calcium signalling. *Nature reviews Molecular cell biology* **1**: 11.

86. Rohrbach P, Friedrich O, Hentschel J, Plattner H, Fink RHA, Lanzer M (2005) Quantitative calcium measurements in subcellular compartments of Plasmodium falciparum-infected erythrocytes. *J Biol Chem* **280**: 27960–27969.

87. Gazarini ML, Garcia CR (2004) The malaria parasite mitochondrion senses cytosolic Ca 2+ fluctuations. *Biochemical and biophysical research communications* **321**: 138–144.

88. Rotmann A, Sanchez C, Guiguemde A, Rohrbach P, Dave A, Bakouh N, Planelles G, Lanzer M (2010) PfCHA is a mitochondrial divalent cation/H+ antiporter in Plasmodium falciparum. *Molecular microbiology* **76**: 1591–1606.

89. Docampo R, Moreno SN (2011) Acidocalcisomes. *Cell calcium* **50**: 113–119.

90. Harper JF, Breton G, Harmon A (2004) Decoding Ca2+ signals through plant protein kinases. *Annu Rev Plant Biol* **55**: 263–288.

91. Nalefski EA, Falke JJ (1996) The C2 domain calcium-binding motif: structural and functional diversity. *Protein Science* **5**: 2375–2390.

92. Raabe A, Berry L, Sollelis L, Cerdan R, Tawk L, Vial HJ, Billker O, Wengelnik K (2011) Genetic and transcriptional analysis of phosphoinositide-specific phospholipase C in Plasmodium. *Exp Parasitol* **129**: 75–80.

93. Martin SK, Jett M, Schneider I (1994) Correlation of phosphoinositide hydrolysis with exflagellation in the malaria microgametocyte. *The Journal of parasitology* 371–378.

94. Ward P, Equinet L, Packer J, Doerig C (2004) Protein kinases of the human malaria parasite Plasmodium falciparum: the kinome of a divergent eukaryote. *BMC genomics* **5**: 79.

95. Weiss GE, Gilson PR, Taechalertpaisarn T, Tham W-H, de Jong NW, Harvey KL, Fowkes FJ, Barlow PN, Rayner JC, Wright GJ, et al. (2015) Revealing the sequence and resulting cellular morphology of receptor-ligand interactions during Plasmodium falciparum invasion of erythrocytes. *PLoS pathogens* **11**: e1004670.

96. Wasserman M, Alarcón C, Mendoza PM (1982) Effects of Ca++ depletion on the asexual cell cycle of Plasmodium falciparum. *The American journal of tropical medicine and hygiene* **31**: 711–717.

97. Glushakova S, Lizunov V, Blank PS, Melikov K, Humphrey G, Zimmerberg J (2013) Cytoplasmic free Ca2+ is essential for multiple steps in malaria parasite egress from infected erythrocytes. *Malar J* **12**: 41.

98. Hotta CT, Gazarini ML, Beraldo FH, Varotti FP, Lopes C, Markus RP, Pozzan T, Garcia CR (2000) Calcium-dependent modulation by melatonin of the circadian rhythm in malarial parasites. *Nat Cell Biol* **2**: 466–468.

99. Brochet M, Collins MO, Smith TK, Thompson E, Sebastian S, Volkmann K, Schwach F, Chappell L, Gomes AR, Berriman M, et al. (2014) Phosphoinositide metabolism links cGMP-dependent protein kinase G to essential Ca2+ signals at key decision points in the life cycle of malaria parasites. *PLoS biology* **12**: e1001806.

100. Collins CR, Hackett F, Strath M, Penzo M, Withers-Martinez C, Baker DA, Blackman MJ (2013) Malaria parasite cGMP-dependent protein kinase regulates blood stage merozoite secretory organelle discharge and egress. *PLoS pathogens* **9**: e1003344.

101. Dvorin JD, Martyn DC, Patel SD, Grimley JS, Collins CR, Hopp CS, Bright AT, Westenberger S, Winzeler E, Blackman MJ, et al. (2010) A plant-like kinase in Plasmodium falciparum regulates parasite egress from erythrocytes. *Science* **328**: 910–912.

102. Giganti D, Bouillon A, Tawk L, Robert F, Martinez M, Crublet E, Weber P, Girard-Blanc C, Petres S, Haouz A, et al. (2014) A novel Plasmodium-specific prodomain fold regulates the malaria drug target SUB1 subtilase. *Nature communications* **5**:

103. Philip N, Waters AP (2015) Conditional degradation of Plasmodium calcineurin reveals functions in parasite colonization of both host and vector. *Cell host \& microbe* **18**: 122–131.

104. Siden-Kiamos I, Ecker A, Nybäck S, Louis C, Sinden RE, Billker O (2006) Plasmodium berghei calcium-dependent protein kinase 3 is required for ookinete gliding motility and mosquito midgut invasion. *Mol Microbiol* **60**: 1355–1363.

105. Ishino T, Orito Y, Chinzei Y, Yuda M (2006) A calcium-dependent protein kinase regulates Plasmodium ookinete access to the midgut epithelial cell. *Mol Microbiol* **59**: 1175–1184.

106. Carey AF, Singer M, Bargieri D, Thiberge S, Frischknecht F, Ménard R, Amino R (2014) Calcium dynamics of Plasmodium berghei sporozoite motility. *Cellular microbiology* **16**: 768–783.

107. Doi Y, Shinzawa N, Fukumoto S, Okano H, Kanuka H (2011) Calcium signal regulates temperature-dependent transformation of sporozoites in malaria parasite development. *Experimental parasitology* **128**: 176–180.

108. Suarez C, Volkmann K, Gomes AR, Billker O, Blackman MJ (2013) The malarial serine protease SUB1 plays an essential role in parasite liver stage development. *PLoS pathogens* **9**: e1003811.

109. McRobert L, Taylor CJ, Deng W, Fivelman QL, Cummings RM, Polley SD, Billker O, Baker DA (2008) Gametogenesis in malaria parasites is mediated by the cGMP-dependent protein kinase. *PLoS biology* **6**: e139.

110. Muhia DK, Swales CA, Deng W, Kelly JM, Baker DA (2001) The gametocyte-activating factor xanthurenic acid stimulates an increase in membrane-associated guanylyl cyclase activity in the human malaria parasite Plasmodium falciparum. *Molecular microbiology* **42**: 553–560.

111. Kawamoto F, Alejo-Blanco R, Fleck SL, Kawamoto Y, Sinden RE (1990) Possible roles of Ca2+ and cGMP as mediators of the exflagellation of Plasmodium berghei and Plasmodium falciparum. *Molecular and biochemical parasitology* **42**: 101–108.

112. Washington NL, Ward S (2006) FER-1 regulates Ca2+-mediated membrane fusion during C. elegans spermatogenesis. *Journal of cell science* **119**: 2552–2562.

113. Lek A, Lek M, North KN, Cooper ST (2010) Phylogenetic analysis of ferlin genes reveals ancient eukaryotic origins. *BMC evolutionary biology* **10**: 231.

114. Helfmann S, Neumann P, Tittmann K, Moser T, Ficner R, Reisinger E (2011) The crystal structure of the C 2 A domain of otoferlin reveals an unconventional top loop region. *Journal of molecular biology* **406**: 479–490.

115. Staub E, Fiziev P, Rosenthal A, Hinzmann B (2004) Insights into the evolution of the nucleolus by an analysis of its protein domain repertoire. *Bioessays* **26**: 567–581.

116. Jiménez JL, Bashir R (2007) In silico functional and structural characterisation of ferlin proteins by mapping disease-causing mutations and evolutionary information onto three-dimensional models of their C2 domains. *Journal of the neurological sciences* **260**: 114–123.

117. Covian-Nares JF, Koushik SV, Puhl HL, Vogel SS (2010) Membrane wounding triggers ATP release and dysferlin-mediated intercellular calcium signaling. *J Cell Sci* **123**: 1884–1893.

118. Davis DB, Doherty KR, Delmonte AJ, McNally EM (2002) Calcium-sensitive phospholipid binding properties of normal and mutant ferlin C2 domains. *Journal of Biological Chemistry* **277**: 22883–22888.

119. Ramakrishnan NA, Drescher MJ, Morley BJ, Kelley PM, Drescher DG (2014) Calcium regulates molecular interactions of otoferlin with soluble NSF attachment protein receptor (SNARE) proteins required for hair cell exocytosis. *Journal of Biological Chemistry* **289**: 8750–8766.

120. Johnson CP (2017) Emerging Functional Differences between the Synaptotagmin and Ferlin Calcium Sensor Families. *Biochemistry* **56**: 6413–6417.

121. Yasunaga S, Grati M, Cohen-Salmon M, El-Amraoui A, Mustapha M, Salem N, El-Zir E, Loiselet J, Petit C (1999) A mutation in OTOF, encoding otoferlin, a FER-1-like protein, causes DFNB9, a nonsyndromic form of deafness. *Nature genetics* **21**: 363.

122. Liu J, Aoki M, Illa I, Wu C, Fardeau M, Angelini C, Serrano C, Urtizberea JA, Hentati F, Hamida MB, et al. (1998) Dysferlin, a novel skeletal muscle gene, is mutated in Miyoshi myopathy and limb girdle muscular dystrophy. *Nature genetics* **20**: 31.

123. Redpath GM, Sophocleous RA, Turnbull L, Whitchurch CB, Cooper ST (2016) Ferlins Show Tissue-Specific Expression and Segregate as Plasma Membrane/Late Endosomal or Trans-Golgi/Recycling Ferlins. *Traffic* **17**: 245–266.

124. Pangr\vsi\vc T, Reisinger E, Moser T (2012) Otoferlin: a multi-C2 domain protein essential for hearing. *Trends in neurosciences* **35**: 671–680.

125. Roux I, Safieddine S, Nouvian R, Grati M, Simmler M-C, Bahloul A, Perfettini I, Le Gall M, Rostaing P, Hamard G, et al. (2006) Otoferlin, defective in a human deafness form, is essential for exocytosis at the auditory ribbon synapse. *Cell* **127**: 277–289.

126. Pangrsic T, Lasarow L, Reuter K, Takago H, Schwander M, Riedel D, Frank T, Tarantino LM, Bailey JS, Strenzke N, et al. (2010) Hearing requires otoferlin-dependent efficient replenishment of synaptic vesicles in hair cells. *Nat Neurosci* **13**: 869–876.

127. Johnson CP, Chapman ER (2010) Otoferlin is a calcium sensor that directly regulates SNARE-mediated membrane fusion. *The Journal of cell biology* **191**: 187–197.

128. Heidrych P, Zimmermann U, Kuhn S, Franz C, Engel J, Duncker SV, Hirt B, Pusch CM, Ruth P, Pfister M, et al. (2009) Otoferlin interacts with myosin VI: implications for maintenance of the basolateral synaptic structure of the inner hair cell. *Human molecular genetics* **18**: 2779–2790.

129. Heidrych P, Zimmermann U, Breß A, Pusch CM, Ruth P, Pfister M, Knipper M, Blin N (2008) Rab8b GTPase, a protein transport regulator, is an interacting partner of otoferlin, defective in a human autosomal recessive deafness form. *Human molecular genetics* **17**: 3814–3821.

130. Davis DB, Delmonte AJ, Ly CT, McNally EM (2000) Myoferlin, a candidate gene and potential modifier of muscular dystrophy. *Hum Mol Genet* **9**: 217–226.

131. Doherty KR, Cave A, Davis DB, Delmonte AJ, Posey A, Earley JU, Hadhazy M, McNally EM (2005) Normal myoblast fusion requires myoferlin. *Development*

132: 5565–5575.

132. Bansal D, Campbell KP (2004) Dysferlin and the plasma membrane repair in muscular dystrophy. *Trends Cell Biol* **14**: 206–213.

133. Bernatchez PN, Sharma A, Kodaman P, Sessa WC (2009) Myoferlin is critical for endocytosis in endothelial cells. *American Journal of Physiology-Cell Physiology* **297**: C484–C492.

134. Robinson JM, Ackerman IV WE, Behrendt NJ, Vandre DD (2009) While dysferlin and myoferlin are coexpressed in the human placenta, only dysferlin expression is responsive to trophoblast fusion in model systems. *Biology of reproduction* **81**: 33–39.

135. Matsuda C, Hayashi YK, Ogawa M, Aoki M, Murayama K, Nishino I, Nonaka I, Arahata K, Brown RH (2001) The sarcolemmal proteins dysferlin and caveolin-3 interact in skeletal muscle. *Hum Mol Genet* **10**: 1761–1766.

136. Huang Y, de Morrée A, van Remoortere A, Bushby K, Frants RR, den Dunnen JT, van der Maarel SM (2008) Calpain 3 is a modulator of the dysferlin protein complex in skeletal muscle. *Hum Mol Genet* **17**: 1855–1866.

137. Ho M, Post CM, Donahue LR, Lidov HG, Bronson RT, Goolsby H, Watkins SC, Cox GA, Brown Jr RH (2004) Disruption of muscle membrane and phenotype divergence in two novel mouse models of dysferlin deficiency. *Human molecular genetics* **13**: 1999–2010.

138. Therrien C, Dodig D, Karpati G, Sinnreich M (2006) Mutation impact on dysferlin inferred from database analysis and computer-based structural predictions. *Journal of the neurological sciences* **250**: 71–78.

139. Cenacchi G, Fanin M, De Giorgi L, Angelini C (2005) Ultrastructural changes in dysferlinopathy support defective membrane repair mechanism. *Journal of clinical pathology* **58**: 190–195.

140. Inoue M, Wakayama Y, Kojima H, Shibuya S, Jimi T, Oniki H, Nishino I, Nonaka I (2006) Expression of myoferlin in skeletal muscles of patients with dysferlinopathy. *The Tohoku journal of experimental medicine* **209**: 109–116.

141. Doherty KR, Demonbreun AR, Wallace GQ, Cave A, Posey AD, Heretis K, Pytel P, McNally EM (2008) The endocytic recycling protein EHD2 interacts with myoferlin to regulate myoblast fusion. *Journal of Biological Chemistry* **283**: 20252–20260.

142. Bernatchez PN, Sharma A, Kodaman P, Sessa WC (2009) Myoferlin is critical for endocytosis in endothelial cells. *Am J Physiol, Cell Physiol* **297**: C484–92.

143. Bernatchez PN, Acevedo L, Fernandez-Hernando C, Murata T, Chalouni C, Kim J, Erdjument-Bromage H, Shah V, Gratton J-P, McNally EM, et al. (2007) Myoferlin regulates vascular endothelial growth factor receptor-2 stability and function.

Journal of Biological Chemistry **282**: 30745–30753.

144. Demonbreun AR, Posey AD, Heretis K, Swaggart KA, Earley JU, Pytel P, McNally EM (2010) Myoferlin is required for insulin-like growth factor response and muscle growth. *The FASEB Journal* **24**: 1284–1295.

145. Turtoi A, Blomme A, Bellahcène A, Gilles C, Hennequière V, Peixoto P, Bianchi E, Noel A, De Pauw E, Lifrange E, et al. (2013) Myoferlin is a key regulator of EGFR activity in breast cancer. *Cancer Res* **73**: 5438–5448.

146. Amatschek S, Koenig U, Auer H, Steinlein P, Pacher M, Gruenfelder A, Dekan G, Vogl S, Kubista E, Heider K-H, et al. (2004) Tissue-wide expression profiling using cDNA subtraction and microarrays to identify tumor-specific genes. *Cancer Res* **64**: 844–856.

147. Volakis LI, Li R, Ackerman IV WE, Mihai C, Bechel M, Summerfield TL, Ahn CS, Powell HM, Zielinski R, Rosol TJ, et al. (2014) Loss of myoferlin redirects breast cancer cell motility towards collective migration. *PloS one* **9**: e86110.

148. Leung C, Yu C, Lin MI, Tognon C, Bernatchez P (2013) Expression of myoferlin in human and murine carcinoma tumors: role in membrane repair, cell proliferation, and tumorigenesis. *The American journal of pathology* **182**: 1900–1909.

149. Posey Jr AD, Demonbreun A, McNally EM (2011) Ferlin proteins in myoblast fusion and muscle growth. *Current topics in developmental biology* **96**: 203.

150. Reisinger E, Bresee C, Neef J, Nair R, Reuter K, Bulankina A, Nouvian R, Koch M, Bückers J, Kastrup L, et al. (2011) Probing the functional equivalence of otoferlin and synaptotagmin 1 in exocytosis. *Journal of Neuroscience* **31**: 4886–4895.

151. Lek A, Evesson FJ, Sutton RB, North KN, Cooper ST (2012) Ferlins: regulators of vesicle fusion for auditory neurotransmission, receptor trafficking and membrane repair. *Traffic* **13**: 185–194.

152. Leung C, Utokaparch S, Sharma A, Yu C, Abraham T, Borchers C, Bernatchez P (2011) Proteomic identification of dysferlin-interacting protein complexes in human vascular endothelium. *Biochemical and biophysical research communications* **415**: 263–269.

153. Achanzar WE, Ward S (1997) A nematode gene required for sperm vesicle fusion. *Journal of cell science* **110**: 1073–1081.

154. Defour A, Van der Meulen JH, Bhat R, Bigot A, Bashir R, Nagaraju K, Jaiswal JK (2014) Dysferlin regulates cell membrane repair by facilitating injury-triggered acid sphingomyelinase secretion. *Cell death \& disease* **5**: e1306.

155. Demonbreun AR, Fahrenbach JP, Deveaux K, Earley JU, Pytel P, McNally EM (2010) Impaired muscle growth and response to insulin-like growth factor 1 in

dysferlin-mediated muscular dystrophy. *Human molecular genetics* **20**: 779–789.

156. Krajacic P, Pistilli EE, Tanis JE, Khurana TS, Lamitina ST (2013) FER-1/Dysferlin promotes cholinergic signaling at the neuromuscular junction in C. elegans and mice. *Biology open* **2**: 1245–1252.

157. Ohsako T, Hirai K, Yamamoto M-T (2003) The Drosophila misfire gene has an essential role in sperm activation during fertilization. *Genes \& genetic systems* **78**: 253–266.

158. Sun X, Zhu Y, Wang L, Liu H, Ling Y, Li Z, Sun L (2017) The Catsper channel and its roles in male fertility: a systematic review. *Reproductive Biology and Endocrinology* **15**: 65.

159. Sodergren E, Weinstock GM, Davidson EH, Cameron RA, Gibbs RA, Angerer RC, Angerer LM, Arnone MI, Burgess DR, Burke RD, et al. (2006) The genome of the sea urchin Strongylocentrotus purpuratus. *Science* **314**: 941–952.

160. Xiong Y, Zhang M, Hong Y, Wei M, Ai D, Meng P, Han Y, Fu Z, Shi Y, Yang J, et al. (2013) Characterization analysis of Schistosoma japonicum plasma membrane repair relative gene myoferlin. *PloS one* **8**: e66396.

161. Mueller A-K, Morath E (2015) Malaria vaccines based on apicomplexan ferlins, ferlin-like proteins and other C2-domain containing proteins.

162. Hall N, Karras M, Raine JD, Carlton JM, Kooij TW, Berriman M, Florens L, Janssen CS, Pain A, Christophides GK, et al. (2005) A comprehensive survey of the Plasmodium life cycle by genomic, transcriptomic, and proteomic analyses. *Science* **307**: 82–86.

163. Franke-Fayard B, Trueman H, Ramesar J, Mendoza J, van der Keur M, van der Linden R, Sinden RE, Waters AP, Janse CJ (2004) A Plasmodium berghei reference line that constitutively expresses GFP at a high level throughout the complete life cycle. *Molecular and biochemical parasitology* **137**: 23–33.

164. Nussenzweig R, Nussenzweig V (1989) Antisporozoite vaccine for malaria: experimental basis and current status. *Clinical Infectious Diseases* **11**: S579–S585.

165. Tsuji M, Mattei D, Nussenzweig RS, Eichinger D, Zavala F (1994) Demonstration of heat-shock protein 70 in the sporozoite stage of malaria parasites. *Parasitol Res* **80**: 16–21.

166. Birago C, Albanesi V, Silvestrini F, Picci L, Pizzi E, Alano P, Pace T, Ponzi M (2003) A gene-family encoding small exported proteins is conserved across Plasmodium genus. *Molecular and biochemical parasitology* **126**: 209–218.

167. Chapman S, Faulkner C, Kaiserli E, Garcia-Mata C, Savenkov EI, Roberts AG, Oparka KJ, Christie JM (2008) The photoreversible fluorescent protein iLOV outperforms GFP as a reporter of plant virus infection. *Proceedings of the National*

Academy of Sciences **105**: 20038–20043.

168. Kooij TW, Rauch MM, Matuschewski K (2012) Expansion of experimental genetics approaches for Plasmodium berghei with versatile transfection vectors. *Molecular and biochemical parasitology* **185**: 19–26.

169. Braks JA, Franke-Fayard B, Kroeze H, Janse CJ, Waters AP (2006) Development and application of a positive-negative selectable marker system for use in reverse genetics in Plasmodium. *Nucleic Acids Research* **34**: e39–e39.

170. Godiska R, Mead D, Dhodda V, Wu C, Hochstein R, Karsi A, Usdin K, Entezam A, Ravin N (2009) Linear plasmid vector for cloning of repetitive or unstable sequences in Escherichia coli. *Nucleic acids research* **38**: e88–e88.

171. Gomes AR, Bushell E, Schwach F, Girling G, Anar B, Quail MA, Herd C, Pfander C, Modrzynska K, Rayner JC, et al. (2015) A genome-scale vector resource enables high-throughput reverse genetic screening in a malaria parasite. *Cell host \& microbe* **17**: 404–413.

172. Schwach F, Bushell E, Gomes AR, Anar B, Girling G, Herd C, Rayner JC, Billker O (2015) PlasmoGEM, a database supporting a community resource for large-scale experimental genetics in malaria parasites. *Nucleic Acids Res* **43**: D1176–82.

173. Grützke J, Rindte K, Goosmann C, Silvie O, Rauch C, Heuer D, Lehmann MJ, Mueller A-K, Brinkmann V, Matuschewski K, et al. (2014) The spatiotemporal dynamics and membranous features of the Plasmodium liver stage tubovesicular network. *Traffic* **15**: 362–382.

174. Bushell E, Gomes AR, Sanderson T, Anar B, Girling G, Herd C, Metcalf T, Modrzynska K, Schwach F, Martin RE, et al. (2017) Functional profiling of a Plasmodium genome reveals an abundance of essential genes. *Cell* **170**: 260–272.

175. Mukherjee A, Walker J, Weyant KB, Schroeder CM (2013) Characterization of flavin-based fluorescent proteins: an emerging class of fluorescent reporters. *PloS one* **8**: e64753.

176. De Koning-Ward TF, Gilson PR, Crabb BS (2015) Advances in molecular genetic systems in malaria. *Nature Reviews Microbiology* **13**: 373–387.

177. Ferré-D'Amaré AR (2010) The glmS ribozyme: use of a small molecule coenzyme by a gene-regulatory RNA. *Quarterly reviews of biophysics* **43**: 423–447.

178. Armstrong CM, Goldberg DE (2007) An FKBP destabilization domain modulates protein levels in Plasmodium falciparum. *Nature methods* **4**: 1007.

179. Nishimura K, Fukagawa T, Takisawa H, Kakimoto T, Kanemaki M (2009) An auxin-based degron system for the rapid depletion of proteins in nonplant cells. *Nature methods* **6**: 917.

180. Siden-Kiamos I, Ganter M, Kunze A, Hliscs M, Steinbüchel M, Mendoza J, Sinden RE, Louis C, Matuschewski K (2011) Stage-specific depletion of myosin A supports an essential role in motility of malarial ookinetes. *Cellular microbiology* **13**: 1996–2006.

181. De Niz M, Helm S, Horstmann S, Annoura T, del Portillo HA, Khan SM, Heussler VT (2015) In Vivo and In Vitro Characterization of a Plasmodium Liver Stage-Specific Promoter. *PloS one* **10**:

182. Laurentino EC, Taylor S, Mair GR, Lasonder E, Bartfai R, Stunnenberg HG, Kroeze H, Ramesar J, Franke-Fayard B, Khan SM, et al. (2011) Experimentally controlled downregulation of the histone chaperone FACT in Plasmodium berghei reveals that it is critical to male gamete fertility. *Cellular microbiology* **13**: 1956–1974.

183. Silvie O, Franetich J-F, Charrin S, Mueller MS, Siau A, Bodescot M, Rubinstein E, Hannoun L, Charoenvit Y, Kocken CH, et al. (2004) A role for apical membrane antigen 1 during invasion of hepatocytes by Plasmodium falciparum sporozoites. *Journal of Biological Chemistry* **279**: 9490–9496.

184. Lavazec C, Moreira CK, Mair GR, Waters AP, Janse CJ, Templeton TJ (2009) Analysis of mutant Plasmodium berghei parasites lacking expression of multiple PbCCp genes. *Molecular and biochemical parasitology* **163**: 1–7.

185. Santos JM, Kehrer J, Franke-Fayard B, Frischknecht F, Janse CJ, Mair GR (2015) The Plasmodium palmitoyl-S-acyl-transferase DHHC2 is essential for ookinete morphogenesis and malaria transmission. *Scientific reports* **5**: 16034.

186. Vogl C, Panou I, Yamanbaeva G, Wichmann C, Mangosing SJ, Vilardi F, Indzhykulian AA, Pangr\vsi\vc T, Santarelli R, Rodriguez-Ballesteros M, et al. (2016) Tryptophan-rich basic protein (WRB) mediates insertion of the tail-anchored protein otoferlin and is required for hair cell exocytosis and hearing. *The EMBO Journal* **35**: 2536–2552.

187. Kobayashi K, Izawa T, Kuwamura M, Yamate J (2012) Dysferlin and animal models for dysferlinopathy. *J Toxicol Pathol* **25**: 135–147.

188. Smith MK, Wakimoto BT (2007) Complex regulation and multiple developmental functions of misfire, the Drosophila melanogaster ferlin gene. *BMC developmental biology* **7**: 1.

189. Beetsma A, van de Wiel TJ, Sauerwein R, Eling W (1998) Plasmodium bergheiANKA: Purification of Large Numbers of Infectious Gametocytes. *Experimental parasitology* **88**: 69–72.

190. Swulius MT, Jensen GJ (2012) The helical MreB cytoskeleton in Escherichia coli MC1000/pLE7 is an artifact of the N-Terminal yellow fluorescent protein tag. *Journal of bacteriology* **194**: 6382–6386.

191. Buckley AM, Petersen J, Roe AJ, Douce GR, Christie JM (2015) LOV-based reporters for fluorescence imaging. *Current opinion in chemical biology* **27**: 39–45.

192. Lacroix C, Giovannini D, Combe A, Bargieri DY, Späth S, Panchal D, Tawk L, Thiberge S, Carvalho TG, Barale J-C, et al. (2011) FLP/FRT-mediated conditional mutagenesis in pre-erythrocytic stages of Plasmodium berghei. *Nature protocols* **6**: 1412.

193. Estévez JM, Somerville C (2006) FlAsH-based live-cell fluorescent imaging of synthetic peptides expressed in Arabidopsis and tobacco. *Biotechniques* **41**: 572–564.

194. Crivat G, Tokumasu F, Sa JM, Hwang J, Wellems TE (2011) Tetracysteine-based fluorescent tags to study protein localization and trafficking in Plasmodium falciparum-infected erythrocytes. *PloS one* **6**: e22975.

195. Nancy H, Laughlin AM, Varner DD, Welsh TH, Forrest DW, Blanchard TL, Johnson L (2004) Gene expression in the spermatogenically inactive “dark” and maturing “light” testicular tissues of the prepubertal colt. *Journal of andrology* **25**: 535–544.

196. Carninci P, Hayashizaki Y (1999) [2] High-efficiency full-length cDNA cloning. In, *Methods in enzymology* pp 19–44. Elsevier.

197. Smith RC, Barillas-Mury C (2016) Plasmodium oocysts: overlooked targets of mosquito immunity. *Trends in parasitology* **32**: 979–990.

198. Janse CJ, Waters AP (2007) The exoneme helps malaria parasites to break out of blood cells. *Cell* **131**: 1036–1038.

199. Wirth CC, Pradel G (2012) Molecular mechanisms of host cell egress by malaria parasites. *International Journal of Medical Microbiology* **302**: 172–178.